Field-Scale Evapotranspiration for the Mission Valley using METRIC

Report submitted to the Montana Department of Natural Resources and Conservation

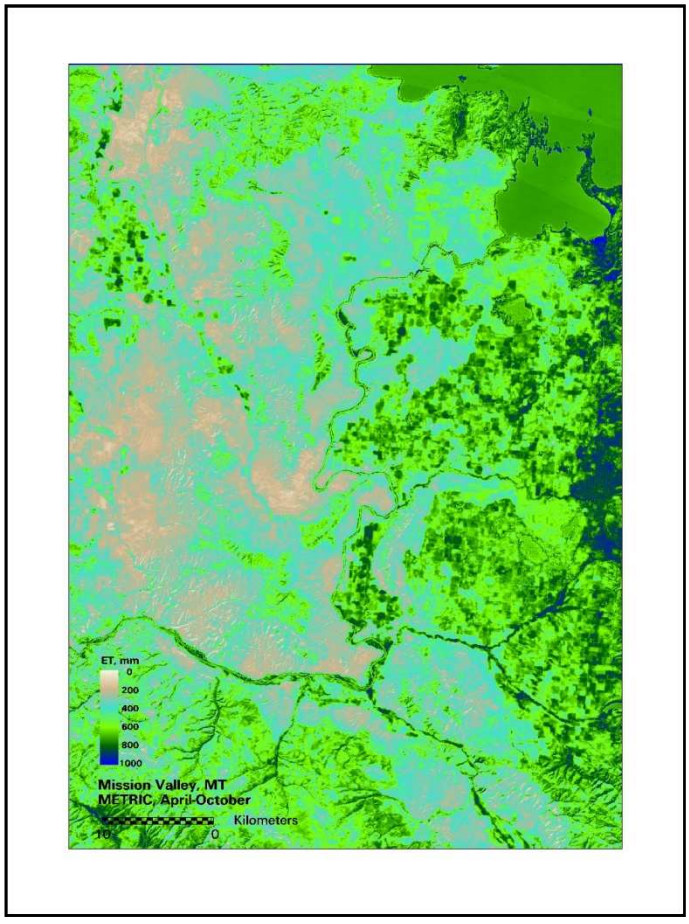

By
Dr. Jeppe Kjaersgaard
Dr. Richard Allen

University of Idaho
Kimberly R&E Center, Idaho

July 2009

Introduction

This report describes the setup and processing of Landsat satellite imagery in the Mission Valley area of Montana using the University of Idaho METRIC (Mapping Evapotranspiration with high Resolution and Internalized Calibration) procedure for determining evapotranspiration (ET). The objective of the study was to produce spatial estimates of monthly and growing season ET over the Mission Valley area. Evapotranspiration is calculated within METRIC using a surface energy balance that produces instantaneous (at 1100 overpass time) and daily values for ET. For the Mission Valley application, eight Landsat image dates were processed over the growing season (April-October). ET was calculated with the same spatial resolution as the satellite image which is 30 m in the case of Landsat. The entire geographic location of the Flathead Reservation is contained within a single Landsat scene, as shown in Fig 1, and the entire Landsat scene (approximately 150 x 150 km) was processed by METRIC. The dates of the satellite images processed using METRIC are listed in Table 1.

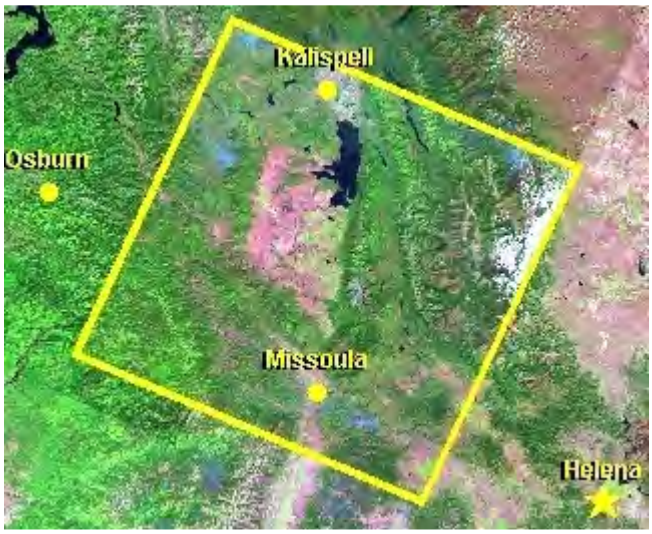

Figure 1. A Landsat image for Landsat path 41 row 27 covering the Mission Valley study area as outlined by the yellow square on this true color mosaic from August 2 2007. Also visible are principal cities and smoke from forest fires.

Table 1. Dates, satellite platform and path/row used to calculate ET for the Mission Valley region.

Date	Satellite	Path	Row
05/10/2006	Landsat 5	41	27
06/27/2006	Landsat 5	41	27
10/01/2006	Landsat 5	41	27
07/16/2007	Landsat 5	41	27
08/01/2007	Landsat 5	41	27
09/02/2007	Landsat 5	41	27
04/13/2008	Landsat 5	41	27
05/31/2008	Landsat 5	41	27

The METRIC procedure utilizes the visible, near-infrared and thermal infrared energy spectrum bands from satellite images and weather data to calculate ET on a pixel by pixel basis. Energy is partitioned into net incoming radiation (both solar and thermal), ground heat flux, sensible heat flux to the air and latent heat flux. The latent heat flux is calculated as the residual of the energy balance and represents the energy consumed by ET. The topography of a region was incorporated into METRIC via a digital elevation model (DEM), to account for impacts of sloped areas on solar radiation, net radiation, terrain roughness and near surface air temperature gradients in the energy balance. In most parts of the agricultural regions of the Mission Valley, the impacts by elevation change are small. METRIC was calibrated for each image using ground based meteorological information and identified 'anchor' conditions (the cold and hot pixels of METRIC) present in each image. A detailed description of METRIC can be found in Allen et al. (2007a,b).

The primary goal for the processing was to estimate ET from the agricultural areas within the Flathead Reservation. Therefore, satellite image dates were selected that were especially free from clouds and smoke over agricultural areas. Clouds and smoke were present at times over some adjacent areas that included rangeland, Flathead and Lolo National Forests, the Rattlesnake Wilderness, and riparian areas along the Flathead River, along canals and around lakes and reservoirs. Because METRIC is unable to compute valid ET estimates for areas affected by clouds, smoke or other conditions of greatly reduced transmissivity of the atmosphere, ET estimates are not available for portions of the adjacent areas on some of the image dates.

This report is organized to decribe the setup and calibration of the satellite image processing and to present some of the results from the application of METRIC. A description of the quality control of supporting meteorological information, Landsat image selection and preparation, selection of supporting information, model improvements and the extrapolation of daily estimates to monthly and seasonal estimates of ET and ET_rF[1] are located in appendices A through G as outlined in Table 2.

Table 2. Content of the appendices

Appendix	Subject
A	Quality control of weather data
B	Selection of Landsat images for the METRIC processing
C	Shift of the thermal band relative to the shortwave bands
D	Selection of a digital elevation map and a land use map
E	Adjustments to METRIC for processing
F	Development of an algorithm to estimate canopy temperature of tall vegetation
G	Estimating monthly and seasonal ET_rF and ET from daily values

[1] ET_rF is the fraction of alfalfa reference ET_r and is a direct product from METRIC. ET_r is used to calibrate METRIC. ET_r is calculated based on meteorological information from a weather station. Typical ranges for ET_rF are 0 to about 1.1. ET_rF is synonymous with the crop coefficient.

1. Data processing

Weather data

METRIC utilizes alfalfa reference ET (i.e., ET_r) as calculated by the ASCE standardized Penman-Monteith equation (ASCE-EWRI 2005) for calibration of the energy balance process and to establish a daily soil water balance to estimate residual soil evaporation from bare soil following precipitation events (Allen et al. 2007a). The ET_r is used as a means to 'anchor' the surface energy balance by representing the ET from locations having high levels of vegetation and cooler surface temperatures. Therefore, high quality estimates of ET_r are needed, which, in turn, require high quality weather data. Therefore, before processing the satellite images, the quality and accuracy of the meteorological data were assessed. The locations and the retrieval and quality control of weather data used during the processing were from the St. Ignatius, Round Butte and Creston Agrimet weather stations located in the Mission Valley. The weather data quality control is described in Appendix A. Based on the assessment of weather station location, local environment and weather data quality, weather information from the St. Ignatius Agrimet weather station was selected to be used during the METRIC processing due to its representativeness of agricultural conditions and more open station surroundings. One exception is for the period July 3 to July 17 2007 where the weather data from St. Ignatius were substituted with weather data from Creston due to exceptional dry local conditions at St. Ignatius during that period as reflected in the relative humidity data.

The calculation timestep for determining ET_r was hourly to produce ET_r for calibration of the METRIC energy balance estimation process at the time of the Landsat overpasses. The hourly ET_r values were then summed to daily totals to provide a basis for producing daily and monthly ET. ET_r was calculated using the RefET software (version 3) of University of Idaho (Allen, 2008).

The daily soil water balance was used to determine whether any residual evaporation existed from exposed soil at the time of each satellite image due to recent rainfall events. The residual evaporation was considered when assigning a value for ET from the 'hot' anchor point during the METRIC calibration process, where the hot anchor point was generally a bare soil condition located within about 20 km of the weather station. The FAO-56 (Allen et al. 1998) soil evaporation model was used to estimate residual evaporation based on a 0.10 m evaporation layer and using soil water holding capacity for the dominant soil in the agricultural regions of the valley. The simulated soil water balance was initiated several months before each image date, hence meteorological data from all of 2006, 2007 and January – August 2008 were used.

Selection and setup of satellite images, land use map and digital elevation map

The satellite images to be processed were selected by PIs from University of Idaho (UI) and MT DNRC based on a list of available Landsat 5 and Landsat 7 image candidates for the years 1997 - 2008 prepared by UI. The selection of the images is described in Appendix B. The eight Landsat 5 images were ordered by and delivered to UI from the USGS Earth Resources Observation Systems (EROS) in Sioux Falls, S.D. The images were ordered as the L1T product, which includes both radiometric, geographic and terrain correction. Based on advice from MT DNRC the

images were ordered in the State Plane Coordinate System Zone 2500 projection and using the NAD83 datum and 30 m pixel size. A copy of the seven-band images was provided to the MT DNRC by UI.

The eight Landsat images ordered and processed span three different years (2006, 2007 and 2008). The multi-year span was necessary, as opposed to a preferred processing of a single year, due to high frequency of clouded images during any individual year. Sequences of clouded images in some part of all years precluded assembling images on an approximately monthly basis for any one year that were sufficiently cloud-free over agricultural areas to process. The months of April and May are especially cloudy in the Mission Valley and some images additionally had a large number of jet contrails due to air traffic. The most cloud-free images were assembled from the three years so that ET information could be produced on about a 3 to 4 week interval. The ET information from the eight images was used to assemble monthly ET images by interpolation of relative ET fractions, based on weather data, between image dates using cubic splines.

It was previously determined (Trezza and Allen, 2008) that the thermal band (band 6) of L1T terrain-corrected Landsat 5 images purchased directly from the USGS EROS data center and processed by EROS using the NLAPS processing system is shifted up to 0, 30, 60 90 or 120 m in the north-south direction as compared to the visible and near-infrared bands. The shift of the thermal band was shifted in the southerly direction. The shift is generally considered to be consistent throughout the image. It is important that the pixels of all seven bands in the Landsat image "line up" in order to perform a correct solution to the surface energy balance during METRIC process. Therefore, prior to processing, the image bands were screened for a possible shift. The vertical shifts determined for each image date are listed in Table 3. The shift and its remedy are described in Appendix C.

Table 3. Vertical (north-south) shift between the shortwave and the longwave bands in the Landsat 5 images.

Image date	Shift (m)
04/13-2008	60
05/10-2006	60
05/31-2008	60
06/27-2006	30*
07/16-2007	60
08/01-2007	60
09/02-2007	60
10/01-2006	60

*When screening the 06/27-2006 image most of the statistics indicated that the shift was 30 m while others suggested 60 m.

A digital elevation map (DEM) is used during the METRIC processing to support the radiation calculation on slopes and to correct the surface temperature for lapse effects caused by elevation variation. A DEM with 30 m resolution was obtained from the USGS seamless server and was resampled into the projection of the Landsat images using cubic convolution

resampling. Maps of slope and aspect (aspect is the cardinal direction of an inclined surface) at 30 m resolution used during the METRIC processing were created using a tool within the ERDAS Imagine processing system based on the DEM.

A land use (LU) map was used to support estimation of aerodynamic roughness and soil heat flux during the METRIC processing. Two LU maps immediately available at 30 m resolution were initially considered for use *viz.* the National Land Cover Dataset (NLCD) 2001 from the USGS and the Satellite Imagery Land Cover from the University of Montana. The properties of the two land use maps and selection of the most suitable one is discussed in Appendix D. The NLCD 2001 land use map was selected and used for the processing. The NLCD land use map was downloaded from the USGS seamless server and was resampled into the projection of the Landsat images using nearest neighbor resampling.

Calibration of METRIC

During the processing of the eight Landsat images the METRIC model was adjusted to account for conditions that deviate from the description of the standard Level 1 METRIC model application. These adjustments are referred to as Level 2 processing (Allen et al., 2008). Some of the Level 2 adjustments have been applied in previous applications of METRIC while other adjustments were made during this study to address factors specific to the Mission valley area. The adjustments are described in Appendices E and F and included adjustment to canopy temperature of forested areas to account for impacts of shadows on the surface temperature measurement, adjustment to albedo of forested areas to account for impacts of shadows, application of a lapse rate in mountain regions that was different from that used in lower lying areas, and improvement in net long-wave radiation estimates in mountainous areas to account for cross valley impacts.

METRIC uses a vertical near surface-to-air difference, dT, to estimate sensible heat flux. Sensible heat flux (H) is the amount of heat that is convected from a surface into the air, thereby reducing the amount of available energy for evaporation. The dT function is generally assumed to be linearly proportional to surface temperature and is defined using the properties of two user selected anchor pixels that represent the extreme conditions encountered within the image (a condition having nearly complete conversion of available energy into evapotranspiration and a condition having nearly zero conversion of available energy into evapotranspiration). The “cold” anchor pixel generally represents a fully vegetated and actively transpiring vegetation, while the “hot” anchor pixel represents a bare and dry or nearly dry agricultural soil with little or no vegetation. The selection of cold and hot anchor pixels by the user is described by Allen et al., (2007b, 2008). These pixels are generally selected from agricultural fields for consistency and to match assumptions made in the estimation of soil heat flux, for example, where that algorithm was developed for agricultural soils.

During the internal calibration of sensible heat flux in METRIC, a fraction of ET_r, ET_rF, is assigned to the hot and cold conditions. ET_rF is equivalent to the crop coefficient (K_c) based on full-cover alfalfa as the reference crop.

During the calibration of the dT function, ET_rF at the cold pixel is normally considered to be 1.05 ET_rF unless vegetation cover is insufficient to support this assumption (for example, early in spring and during winter when full, robust vegetation cover is rare). The cold pixel is selected from a population of fields having full cover and relatively cold temperatures. Ideally, an alfalfa field is preferred for calibration, since the ASCE Penman-Monteith equation is calibrated to an alfalfa reference. However, Wright (1982) has shown that most agricultural crops, when at full cover, transpire at levels very similar to those of alfalfa. Therefore, the selected location for the cold pixel does not need to be alfalfa, but can be any pixel from within the interior of a fully vegetated, cool, field (crop type is generally unknown when applying METRIC). The 1.05 multiplier on ET_rF is used to account for the variation in ET inherent within a large population of fully vegetated fields. Because the colder 'portion' of the 'full-cover' population is generally used in selecting the cold pixel, the ET from that portion of the full-cover population is likely to be about 5% greater than the reference ET estimate, which is intended to represent the average rate from full-cover alfalfa (Allen et al., 2007a).

For the April 13 2008 image we were unable to locate fields that appeared to have full vegetation cover. Therefore, the ET from the agricultural fields evaluated on that date is expected to be lower than that from the alfalfa reference and ET_rF was therefore calculated using the following relationship between ET_rF and the normalized difference vegetation index (NDVI) $ET_rF_{cold\_041308}$=1.25NDVI (Tasumi et al., 2005, Burnett, 2007). NDVI generally ranges from about 0.1 to 0.15 for bare soil to 0.75 to 0.85 for full vegetation cover.

The hot pixel is generally considered to be a dry, bare soil having no residual evaporation (i.e. ET_rF=0). This is generally true if there have been no precipitation events for several weeks prior to the image overpass date. In the case where there have been recent precipitation events, the soil may not be dry and there will likely be some residual evaporation from the soil that must be recognized during calibration of energy balance parameters and processing of ET for satellite images.

A daily soil water balance was applied to the entire years of 2006 and 2007, and January-August 2008 using precipitation and ET_r for the St. Ignatius weather station. The water balance estimated residual evaporation on each of the image dates. The soil water balance is based on the two-stage daily soil evaporation model of the United Nations Food and Agriculture Organization's Irrigation and Drainage Paper 56 (Allen et al. 1998; 2005). Fig. 2 shows a simulation of evaporation from the upper 0.1 m of soil. The typical soil type for irrigated areas of the region was assumed to have a plant available water content (difference between field capacity and the wilting point) of 0.17 cm^3/ cm^3, based on the NRCS Soil database.

During the drying cycle after a wetting event, a typical bare agricultural soil can be expected to continue to evaporate at a small rate beyond the first several weeks due to diffusion of liquid water and vapor from beneath the upper soil layer. This evaporation can continue for an additional several weeks provided no new wetting event occurs, especially from tilled soils that have a moderate amount of water stored within the soil profile. This is typical of agriculture. The medium-term residual evaporation is not simulated by the FAO model. Becasue wetting

events generally occur relatively frequently in the St. Ignatius area, a minimum ET_rF value of 0.1 was used as a floor for evaporation from the bare soil selected as the hot calibration pixel for all image dates (desert and range soils having low water profiles are expected to go lower than the 0.1 residual). If the soil water balance predicted a higher ET_rF value for bare soil than the residual evaporation, the higher value was used as shown in Eq. 1:

$$ET_rF_{\text{bare soil for the hot pixel}} = \text{Maximum(Soil water balance model estimate, 0.1)} \quad (1)$$

Table 4 lists the ET_rF assigned to and location of the hot and cold pixels for the eight image dates.

Desert and range soils typically run 'hotter' in terms of surface temperature than bare agricultural soils. Reasons for this include effects of organic mulches, shielding of the soil surface by sparse live or dead vegetation, delamination of soil crusts, and increased soil porosity caused by animals and roots that is common to these land uses, but not to bare agricultural soils. To prevent the higher temperatures in desert and range from overestimating the near surface air temperature gradient (dT) and thus H, thereby causing ET from the energy balance to even go negative at times, adjustments were made to the dT estimation and estimation of soil heat flux when surface temperature exceeded a threshold temperature. On all image dates the soil heat flux and the slope of the dT function were reduced for those pixels where the surface temperature exceeded the surface temperature of a dry agricultural pixel as described by Allen et al. (2007b). Applications of METRIC in southern Idaho and some other areas have included an 'excess resistance' for desert areas containing sage brush to account for the shielding phenomenon by sparse, brushy vegetation on surface temperature. However, based on a visual assessment of the general vegetation type, height, density and vigor in the range land areas of the Mission Valley, no excess resistance was applied in this METRIC application.

A surface temperature lapse rate is used during the METRIC process to normalize the surface temperature image for changes in temperature caused by normal lapse effects associated with elevation changes within the image. This normalization is needed in any energy balance process before estimating near surface air temperature gradients and the associated sensible heat flux (Allen et al., 2007a). The temperature lapse rate changes with air humidity and weather conditions and is therefore not necessarily the same for all image dates. An analysis based on behavior of surface temperature for fully vegetated fields at north and south extremes in the images are described in Appendix E, section 1.

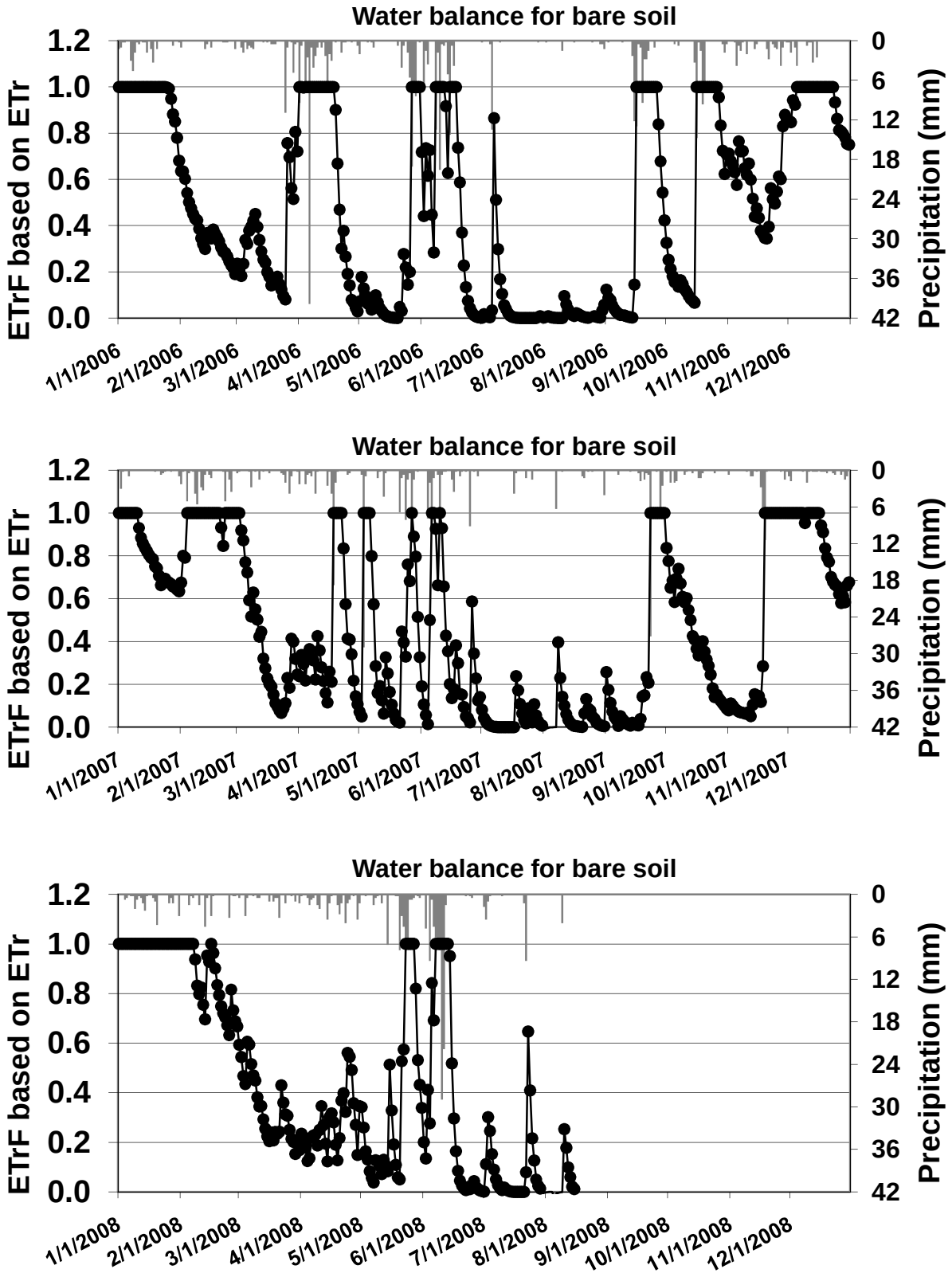

Figure 2. Daily ET_rF for bare soil estimated from the soil water balance for 2006 (top), 2007 (middle) and January-August 2008 (bottom).

Table 4. ET_rF values assigned to and locations (X, Y coordinate) of the hot and cold pixels.

			Hot pixel		Cold pixel	
Image date	ET_rF_{hot}	ET_rF_{cold}	X	Y	X	Y
04/13-2008	0.19	0.86	236460	359281	236312	360785
05/10-2006	0.1	1.05	237929	385917	245030	366715
05/31-2008	0.34	1.05	237887	359895	236516	359345
06/27-2006	0.1	1.05	248458	369872	253497	375541
07/16-2007	0.1	1.05	244144	362972	250441	389461
08/01-2007	0.1	1.05	248208	369529	250770	384814
09/02-2007	0.17	1.05	251630	388285	250445	377078
10/01-2006	0.33	1.05	253859	378265	240431	384873

2. Results

Reference ET

Daily ET_r was calculated by summing hourly ET_r to 24-h periods. Hourly ET_r was calculated using meteorological information from the St. Ignatius weather station. Daily (24-h) totals for the processed image dates are listed in Table 5.

Table 5. Day of year and calculated alfalfa based ET, ET_r for the satellite image dates

Image date	Day of year	ET_r (mm/day)
04/13-2008	104	5.89
05/10-2006	130	6.04
05/31-2008	152	6.55
06/27-2006	178	7.86
07/16-2007	197	7.26
08/01-2007	213	7.60
09/02-2007	245	5.69
10/01-2006	274	3.60

Daily ET_rF

Maps of reflectance of short wave radiation, vegetation indices (NDVI and LAI), surface temperature, net radiation and soil heat flux are generated as intermediate products during METRIC processing. The final output from the METRIC model is comprised of images of instantaneous ET_rF (fraction of alfalfa based reference ET, ET_r) at the satellite overpass time. The estimate of daily ET_rF is set equal to the instantaneous at the satellite overpass time, based on extensive ET measurements made using precision weighing lysimeters at Kimberly, Idaho (Allen et al. 2007b, 2008). An estimate of daily ET in mm/day is calculated by multiplying the ET_rF by daily ET_r. The procedures for obtaining daily estimates of ET and ET_rF are detailed in appendix G.

Maps of ET_rF for the area around Pablo Reservoir for the 05/10-2006, 06/27-2006 and 10/01-2006 image dates are shown in Fig. 3. Contrasts in spatial ET_rF and change over time are apparent. The 05/10-2006 image contains many fields having low vegetation due to bare agricultural fields around the Pablo Reservoir. By 06/27-2006 these fields are covered by crops having apparently good vigor that are evapotranspiring water at close to the reference level. Many of these crops were harvested or senescenced by 10/01-2006 causing lower ET rates. Other fields have some vegetation cover on all three image dates indicating a more permanent vegetation cover such as pasture or a back-to-back winter cereal rotation.

Daily ET values in mm/day for the satellite overpass dates are obtained by multiplying the ET_rF values by the value for ET_r from Table 4.

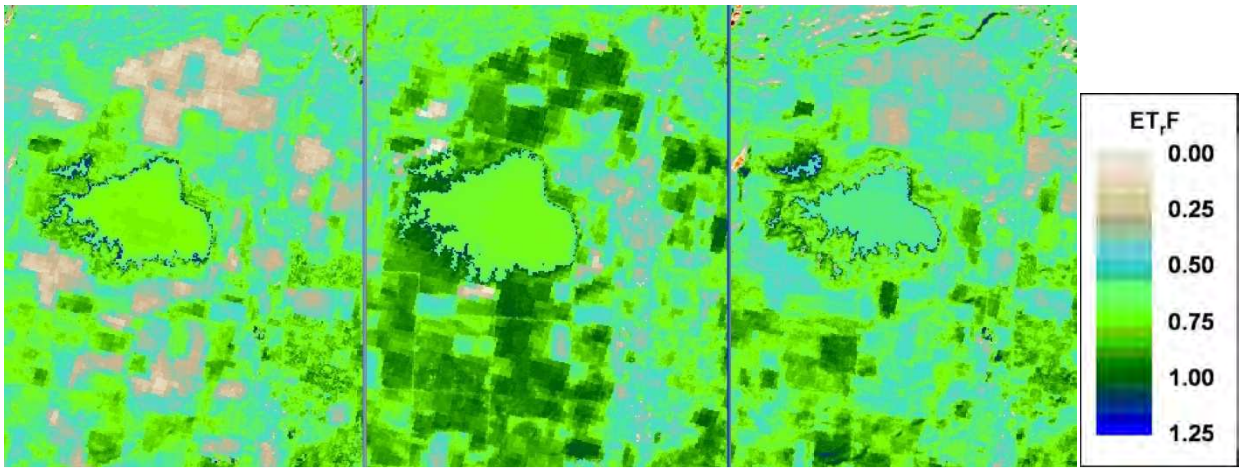

Figure 3. Daily ET expressed as ET_rF for 05/10-2006 (left), 06/27-2006 (center) and 10/01-2006 (right) for the area around the Pablo Reservoir.

The ET_rF maps in the following figures 4 and 5 show the ET_rF on the satellite overpass dates for the central part of the Mission Valley. The Flathead River is seen towards the center of the image dividing the irrigated agricultural areas in the eastern part of the valley and the drier portions of the western part of the valley. The values and ranges of ET varied with time of year, with peak values reached during early summer for many crops and low values during winter when most vegetation was dormant and evapotranspiration potentials were low. The values for ET are impacted by the weather data on the satellite overpass date, and therefore do not paint as clear a picture of ET evolution as do the images of ET_rF. The ET_rF images show a progressive increase in ET_rF through spring and early summer and subsequent decrease into the fall and winter.

Some ET_rF (and ET) images show some striping artifacts that were caused by striping in some of the individual bands of the Landsat 5 satellite. These stripes do not create measurable error in the final ET products. Some images had cloud cover in portions of images, usually away from the LRG valley. Prior to integration of ET over months and growing season, the clouded areas were manually identified, masked, and then filled in by interpolating ET_rF information from adjacent images in time.

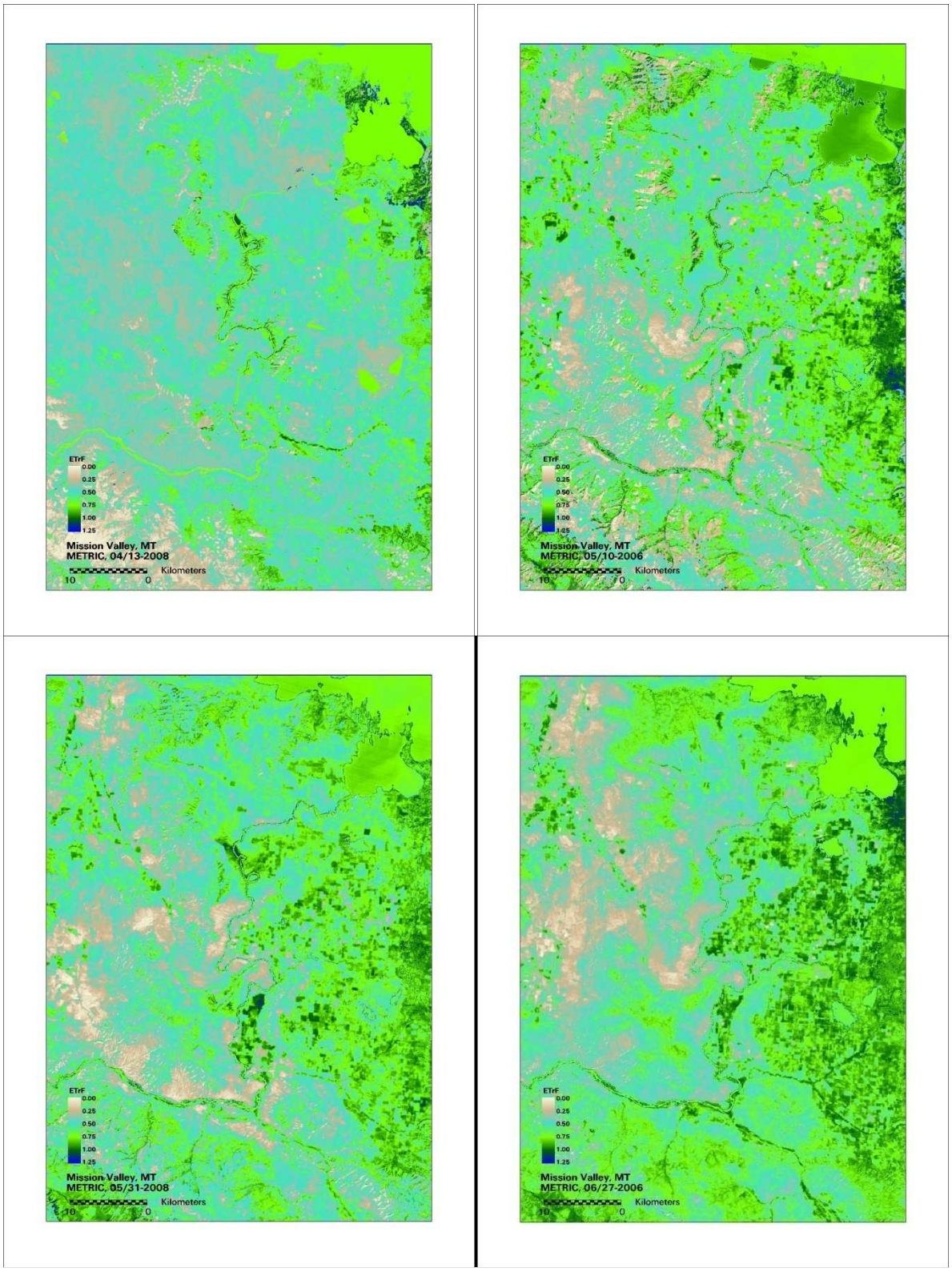

Figure 4. Maps of ET_rF at satellite overpass dates for 04/13-2008 (top left), 05/10-2008 (top right), 05/31-2008 (bottom left) and 06/27-2006 (bottom right).

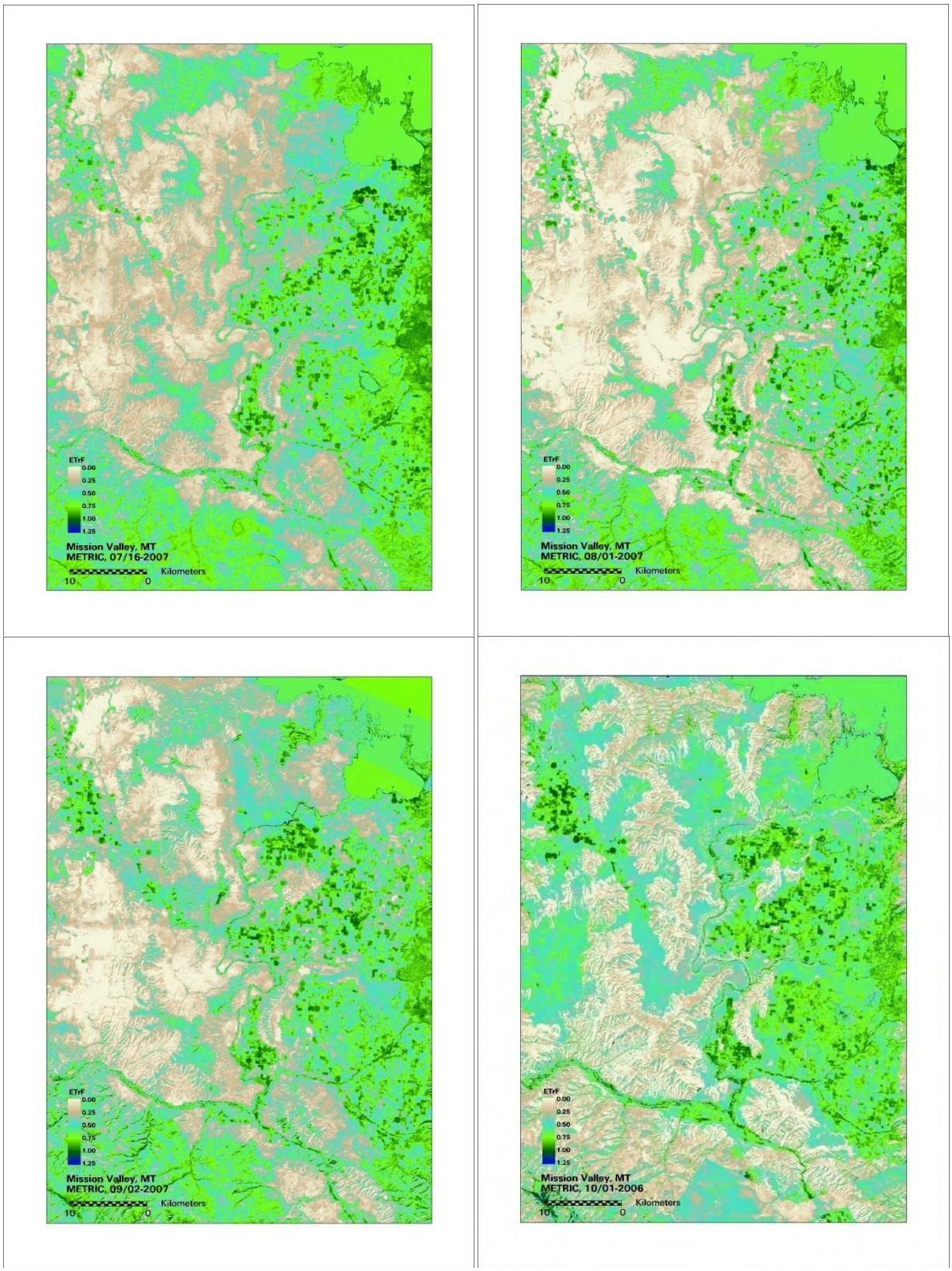

Figure 5. Maps of ET_rF at satellite overpass dates for 07/16-2007 (top left), 08/01-2007 (top right), 09/02-2007 (bottom left) and 10/01-2006 (bottom right).

Monthly and seasonal ET_rF and ET

Maps showing monthly and seasonal ET in mm were produced by interpolating the values of daily ET_rF on satellite overpass dates between dates using a cubic spline function. Values for ET_rF for each day between images were multiplied by ET_r for that day and then integrated over the specific month. The splining and integration process is described in Appendix F.

The satellite images processed using METRIC were from three different years and consequently the estimates of monthly and seasonal ET and ET_rF will show some dependence on which year's weather data are used to calculate ET_r. For this reason, monthly and seasonal ET was calculated for all three years using the same ET_rF image series, but using ET_r for each year from the St. Ignatius weather station, as summarized in Table 6

Table 6. Source years of meteorological information used to calculate ET_r.

Method Reference	Calculation of ET_r (based on data from the St. Ignatius agrimet weather station)
2006	2006 weather data
2007	2007 weather data
2008	2008 weather data
Mean	Average ET_r from 2006, 2007 and 2008

The seasonal ET and ET_rF for the Mission Valley were integrated over the period April 1 – October 31 for each year.

ET from desert areas in the western part of the Mission valley was similar to or slightly higher than reported rainfall amounts, which averaged 238 and 258 mm (9.4 and 10.2 inches) at the Round Butte and St. Ignatius weather stations during April 1 – October 31 for 2006 through 2008. The additional ET from these areas is likely from the difference in soil moisture between April 1 and October 31. On April 1 there was still residual moisture in the soil from winter precipitation, and the soil profile dried as the summer progressed.

Because of the high degree of cloudiness within the images for areas surrounding the Mission Valley, some of the monthly and the seasonal estimates of ET are based on values that had to be interpolated and scaled from the previous and/or following month. This increases the uncertainties in the estimates of ET and ET_rF for the affected areas, since the estimates are based on interpolated values and not on actual values for that month. For this reason, users are encouraged to review the data availability section of Appendix G and use caution before using the ET estimates for areas outside of the Mission Valley.

The surface energy balance of water bodies varies substantially depending on their properties, especially depth, temperature profiles and turbidity. The METRIC model can attempt to account for variations among open water bodies, provided the water bodies are classified and partitioning algorithms between water heat storage and net radiation are adjusted. The partitioning can change with time of year. Because such classification and description of

partitioning were not available and because the primary project goal was to estimate ET from agricultural crops, the evaporation from open water bodies (lakes, rivers, canals, reservoirs, farm ponds etc) was estimated using a single algorithm regardless of body size, depth and turbidity. The algorithms used to estimate open water ET represents assumed ”average” water body properties which may increase the uncertainty of ET from the water within the image. Results reported by Allen and Tasumi (2005) indicate that this algorithm may overestimate the ET from large water bodies such as the Flathead Lake by 10 % or more. For this reason, users are cautioned if extracting estimates of open water evaporation from the maps of ET or ET_rF.

The panels on the following pages show the monthly ET_rF products and seasonal ET product in mm and as ET_rF for the period April 1 – October 31 using ‘mean’ ET_r representing the three year period (Table 6). These images have resolution of 30 m, so that monthly and seasonal ET data can be extracted for each 30 m on a grid. The white rectangle in Figure 6 indicates the area that is included in the panels.

Figure 6. Area that is included in the following panels of monthly ET_rF and seasonal ET and ET_rF.

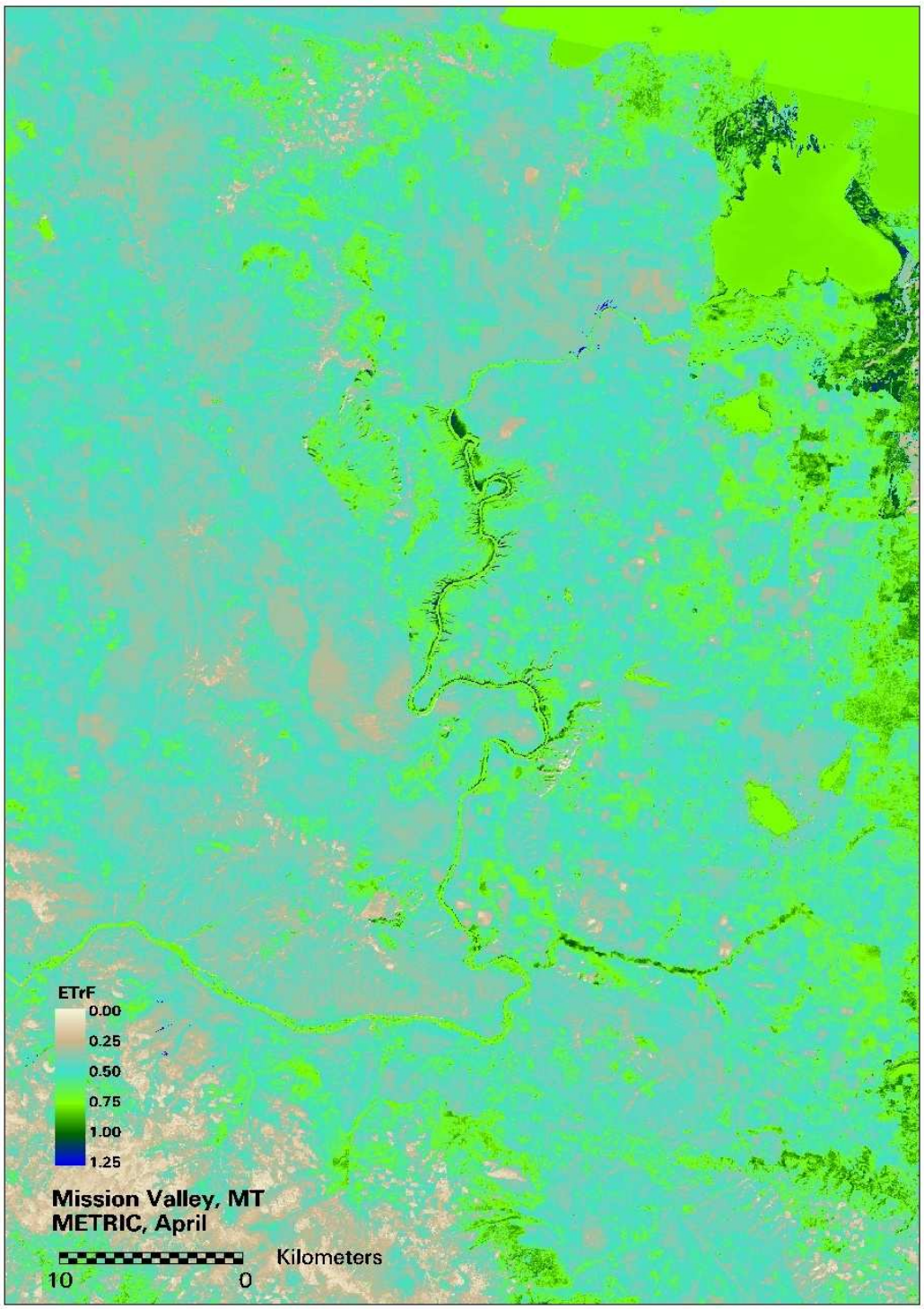

Panel 1. ET_rF estimated for April.

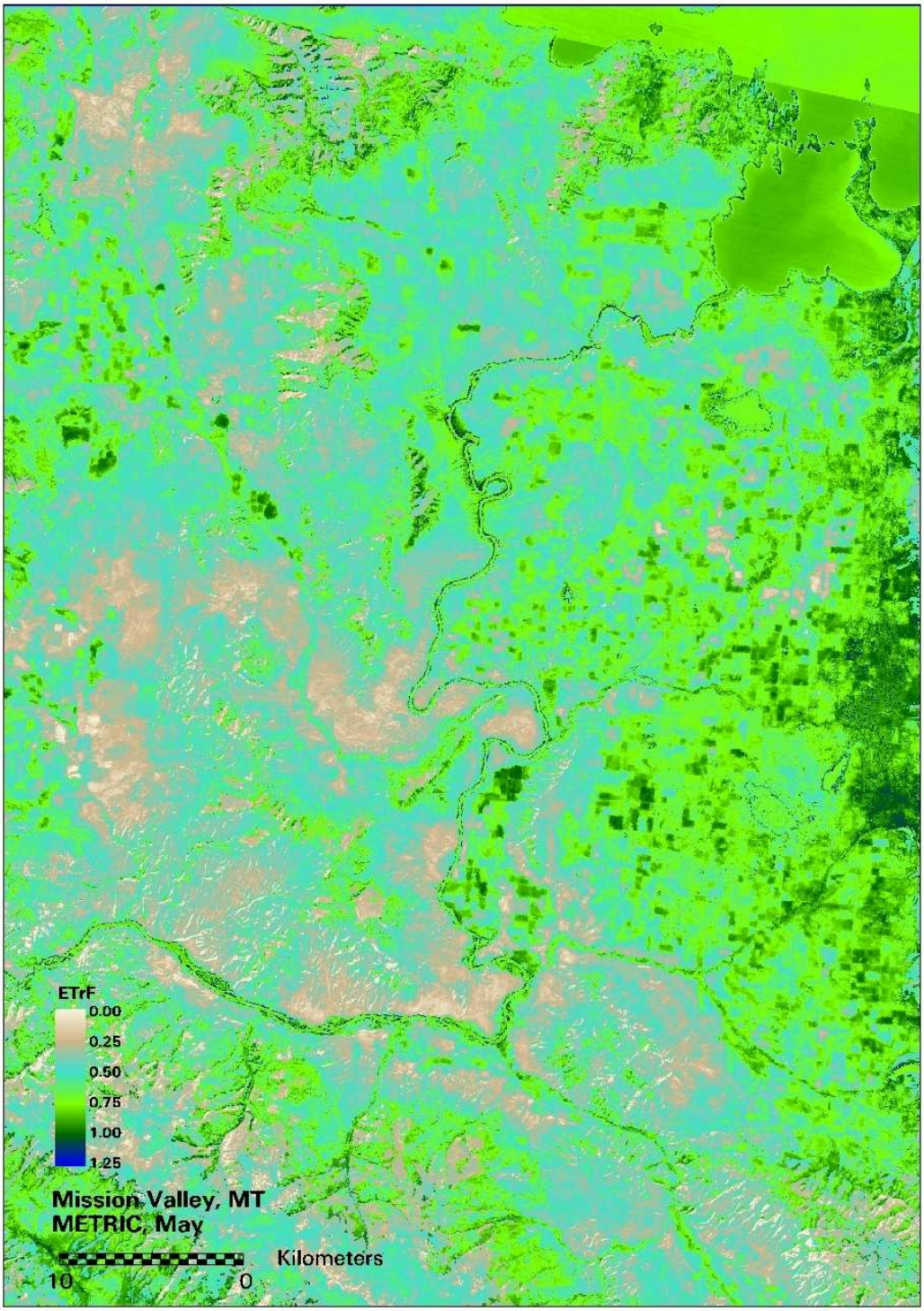

Panel 2. ET_rF estimated for May.

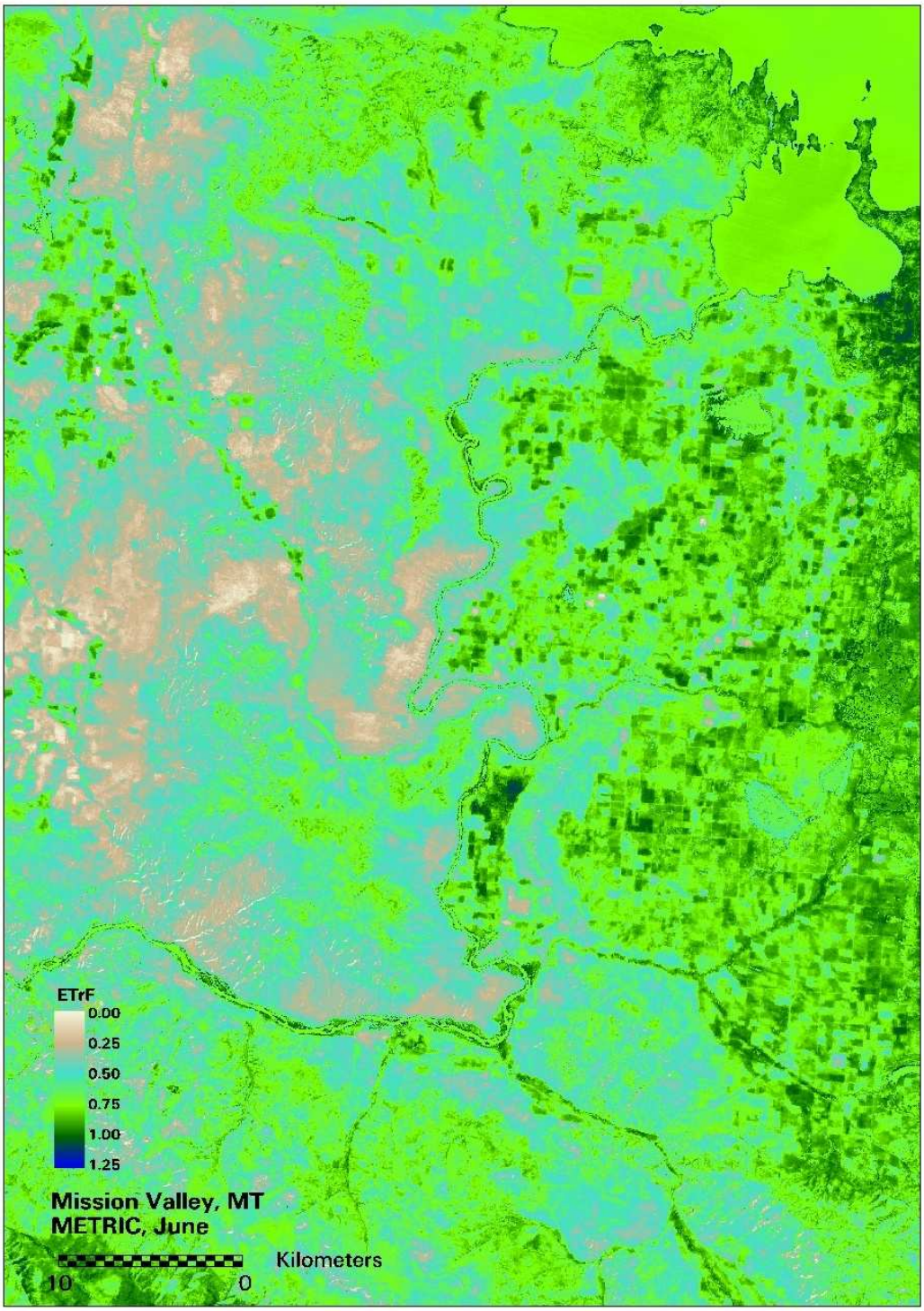

Panel 3. ET_rF estimated for June.

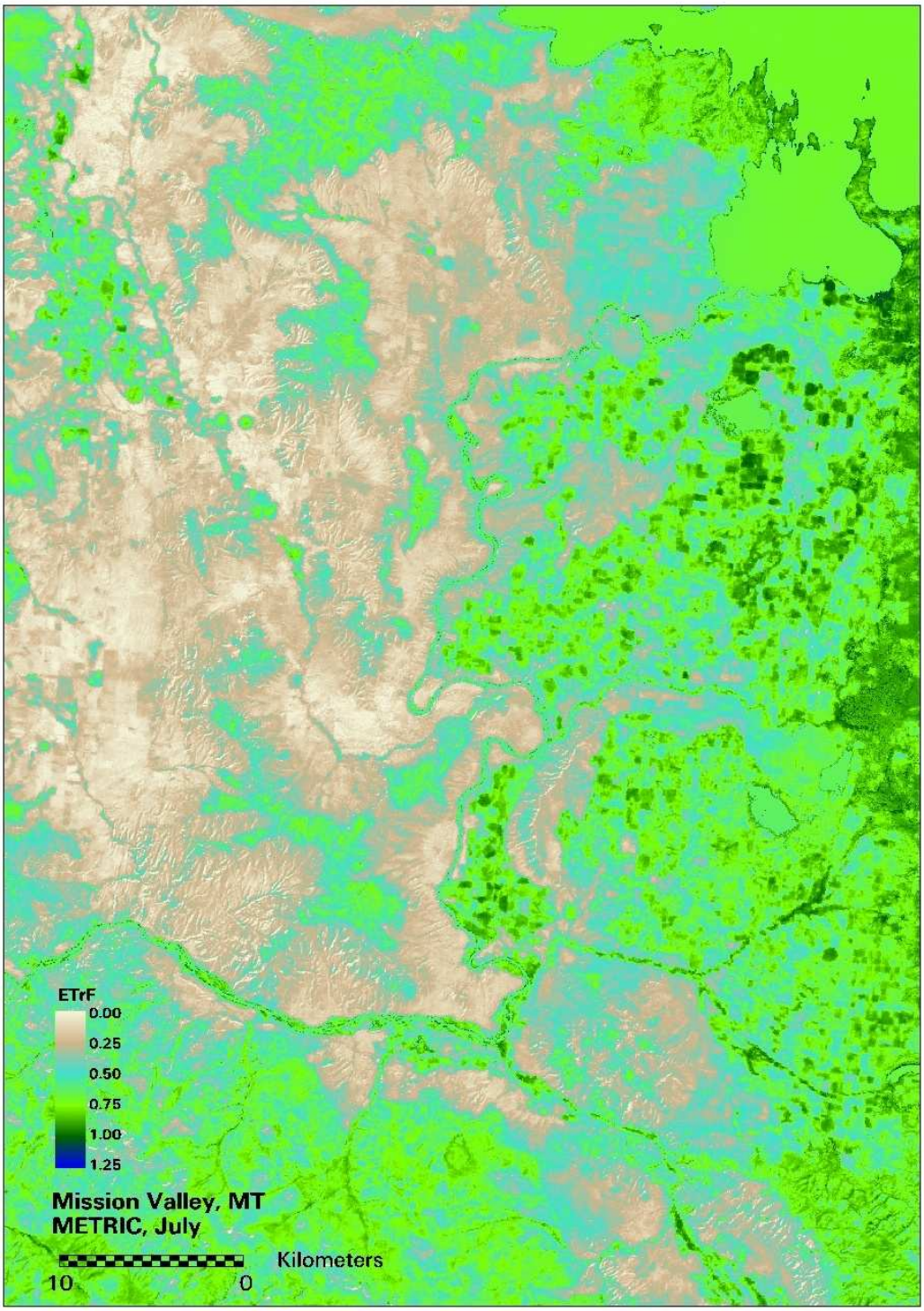

Panel 4. ET_rF estimated for July.

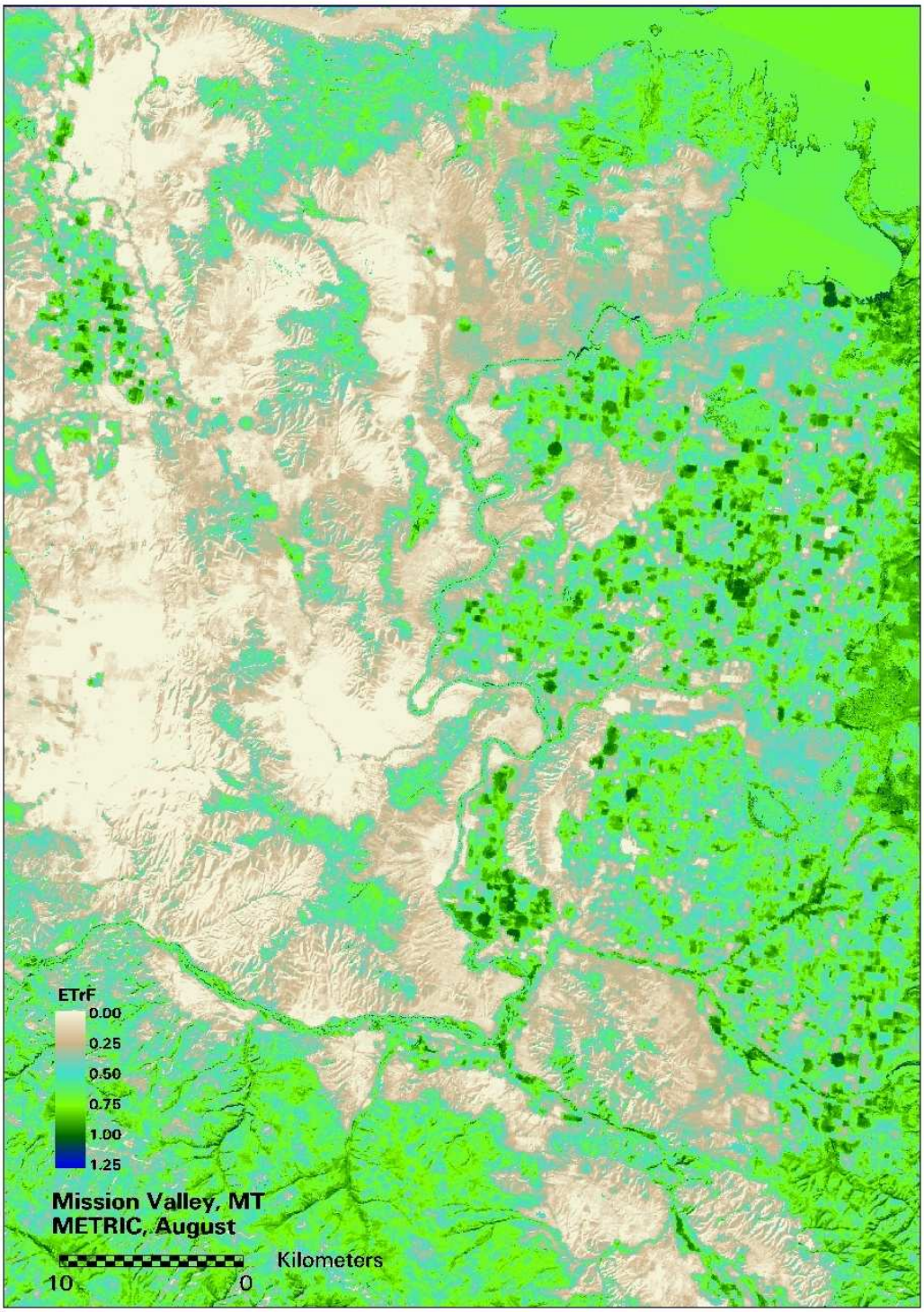

Panel 5. ET_rF estimated for August.

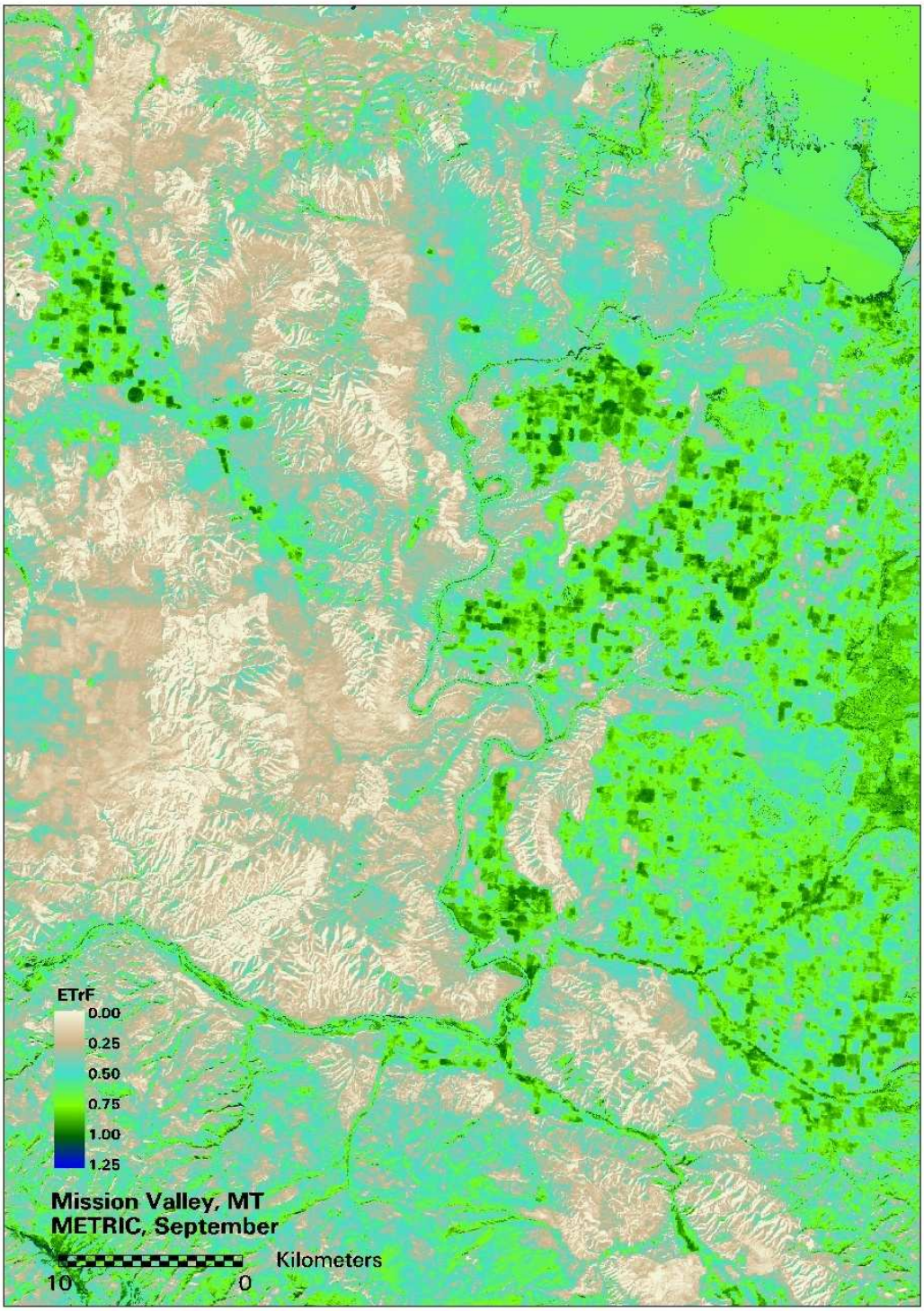

Panel 6. ET_rF estimated for September.

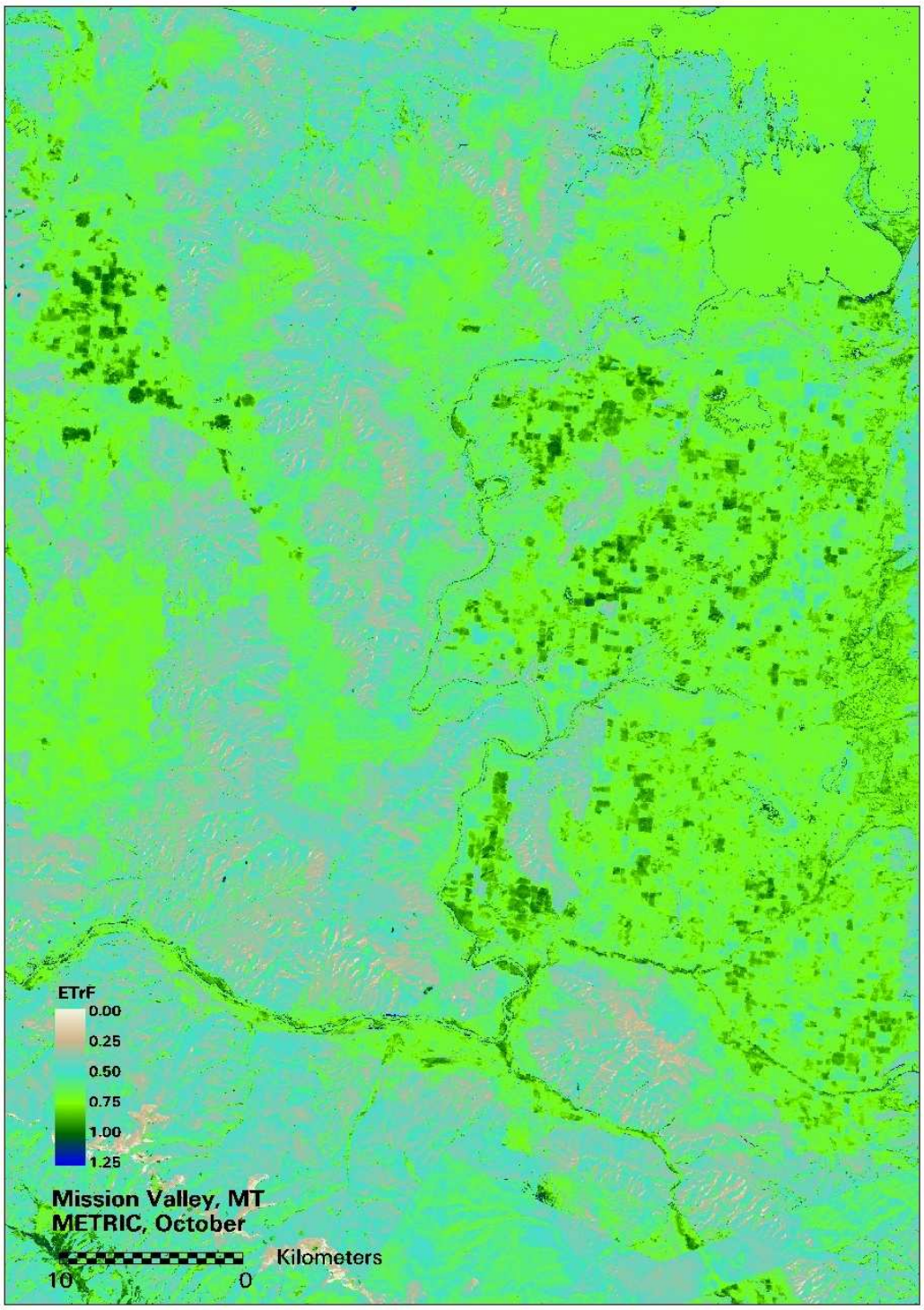

Panel 7. ET_rF estimated for October.

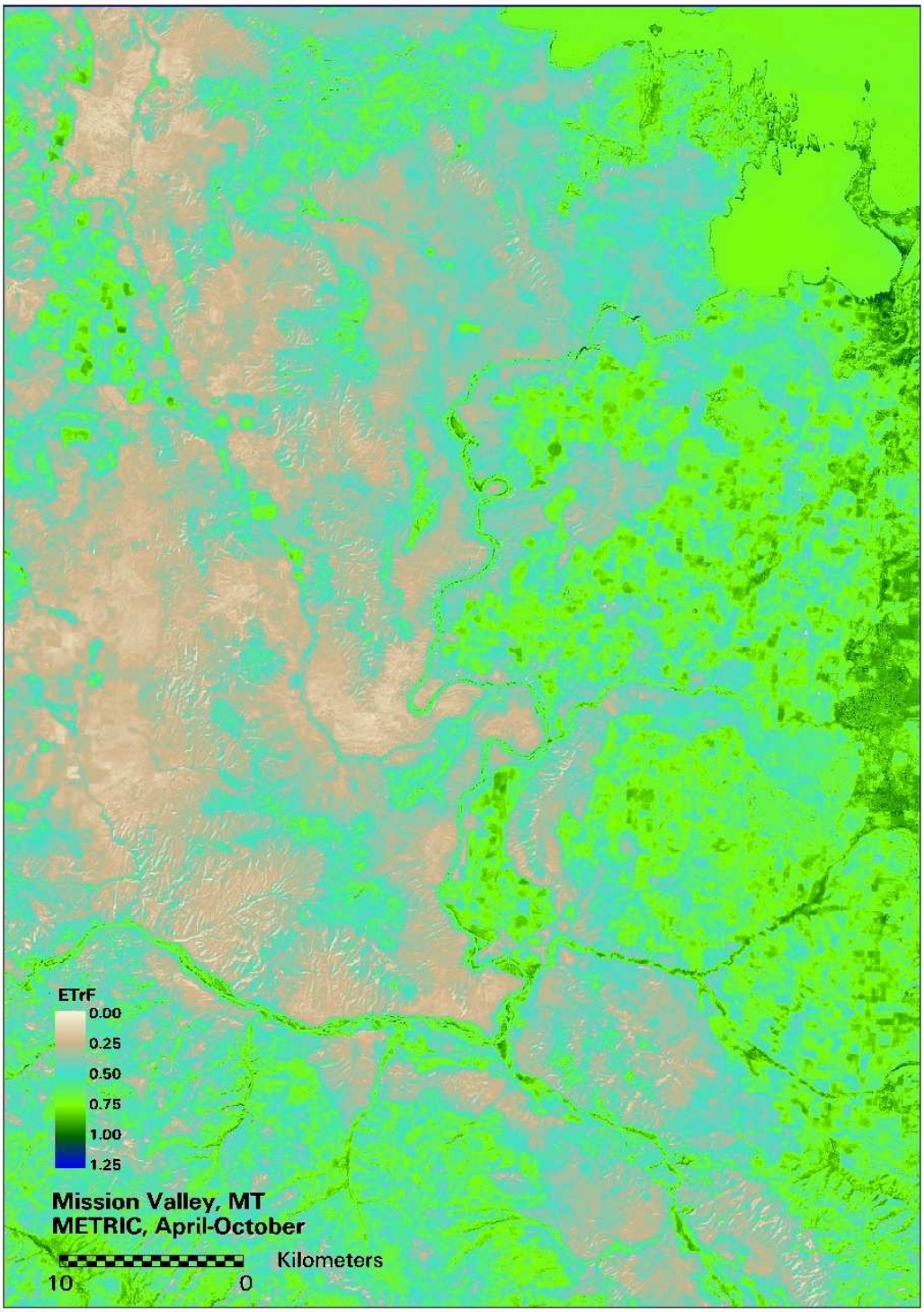

Panel 8. Average ET_rF over April 1 through October 31.

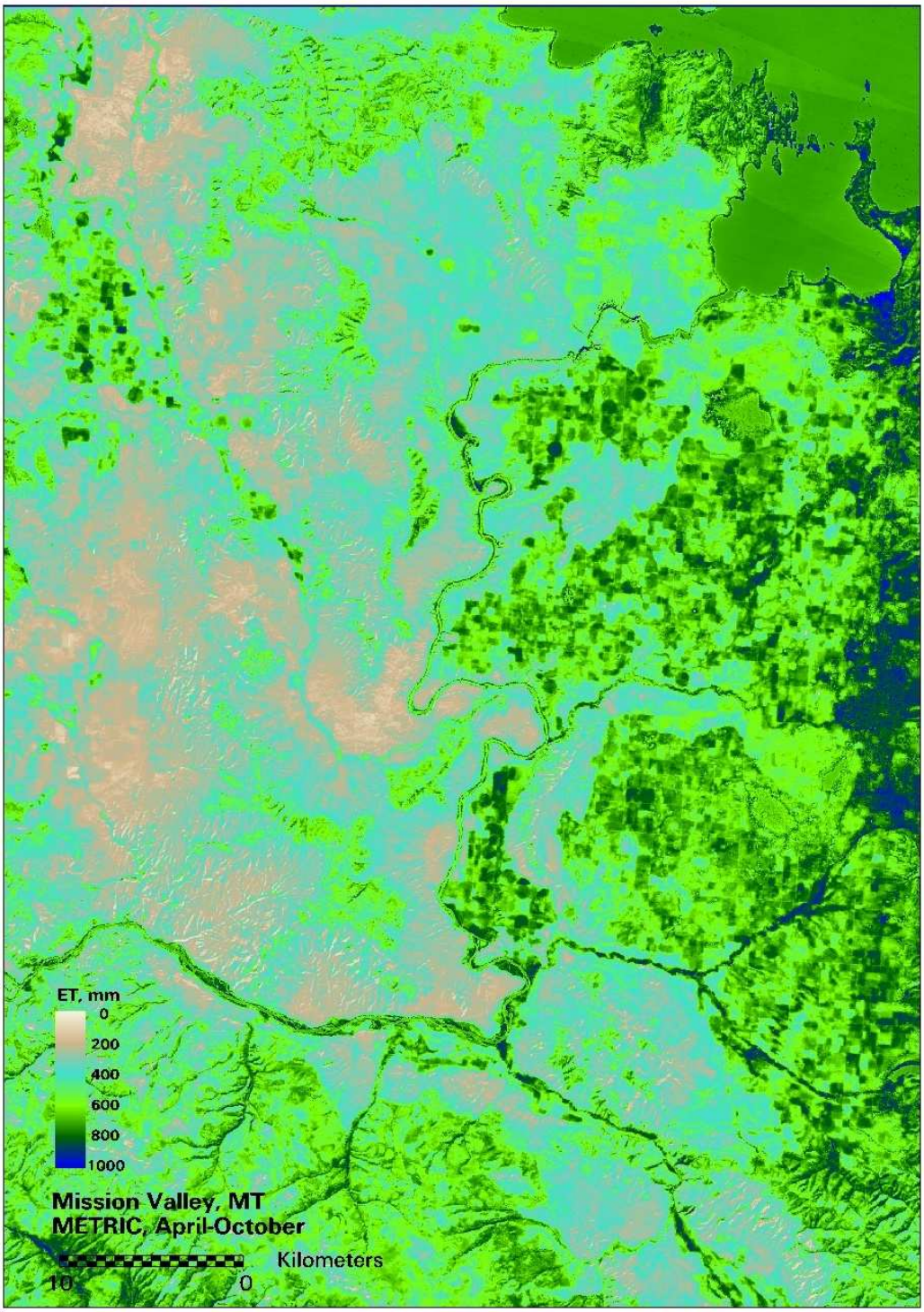

Panel 9. ET estimated for April 1 through October 31.

3. Summary

The METRIC (Mapping Evapotranspiration with high Resolution and Internalized Calibration) procedure for determining evapotranspiration (ET) from satellite imagery was applied to the Mission Valley MT area. ET is calculated within METRIC using a surface energy balance applied to Landsat images and augmented by local weather data. Processing was conducted for eight Landsat image dates. Due to high degree of cloudiness in the project area images from three years were selected to provide a uniform coverage of the growing season. ET is calculated with a spatial resolution of 30 m. The daily ET maps by METRIC were extrapolated into monthly and seasonal (April 1-October 31) ET estimates. The primary focus areas for the METRIC processing were irrigated areas in the Mission Valley within the Flathead Reservation. Land areas adjacent to the Mission Valley including surrounding forest and wilderness areas, agricultural and wetland areas north and west of the Flathead Lake and along water ways were additionally processed.

Because of the high degree of cloudiness present within the images, large portions of some of the images had to be masked out. The affected areas were primarily the mountain areas surrounding Mission Valley. The resulting gaps were filled with data from previous and following image dates which increases the uncertainties in the ET and ET_rF estimates for the mountain areas.

Special METRIC processing was conducted during the Mission Valley application, including estimation of aerodynamic roughness lengths for tall vegetation following a procedure that adjusts both roughness length and zero-plane displacement according to the density of the vegetation; improvement of estimated hemispherical albedo (reflectance) from trees and other tall vegetation to compensate for the nadir (vertical) viewing angle of Landsat; and improvement in the estimated temperature of leaf canopies of trees, where most evaporation and energy exchange occurs, to compensate for impacts of shaded and sunlit soil viewed by the nadir (vertical) viewing Landsat satellite.

Monthly and growing season (April-October) ET and ET_rF (fraction of alfalfa reference ET) was calculated by splining the ET fraction determined for each satellite image over each month and multiplying by reference each day. All ET data products are available for each image date, month, and growing season as ERDAS Imagine (.img) files.

4. References

Allen, R.G., 2008. REF-ET: Reference Evapotranspiration Calculation Software for FAO and ASCE Standardized Equations. University of Idaho, 82 pp. [http://www.kimberly.uidaho.edu/ref-et/index.html]. Contact author for updates.

Allen, R.G., Pereira, L.S., Raes, D., Smith, M., 1998. Crop Evapotranspiration. Guidelines for computing crop water requirements. FAO Irrigation and Drainage Paper 56. FAO, Rome, 300 pp.

Allen, R.G., Pereira, L.S., Raes, D., Smith, M., Wright, J.L., 2005. FAO-56 Dual Crop Coefficient Method for Estimating Evaporation from Soil and Application Extensions. J. Irrig. Drain. Engr., 131(1), 2-13.

Allen, R.G., Tasumi, M., 2005. Evaporation from American Falls Reservoir in Idaho via a Combination of Bowen Ratio and Eddy Covariance. Proceeding of the EWRI World Water and Environmental Resources Congress 2005: Impacts of Global Change. May 15-19 2005, Anchorage, Alaska. 17 pp.

Allen, R.G., Tasumi, M., Morse, A., Trezza, R., Wright, J.L., Bastiaanssen, W., Kramber, W., Lorite, I., Robison, C.W., 2007a. Satellite-Based Energy Balance for Mapping Evapotranspiration with Internalized Calibration (METRIC) – Applications. J. Irrig. Drain Engr., 133(4), 395-406.

Allen, R.G., Tasumi, M., Trezza, R., 2007b. Satellite-Based Energy Balance for Mapping Evapotranspiration with Internalized Calibration (METRIC) – Model. J. Irrig. Drain Engr., 133(4), 380-394.

Allen, R.G., Tasumi, M., Trezza, R., Kjaersgaard, J.H., 2008. Metric. Mapping Evapotranspiration at High Resolution. Applications Manual, V 2.0.4. University of Idaho. 166 pp.

ASCE-EWRI, 2005. The ASCE Standardized Reference Evapotranspiration Equation. ASCE, Reston, Virginia.

Burnett, B., 2007. A Procedure for Estimating Total Evapotranspiration using Satellite-Based Vegetation Indices with Separate Estimates from Bare Soil. M.Sc. Thesis, University of Idaho. 175 pp.

Tasumi, M., Allen, R.G., Trezza, R., Wright, J.L., 2005. Satellite-Based Energy Balance to assess Within-Population Variance of Crop Coefficient Curves. J. Irrig. Drain. Engr., 131(1), 94-109.

Trezza, R., Allen, R.G., 2008. Analysis of vertical shift in Band 6 of Landsat 5 images in the EROS L1T product. University of Idaho, Kimberly, Idaho. 25 pp. Accessed online on June 17 2009 at http://www.idwr.idaho.gov/GeographicInfo/PDFs/trezza-allen-thermal-band-shift.pdf

Wright, J.L., 1982. New evapotranspiration crop coefficients. J. Irrig. Drain. Engr., 108(1), 57-74.

Appendices

Appendix A
QA/QC of weather data from St. Ignatius, Round Butte and Creston Agrimet weather stations for 2006 – August 2008.
By J. Kjaersgaard and R.G. Allen, September 2008

This report describes the location, methods for downloading and how to summarize the weather data from the St. Ignatius, Round Butte and Creston electronic weather stations, including a quality control of the meteorological information. The three weather stations are part of the Pacific Northwest Cooperative Agricultural Weather Network (generally abbreviated Agrimet), operated by the Bureau of Reclamation. The quality control protocol follow the general procedures and methods for quality control of meteorological data described by Allen, 1996 and ASCE-EWRI, 2005 (Appendix D).

These three weather stations are of interest because they measure and report weather information relevant to the estimation of alfalfa reference evapotranspiration (ET_r) calculated using the ASCE standardized Penman-Monteith equation (ASCE-EWRI, 2005), which in turn is a required input for satellite image processing using METRIC. The meteorological parameters needed are hourly values of solar radiation (R_s), air temperature (T_a), air humidity (expressed as relative humidity, RH; dew point temperature, T_d; or vapor pressure, e_a) and wind speed (WS). Additionally, daily values of precipitation are normally required to establish a water balance for the upper soil layers.

Location of the weather stations
The St. Ignatius and Round Butte stations are located within the Flathead Indian Reservation in the Mission Valley, MT while the Creston station is located north of the reservation. The station locations are shown in Fig. 1 and station elevation, latitude and longitude are listed in Table 1.

Figure 1. Location of the Agrimet weather stations in the Flathead Lake, MT area.

Table 1. Location, elevation, latitude and longitude of the Agrimet weather stations in the Flathead Lake, Montana area.

Station name	Station ID	Location	Elevation (m)	Latitude (°N)	Longitude (°W)
St. Ignatius	SIGM	St. Ignatius Airport	911	47.301	114.098
Round Butte	RDBM	8 miles W of Ronan	927	47.539	114.281
Creston	CRSM	MT State U. Agric. Farm, Creston	899	48.188	114.128

St. Ignatius

The St. Ignatius weather station is located at the airport in St. Ignatius. Photos from the weather station are shown in Fig. 2. The station was installed on 3/28 1991 at a site east of the airport buildings. Due to construction the station was relocated to a site south of the buildings within the airport in July 2008.

The local area around the St. Ignatius airport is irrigated pasture but has non-irrigated rangeland farther north, irrigated farmland to the east and south and the town of St. Ignatius and non-irrigated farmland to the west. With winds from north and west the air temperature and air humidity may not have been as impacted by ET from irrigated fields compared to wind directions from east and south. In addition the air temperature may be affected by the station

Figure 2. St. Ignatius Agrimet weather station looking north (top left), east (top right), south (bottom left) and west (bottom right). Photos from the Agrimet website.

being located in the airport; an expanse consisting of non-irrigated vegetation and consolidated areas (runway, hangars, parking lots etc). The wind speed may be impacted by the vegetation (tall grass and hip bushes) in the immediate vicinity of the station.

Round Butte

The Round Butte weather station is located approximately 8 miles west of Ronan and ½ mile north of Round Butte Road W/MT-211 near a farmstead. The station was installed 5/23 1989. Photos from the Round Butte station are shown in Fig. 3.

The station is surrounded by irrigated fields except a reservoir/wetland area and rangeland to the north-east. The reservoir is up to about one-half mile in size when full and dries up some years. The solar radiation readings are impacted from shading by tall trees east of the station when the sun angle is low during early morning hours. Wind speed from easterly directions is impacted by tall trees and buildings and may be impacted seasonally by tall grass in the immediate vicinity of the station.

Figure 3. Round Butte Agrimet weather station looking north (top left), east (top right), south (bottom left) and west (bottom right). Photos by J. Kjaersgaard, June 28 2008.

Creston

The Creston weather station is located approximately ½ mile west of Creston and ¼ mile south of MT hwy 35 between two fields belonging to the Montana State University Northwestern

Agricultural Research Center. The station was installed 5/7 1988. Photos from the Creston station are shown in Fig. 4.

The Creston station is surrounded by irrigated agricultural fields. Some of the fields are smaller research type fields with different crops. The terrain is flat and slops gently to the south with a relative abrupt increase in slope approximately 100 feet south of the station.

Figure 4. Creston Agrimet weather station looking north (top left), east (top right), south (bottom left) and west (bottom right). Photos by J. Kjaersgaard, June 29 2008.

Agrimet weather data format and retrieval

Meteorological information from the Agrimet Weather stations is downloadable from the Pacific Northwest Agrimet web site at http://www.usbr.gov/pn/agrimet/. Data may be downloaded 15-min values (i.e. four output readings per hour and 96 readings per day), hourly values (i.e. 24 output readings per day) or daily values. The 15-min values are the highest available temporal resolution from the website available for the three stations. Wind run, R_s and P are only reported once per hour (on top of the hour) in the 15-min datasets. For the remaining time increments in the 15-min datasets values are reported as “Missing”.

The format and configuration of the 15-min meteorological data from the Agrimet network are somewhat unusual compared to the reporting format of other meteorological networks. A summary of the standard measurement program and notations is shown in Table 2.

Table 2. Agrimet header codes and units, measurement increment and the notation and units commonly used for the meteorological parameters.

Agrimet notation	Agrimet unit	Measurement increment	Meteorological parameter	Common notation	Common unit
OB	°F	Instantaneous	Air Temperature	T_a	°C
TU	%	Instantaneous	Relative Humidity	RH	%
TP	°F	Instantaneous	Dew Point Temperature	T_d	°C
WD	° azimuth	15 min vector mean	Wind Direction	WD	° azimuth
WG	Miles/h	Peak during last 15 min	Wind gust	WG	m/s
WS	Miles/h	15 min average	Wind speed	WS	m/s
UI	Miles	Cumulative	Wind run	-	m
SQ	Ly/h (cal/cm^2/h)	Cumulative	Solar Radiation	R_s	W/m^2
PC	Inch	Cumulative	Precipitation	P	mm

The Agrimet website provides the following description for the 15-min values (excerpt): “Many values, such as air temperature and relative humidity, are *instantaneous* values at the time of observation. Other observations, such as solar radiation, wind run, and precipitation, are *cumulative* values. Wind speed and wind direction are *average* values for the reporting period (typically 15 minutes).” … “AgriMet weather data is reported in local time (Mountain and Pacific time zones). The reported time also reflects daylight savings time (DST) when in effect.”

The Agrimet weather data are also available for download as hourly values from the Agrimet website. However, air temperature and dew point temperature reported in the hourly values are not averages of the four instantaneous measurements for a whole hour, but only the instantaneous top-of-hour reading. Similarly, wind speed reported in the hourly values are not average wind speeds for the whole hour, but only the average of the last 15 minutes before top-of-hour. Hence, to retain the highest degree of information about air temperature, air humidity and wind speed for the full hour, it is recommended that data are downloaded as 15-min values and converted to hourly values by the user.

15-min data from the St Ignatius, Round Butte and Creston weather stations from the period January 1 2006 – August 10 2008 have been downloaded to be used as supporting information for the METRIC processing. The downloaded data file has over 91,000 lines of data per weather station. Gap filling and quality control of these data are described in the following.

Initial data screening and gap filling

The 15-min dataset was screened to assess the occurrence of missing values to avoid gaps in the time sequence. The raw data sets contain invalid data throughout. Invalid data in the Agrimet file consist of either 1) Data have been replaced by the word “Bad”, possibly assigned during a (rough) manual or automated post measurement quality control, 2) The word “Missing”, indicating no data are available, and 3) Some time steps are missing entirely, which may be caused by equipment failure, maintenance or servicing of the equipment, transmission error and similar.

Re 1), the designation "Bad" generally occurs for isolated 15-min timestamps (and commonly for all meteorological parameters at the same time step). For air temperature, air humidity and wind speed these time steps (< 100 per dataset) were ignored when calculating hourly values. For solar radiation, time steps designated as "Bad" (< 25 per dataset) were replaced with a value calculated as

$$R_{s\_t} = R_{s0\_t} \times \frac{R_{s\_t-1}}{R_{s0\_t-1}} \qquad (1)$$

where R_{s0} is calculated clear sky solar radiation, and subscripts *t* and *t-1* is the current and the previous hour, respectively. At night, the fraction after the multiplication sign in Eq. 1 is zero. For precipitation, which is reported as a cumulative value on an hourly basis, "Bad" designated time steps (< 25 per dataset) were replaced with a value equal to the previous (cumulative) reading.

Re 2), the designation "Missing" was only found for the three out of four 15-min timestamps for wind run, solar radiation and precipitation.

Re 3), missing time steps (e.g. one or multiple consecutive complete data lines missing) occurred in all datasets (< 25). Typically, 4 consecutive 15-min values were missing. The missing time steps were filled in in the 15-min dataset. For air temperature, air humidity and wind speed gaps were filled using a weighted average of the previous and next measurement, as exemplified in Table 3. Solar radiation data were filled using Eq. 1. Precipitation was filled in using the same cumulative value as the previous hour.
Several consecutive days were missing entirely at the end of November and beginning of December 2006 at Creston. Since this period is of very little importance for the METRIC processing it was not gap filled.

Table 3. Schematic example of gap filling of air temperature, air humidity and wind speed for four consecutive missing 15-min time steps. Bold font represent valid data, normal font is for missing time steps.

Time step	Equation	Example
Last previous time step with good data	**P**	**20**
Time step with missing data 1	(4P+1N)/5	18
Time step with missing data 2	(3P+2N)/5	16
Time step with missing data 3	(2P+3N)/5	14
Time step with missing data 4	(1P+4N)/5	12
First following time step with good data	**N**	**10**

Unlike the other information used during the METRIC processing, which does not reflect day light savings, the three Agrimet weather datasets reflect day light savings. To avoid misinterpretations the 15-min datasets were converted to be entirely 'Standard time' by removing one hour of data (while maintaining the timestamps) between 2.00 and 3.00 am on April 2, 2006; March 11, 2007 and March 9, 2008. Similarly, one hour of data was added (while maintaining the timestamps) at 2.00 am on October 29, 2006 and November 4, 2007. Values for

the meteorological parameters for the added time step were calculated as described in bullet 3 above.

Aggregation of data from 15-min to hourly values

Due to the non-conventional format of the Agrimet weather data the conversion from 15-min to hourly values requires tailored solutions for each meteorological parameter. The time label in the resulting hourly dataset is reported for the endpoint of the hourly measurement period, with time steps 00.00 (representing the hour 23.00 to 24.00 (from the previous day)) through 23.00.

Air Temperature, T_a

T_a is measured as instantaneous values each 15 minutes, i.e. the reporting time steps may be viewed as a "midpoint" reading; e.g. the 10.00 time stamp is representative for the period 09.52:30 – 10.07:30. To account for this relative "shift" of 7.5 minutes, average hourly T_a is calculated using half weight of the two top-of-hour 15-min time step and full weight of the intermediate time steps. An example of this calculation of average air temperature for the 11.00 time label is shown in Eq. 2.

$$(0.5*[10.00T_a] + [10.15T_a] + [10.30T_a] + [10.45T_a] + 0.5*[11.00T_a]) / 4 \qquad (2)$$

where the values in square brackets are the measured air temperature at the indicated time stamps.

Air temperatures are converted from °F to °C. Daily values of T_a are calculated as a mean of the hourly values. Additionally, daily minimum and maximum T_a from the 15-min readings are output along with the daily average T_a.

Air Humidity

Air humidity is reported as both relative humidity (RH) and dew point temperature (T_d) in the Agrimet datasets. T_d was used to estimate hourly and daily air humidity. Due to the non-linearity of the relation between saturation vapor pressure and T_a, it is undesirable to use RH when averaging humidity to hourly and (particularly) daily values. Dew point temperatures are converted from °F to °C.

T_d is averaged to hourly and daily values following the same procedure as for T_a. Daily minimum and maximum RH was extracted from the hourly values of T_d.

Solar Radiation, R_s

As seen from Table 1, measurements of R_s are accumulated at hourly increments, and the amount of R_s received is the difference between the present and the previous hour. Hourly R_s, expressed as Langleys per hour (ly/hr), is accumulated until a predefined rollover value is reached, after which the accumulated value reverts to zero to continue the count. The accumulation principle is visualized in Figure 5 for the period June 7 – June 20 2007 for R_s measured at St. Ignatius. The threshold is not constant between stations and is normally adjusted every year for each station. At the time for the annual station maintenance in 2007

the weather conditions prevented calibration of new rollover values hence the values obtained in 2006 carried over. Rollover values for the three stations are shown in Table 4.

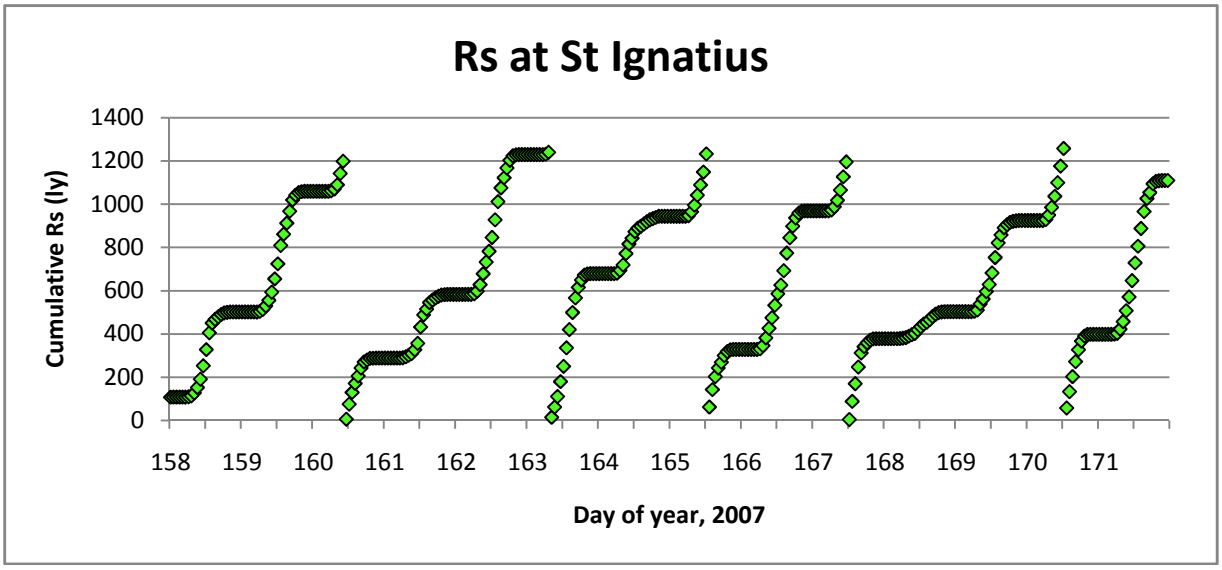

Figure 5. Reporting system of solar radiation, R_s, from Agrimet. Each green diamond is the value reported at hourly increments.

Table 4. Rollover values for solar radiation (Ly/hr) at the St. Ignatius, Round Butte and Creston Agrimet weather stations.

Station	Begin date	End date	R_s rollover number
St. Ignatius	6/14 2005	6/13 2006	1509.33
	6/13 2006	7/23 2008*	1262.67
Round Butte	6/14 2005	6/13 2006	1349.16
	6/13 2006	7/23 2008*	1070.93
Creston	6/14 2005	6/13 2006	1477.28
	6/13 2006	7/23 2008*	1145.14

*The annual station maintenance for 2008 was carried out around 7/23 2008 for the three stations. According to Mr. Peter Palmer, Agrimet Program Coordinator, "There will probably be no updates this year (2008, red) due to cloudy conditions."

Hourly R_s is obtained by subtracting the reported value from the previous hour from the value reported at a given hour. At the hour where the measurements reaches the rollover value R_s is calculated as

$$R_{s\_r} = V_r - R_{s\_r-1} + R_{s\_r\_app} \qquad (3)$$

where R_{s_r} is the amount of solar radiation measured for the hour where the rollover value is exceeded, V_r is the rollover value (Table 4), $R_{s\_r\text{-}1}$ is the cumulative R_s reading for the previous hour and $R_{s\_r\_app}$ is the cumulative reading for the hour where the rollover value is exceeded and the reported value has started the count from zero. Units are in Ly/hr.

R_s is converted from Ly/hr to W/m^2 before averaging to daily values, using 0.08598 ly/hr = 1 W/m^2.

Wind speed, WS

WS is reported as the average for each 15-minute increment in mph with two decimals in the raw datasets. Hourly WS is calculated as the average of the four 15-min values. The maximum wind gust in mph with two decimals is an output in the 15-min dataset, and is retained in the hourly and daily datasets for use in the quality control of the weather data. Units for wind speed are converted from mph to m/sec using 1 mph = 0.447 m/sec.

Daily average WS is calculated as the average of hourly WS values. Wind direction at the top of the hour is retained in the hourly datasets.

Precipitation, P

P is reported in a cumulative manner much comparable to the reporting format of R_s. As seen from Table 1, P is accumulated at hourly increments, and the amount of P received is the difference between the present and the previous hour.

The precipitation gauges at the three stations are of the “storage” type, where precipitation is accumulated in a bucket placed on a weighing scale. The capacity of the bucket corresponds to 12 inches of liquid precipitation. The buckets are charged with an antifreeze solution to melt solid precipitation and mineral oil to prevent evaporation from the bucket. When the bucket approaches its capacity the accumulated water is discarded manually and the bucket recharged before being placed back on the scale. Hence, water is discarded at irregular intervals by Agrimet personnel, and the bucket is not ‘empty’ when a new counts starts (due to antifreeze and mineral oil that is added to the empty bucket).

Due to the sensitivity of the weighing device the accumulated precipitation value may fluctuate (typically 0.01 inch), but is fairly consistent when hourly values are summed to daily values. One notable exception is an error that occurred over a period in July 2008 at the Creston station, as shown in Figure 6. On July 1 a major precipitation event caused the bucket to overflow, whereby the oil floating on top of the water was washed out of the bucket. Without this oil layer preventing evaporation some water evaporated out of the bucket the following three weeks thereby decreasing the weight of the bucket.

The bucket is generally emptied 3 – 4 times per year. The roll-over values where the bucket was emptied have been identified manually and are listed in Table 5. Units for precipitation are converted using 1 inch = 25.4 mm.

The hourly precipitation values are summed to obtain daily values.

Table 5. Roll-over values (inch) from when the rain gauge bucket has been emptied and corresponding depth of water (inches) of the recharged bucket at the St. Ignatius, Round Butte and Creston Agrimet weather stations.

St. Ignatius			Round Butte			Creston		
Date	Threshold	Revert to	**Date**	Threshold	Revert to	**Date**	Threshold	Revert to
01/13-06	8.24	1.76	**01/25-06**	8.01	2.78	**01/12-06**	11.46	2.20
06/13-06	10.75	2.73	**03/21-06**	3.38	1.68	**06/13-06**	10.81	2.61
01/23-06	7.71	2.06	**06/14-06**	8.04	1.68	**10/23-06**	9.78	2.55
06/05-07	10.39	2.20	**09/07-06**	3.54	2.78	**06/05-07**	11.22	2.19
11/19-07	7.59	2.23	**04/19-07**	10.61	1.59	**11/19-07**	6.29	2.27
06/12-08	11.32	2.75*	**09/04-07**	5.28	2.78	**07/22-08**	10.61	4.67
			03/25-08	7.2	1.68			

*The bucket was charged on 06/19-08

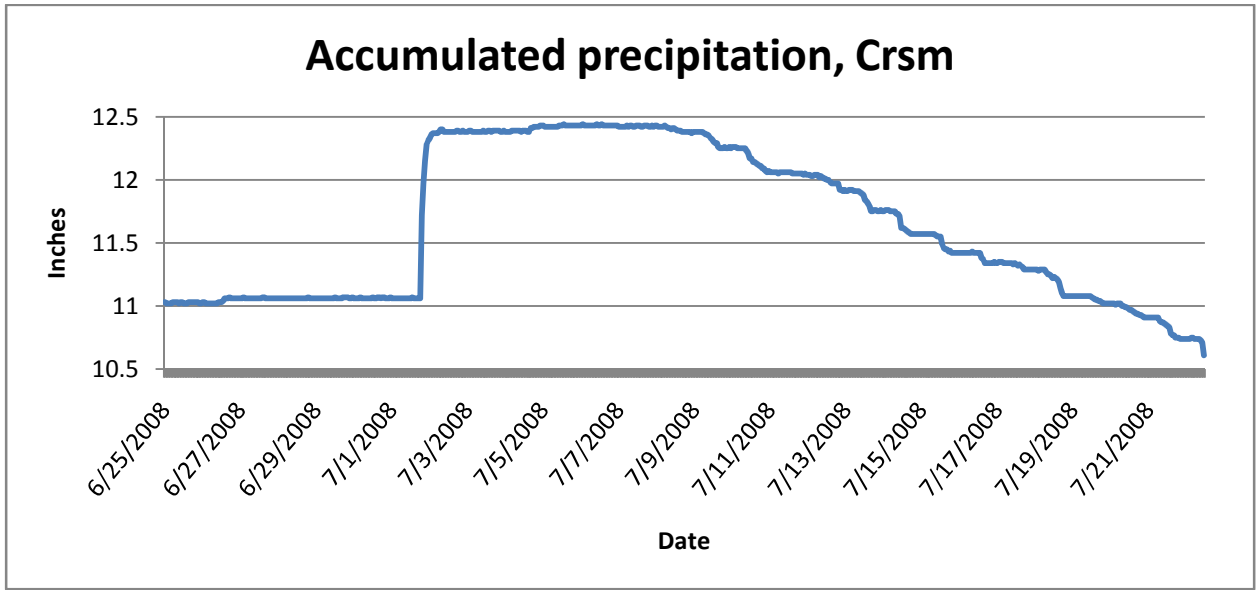

Figure 6. Accumulated precipitation at the Creston weather station during the period 6/25-08 – 7/22-08.

Calculation of ET_r

For the purpose of calculating ET_r using the Standardized Penman-Monteith equation, hourly values of T_a, T_d, R_s and WS along with information of year, month, date and time-of-day for each time step were exported to a comma separated text file.

ET_r is calculated using the RefET V3.1 software, developed by Dr. Rick Allen, University of Idaho. RefET computes ET_r following the recommendations of ASCE-EWRI (2005). RefET is very flexible regarding the units of the individual weather parameters in the input file, and units for the output file is selected by the user; metric units are preferred to be congruent with the units used in METRIC (no pun intended), as shown in Table 1.
The software and additional information, including a user manual, is available from http://www.kimberly.uidaho.edu/ref-et/index.html.

Daily ET_r is calculated by summing hourly ET_r estimates to 24-h values. It should be noted, that it is recommended (Allen et al., 2006; ASCE-EWRI, 2005) to calculate daily ET_r as the sum of hourly values rather than summing or averaging hourly input parameters (T_a, T_d, R_s and WS) to daily values before calculating ET_r.

Weather data quality control

Generally, the three stations have a few minor problems arising from the station designs and locations compared to "ideal" reference conditions (ASCE-EWRI, 2005). The design of the stations is such that the wind speed and wind direction are modified by other sensors and installations on the tripod. Wind speed may additionally be impacted by tall vegetation around the station during part of the year.

The stations are located downwind of fields growing annual crops that may not be at full ground cover during some times of the year. As a result, the air temperature and air humidity at the stations does not tend to be 'conditioned' by evaporative cooling and evapotranspiration (ET) from irrigated agriculture during part of the year.

A description of procedures and thresholds for quality control of weather data is in appendix D of ASCE-EWRI (2005). This publication further provides insight and methods for calculating a theoretical clear sky solar radiation curve, which is a powerful parameter to use for indicating not only possible errors in R_s (e.g. calibration errors, sensor misalignment, damaged sensor etc), but also errors in datalogger time stamps and internal clock.

Air temperature is analyzed by subtracting the average of 24 hourly T_a from the difference between daily temperature extremes (minimum and maximum T_a). Systematic differences greater than 2-3 °C may indicate erroneous extremes in air temperature or impacts of missing data. Daily 24-h temperatures are screened in order to check the dataset for outliers and the expected annual occurrence of maximum and minimum temperatures.

Air humidity is shown as minimum and maximum daily RH. In relatively arid regions such as the Mission Valley, daily minimum RH may run as low as 15 – 20 % during the dry part of the year. Daily maximum RH is generally in the range of 80 - 100 % for irrigated areas with sufficient fetch and adequate water supply, especially during "wet" portions of the year.

Daily average wind speed is plotted as a function of day of year (DOY) to check for outliers. Continuous periods with wind speeds less than 1 m/s may indicate problems with the anemometer. Also, daily wind speed is compared among the three stations to evaluate spurious high values and systematic higher wind speeds compared to the other stations. The gust factor, calculated as the ratio of maximum daily wind speed to mean daily wind speed, is plotted to evaluate the functioning of the anemometer. If the gust factor over time shows a period of large values the anemometer may be malfunctioning. Also, if the gust factor drops to a value of 1 the sensor may be failing completely.

Daily values of precipitation are compared for the four stations to evaluate the temporal occurrence of precipitation and the amount received. Generally precipitation is very

heterogeneous, however if one of the stations systematically records substantially less precipitation this may indicate a dirty or malfunctioning rain gauge.

In the following a sample of the results from the quality analysis for solar radiation, air temperature, air humidity, wind speed and precipitation is presented.

Solar radiation

Daily R_s is compared to calculated clear sky solar radiation, R_{s0}. R_{s0} is calculated based atmospheric pressure, sun angle and precipitable water in the atmosphere. On clear sky days the measured R_s should approach the value of R_{s0}. The R_{s0} curve may be obtained as one of the outputs from the RefET software.

Figure 7 shows daily solar radiation from the three weather stations for the entire 2 ½ year period. At St. Ignatius and Creston the R_s data runs higher than the R_{s0} curve after medio 2006. This pattern is also seen from Figure 8 showing hourly solar radiation values for a seven-day period prior to a few of the satellite overpass dates. In early May 2006 R_s at St. Ignatius follows the R_{s0} curve, while the values lie above the curve in June 2006 and (to a lesser extent) in ultimo August 2007. From the June 2006 graph a hesitation in R_s at Round Butte is seen during early morning hours which is likely caused by nearby trees shading the pyranometer.

The errors in R_s are rectifiable by applying appropriate multiplication factors. R_s at St. Ignatius and Creston were modified using the correction factors shown in Table 6.

Table 6. Correction factors for R_s measured at the St. Ignatius and Creston Agrimet weather stations.

Station	Begin date	End date	Multiplier
St. Ignatius	01/01-06	06/12-06	1.0
	06/13-06	08/15-08	0.95
Creston	01/01-06	06/30-06	1.0
	07/01-06	08/15-08	0.96

Daily R_s at St. Ignatius and Creston after correction are shown in Figure 9 and hourly R_s for two seven day periods prior satellite overpass are shown in Figure 10.

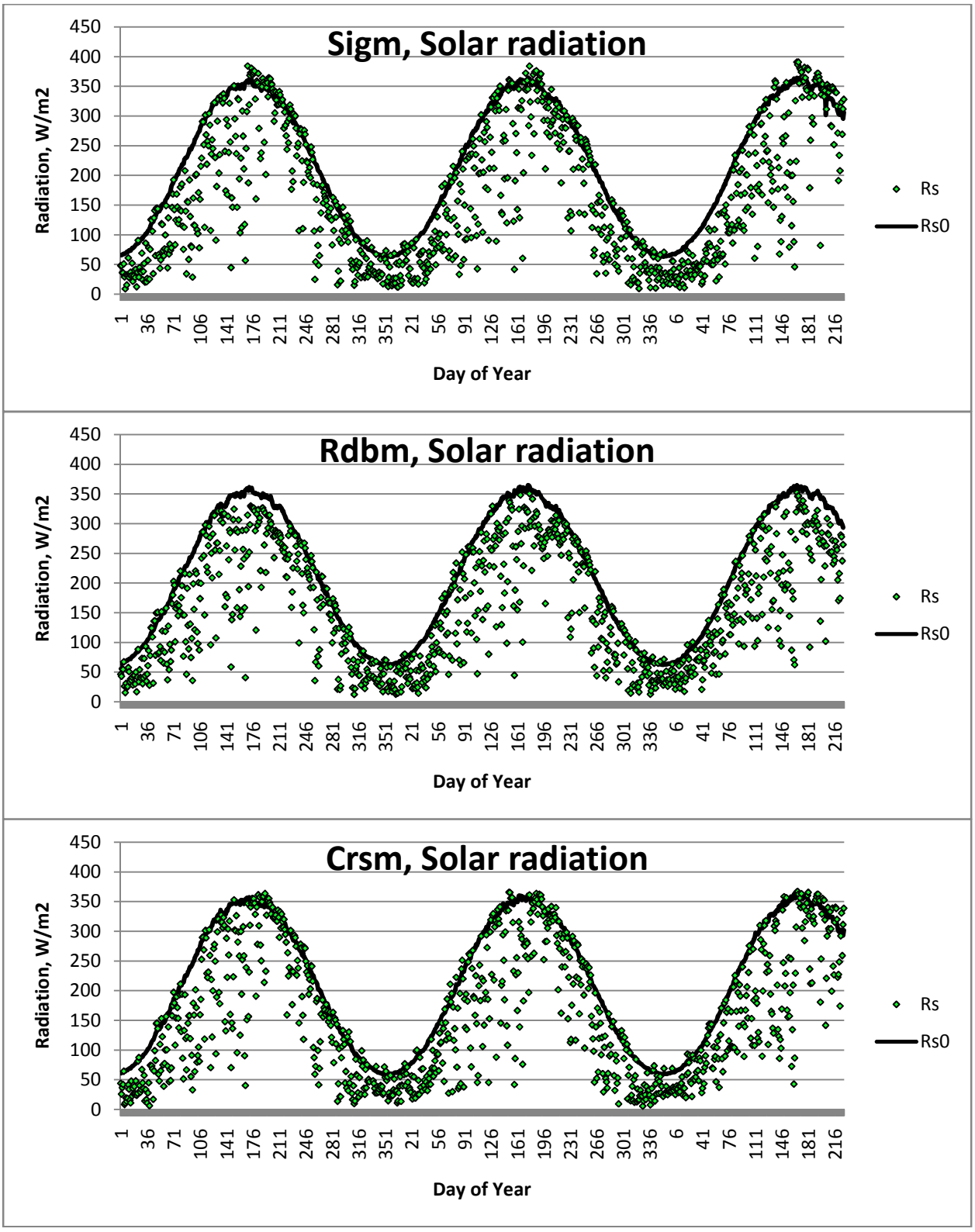

Figure 7. Daily recorded solar radiation and theoretical clear sky radiation curve for the St. Ignatius (Sigm), Round Butte (Rdbm) and Creston (Crsm) Agrimet weather stations between Jan 1 2006 and Aug 15 2008 *before* correction.

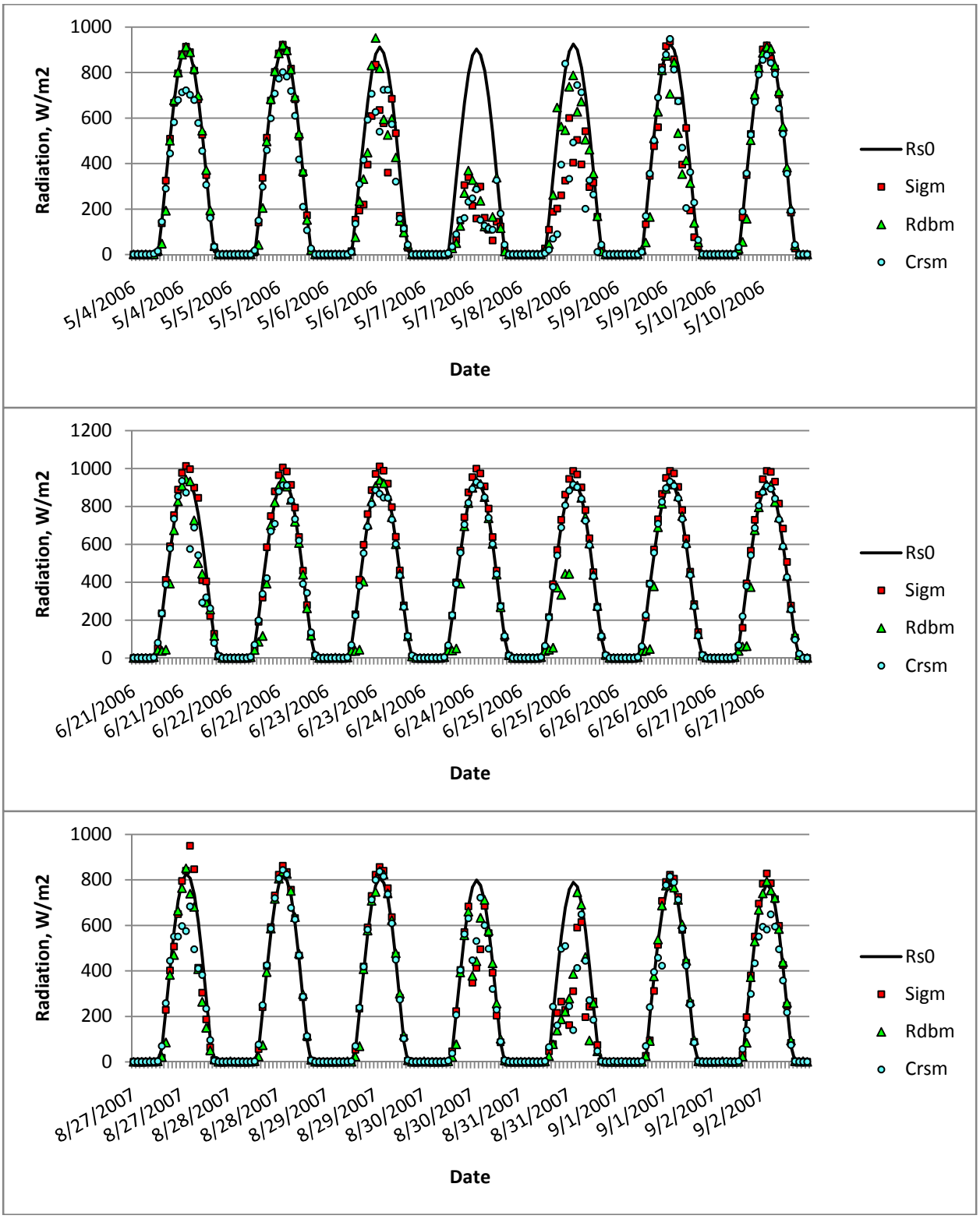

Figure 8. Hourly solar radiation and theoretical clear sky solar radiation curve (R_{s0}) for 7-day periods before a satellite overpass date *before* correction at the St. Ignatius (Sigm), Round Butte (Rdbm) and Creston (Crsm) Agrimet weather stations.

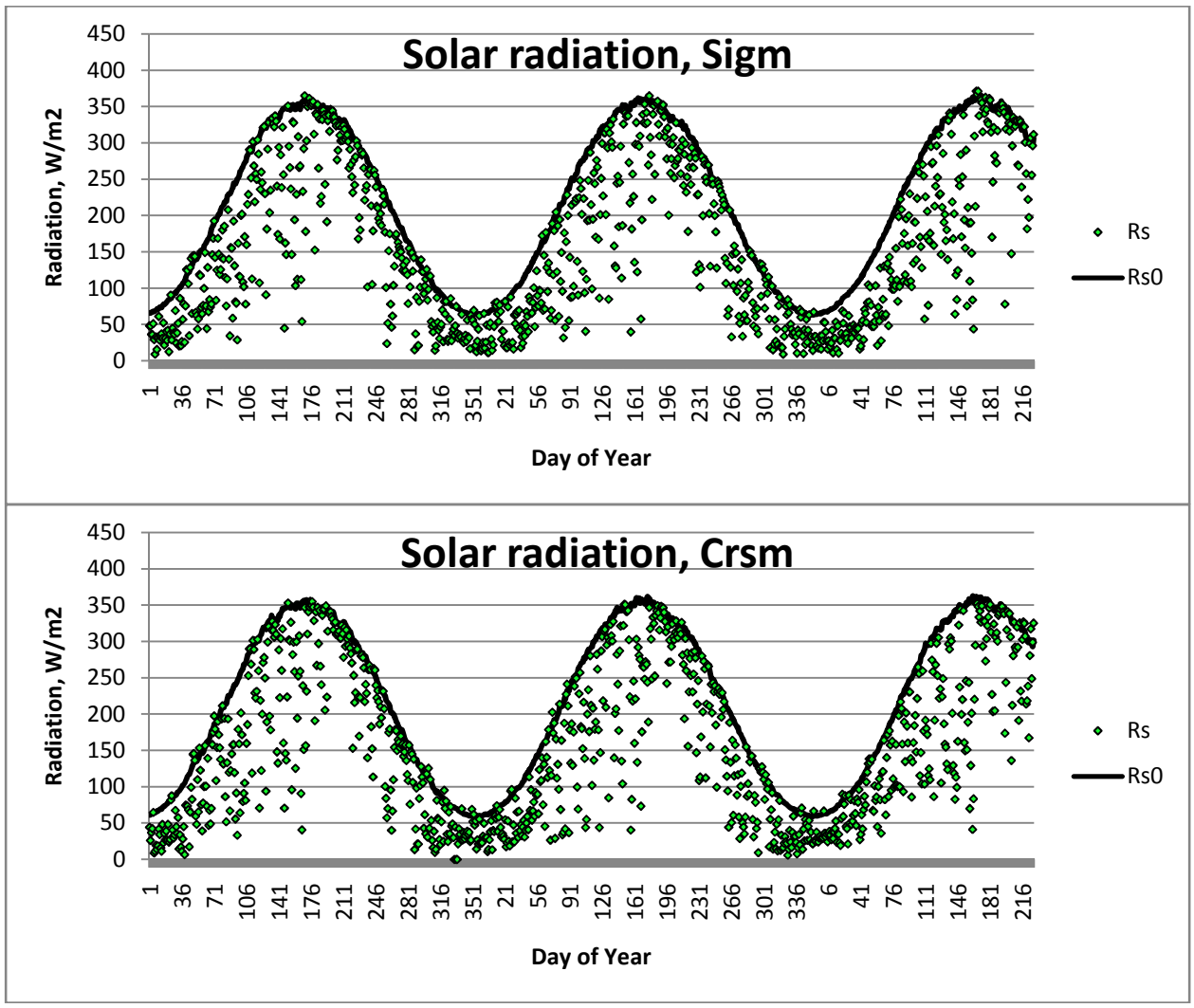

Figure 9. Daily recorded solar radiation and theoretical clear sky radiation curve for the St. Ignatius (Sigm), and Creston (Crsm) Agrimet weather stations between Jan 1 2006 and Aug 15 2008 *after* correction.

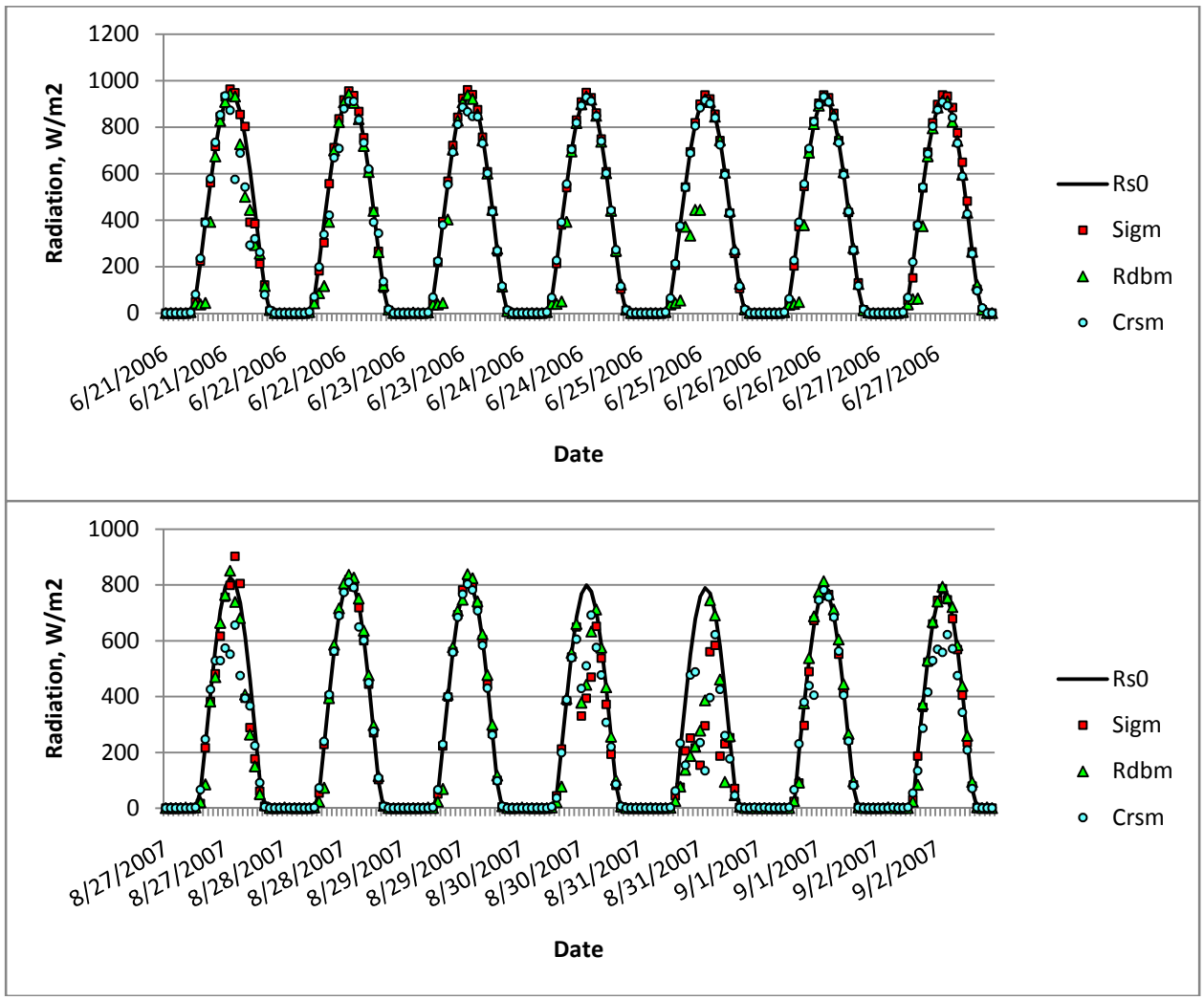

Figure 10. Hourly solar radiation and theoretical clear sky solar radiation curve (R_{s0}) for 7-day periods before a satellite overpass date *after* correction at the St. Ignatius (Sigm), Round Butte (Rdbm) and Creston (Crsm) Agrimet weather stations.

Air temperature

Hourly air temperature for three seven-day periods is shown in Figure 11. The temperature observations generally track each other well among the stations.

After a longer period of no or very little rainfall during the growing season the temperature at St. Ignatius ran up to a few degrees warmer than Creston at night time as seen in Figure 11, bottom. No or very little rainfall was recorded during the July and August 2007. The airport location surrounding the St. Ignatius station is not irrigated, and may experience less evaporative cooling during daytime compared to Creston thereby releasing more sensible heat and emitting more long-wave radiation. As a result, air may be heated more by the surface at St. Ignatius than at Creston but not enough to cause instability or buoyancy at nighttime. Wind ensures sufficient mixing of the near-surface air mass to remove heat convected from the ground and cool the radiation shield during daytime, whereas there is little vertical air movement to mix the near-surface air mass at nighttime causing the air temperatures being indicative of a more local environment.

Air temperature was analyzed by subtracting the average 24-h T_a from the difference between daily temperature extremes (minimum and maximum T_a). The difference is generally within 3 °C indicating no abnormal systematic measurements and a well working instrument.

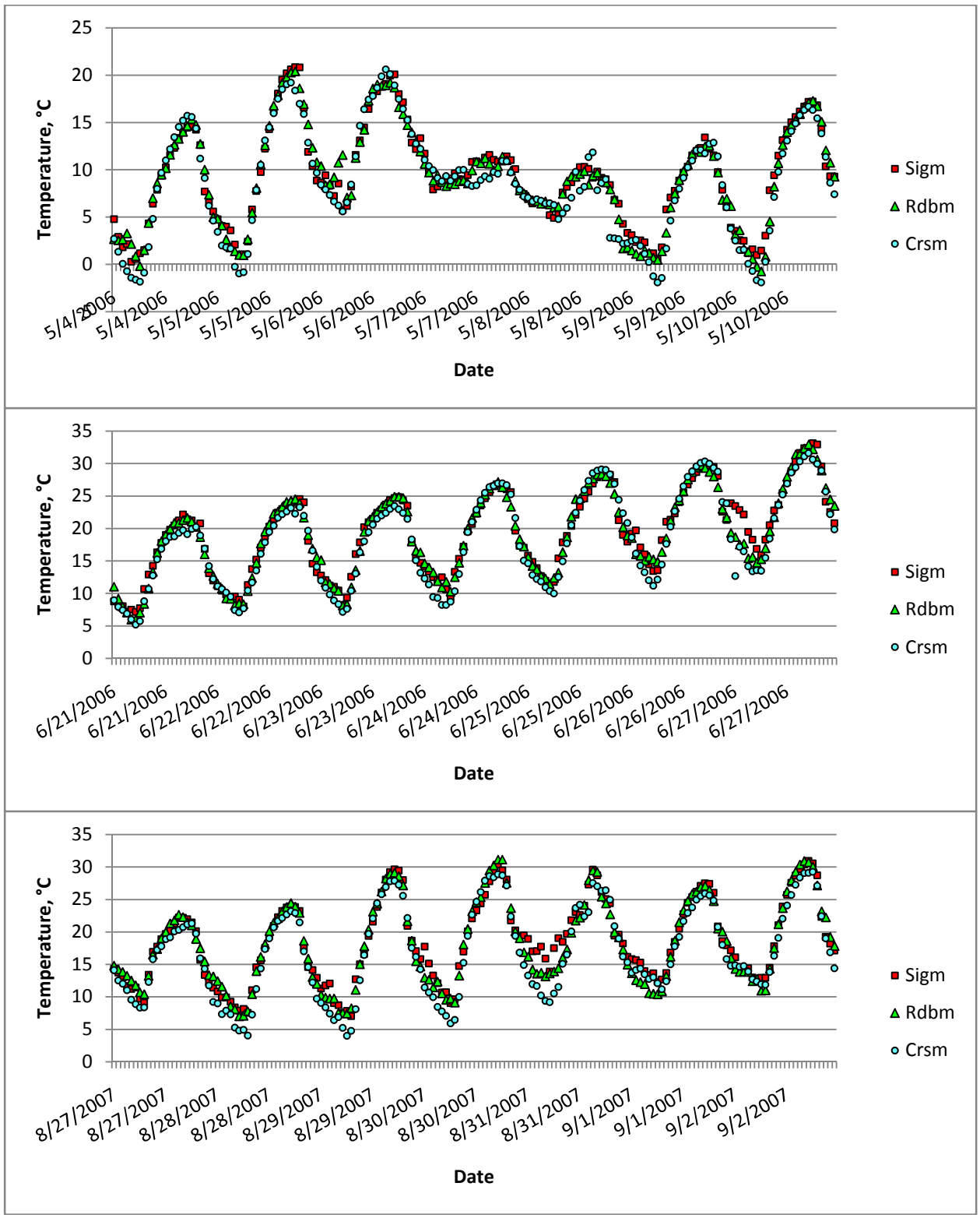

Figure 11. Hourly air temperature (°C) at St. Ignatius (Sigm), Round Butte (Rdbm) and Creston (Crsm) for a 7-day periods before satellite overpass dates.

Air humidity

Figure 12 shows daily minimum and maximum relative humidity for the entire 2 ½ year period. For a weather station located in reference conditions, maximum RH normally occurs in the early morning hours while minimum RH normally occurs mid-afternoon. Maximum RH was generally between 80 and 100 % at Creston which is indicative of this station being situated in near reference conditions. At St. Ignatius maximum RH fell below 60 % during the drier mid-to-end portion of the growing season indicating this station is located in a somewhat environment. Maximum RH may run a few % too low at Round Butte.

Hourly dew point temperature during a seven-day period prior to a satellite overpass date is shown in Figure 13. The patterns for dew point temperatures were similar among the three stations all year, which is a good indication of good performance by the relative humidity sensors. The drier environment St. Ignatius is seen in the bottom part of figure 13, which follows a period with no or very little rainfall during July and August 2007.

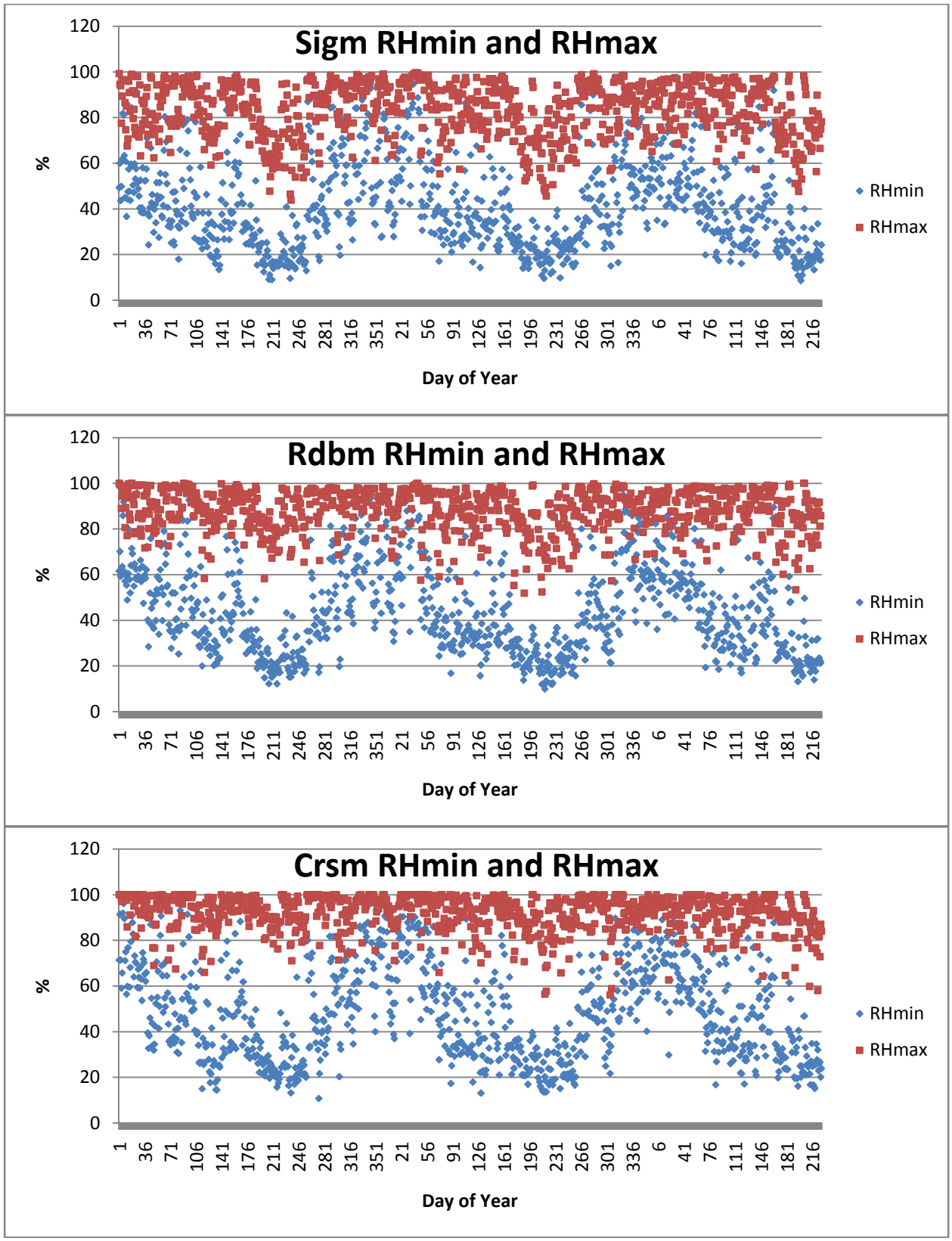

Figure 12. Daily minimum and maximum relative humidity (RH) at the St. Ignatius (Sigm), Round Butte (Rdbm) and Creston (Crsm) Agrimet weather stations between Jan 1 2006 and Aug 15 2008.

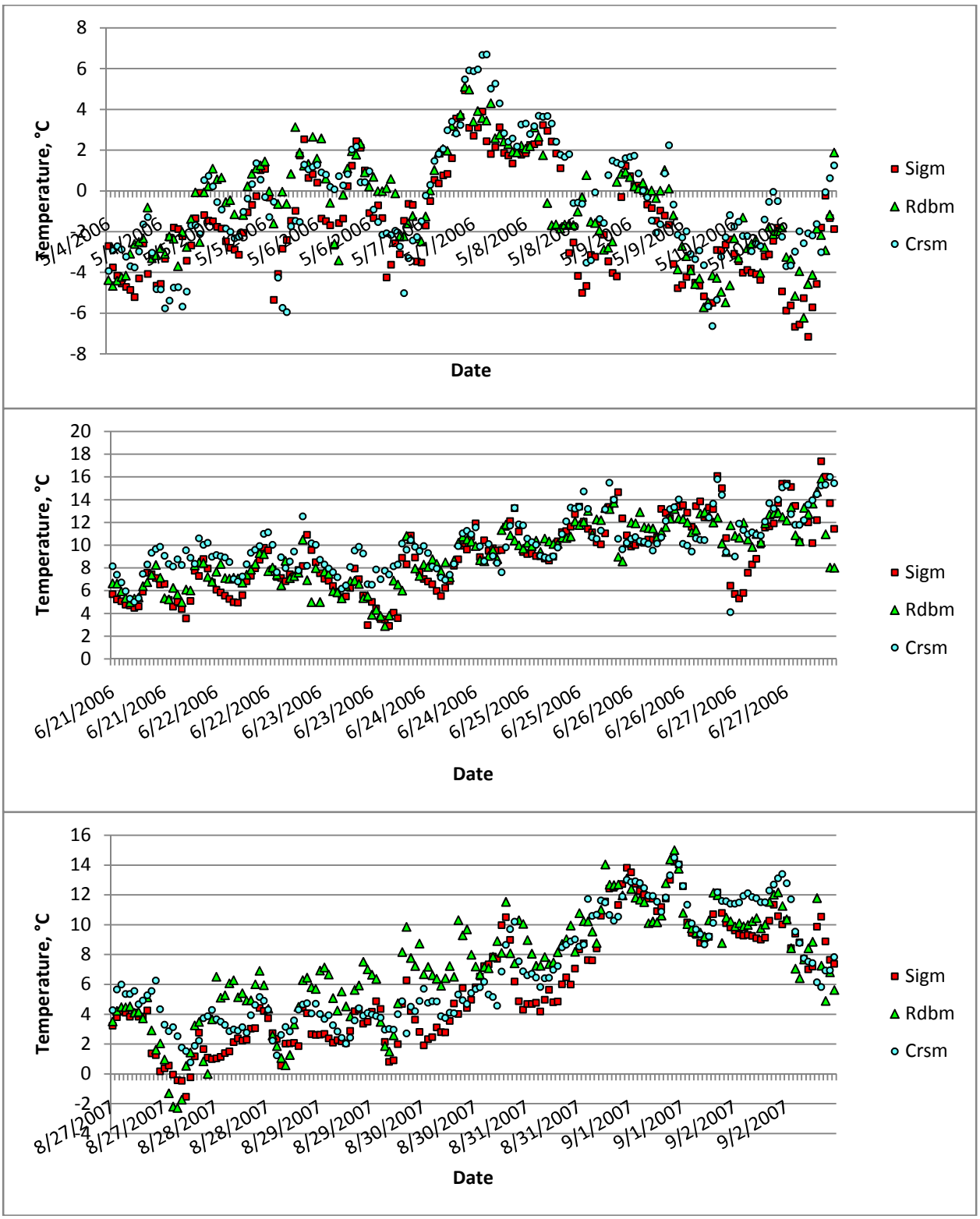

Figure 13. Hourly dew point temperature (°C) at St. Ignatius (Sigm), Round Butte (Rdbm) and Creston (Crsm) for 7-day periods before a satellite overpass date.

Wind speed

Wind speed recorded at Round Butte is lower than at the two other stations, as shown with cumulative values in Figure 14. After breaking wind speed down by wind direction, Figure 15, it is seen that the average wind speed recorded at Round Butte is lower than the two other stations when winds are from an easterly directions. This is likely caused by the trees, buildings and other physical obstructions located 100 – 150 feet east of the Round Butte weather station.

The wind speed is particularly higher at Creston compared to the other stations when the wind is from the south. This may be caused by its location in the north end of the valley where the wind can pick up speed, compared to the southern end of the valley at St. Ignatius, where mountains slows down the wind. Also, Creston is located on an almost horizontal terrace which a relatively sudden increase of slope about 100 feet south of the station. The Venturi effect created by this change in slope may cause higher wind speeds locally.

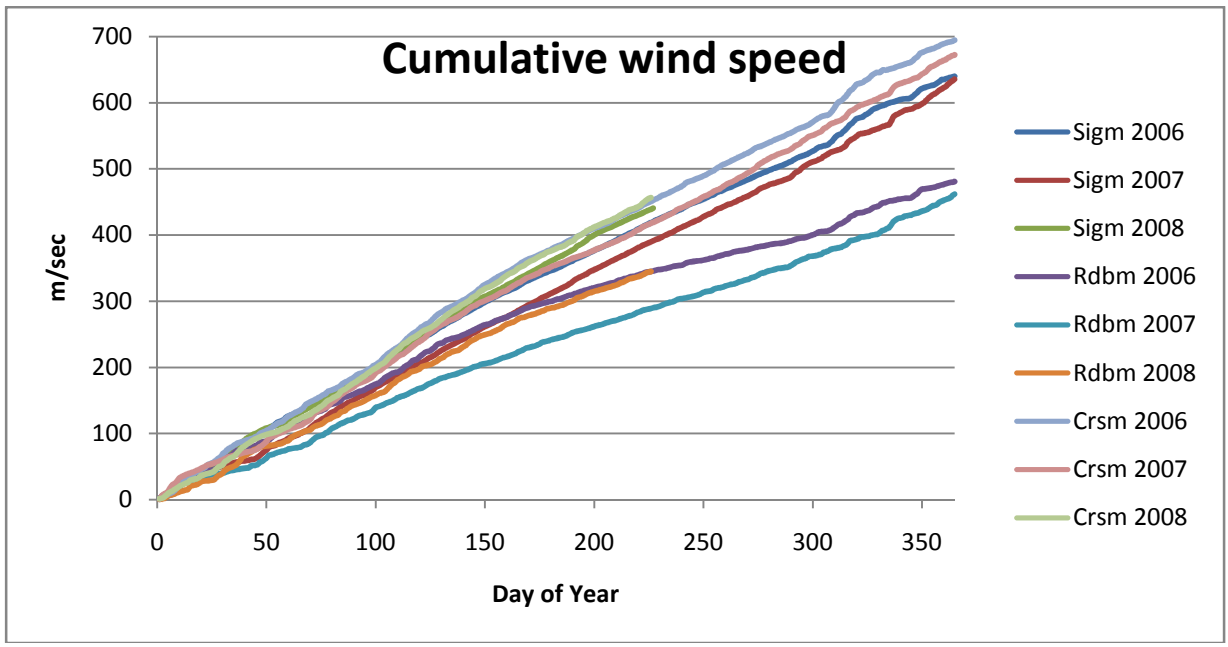

Figure 14. Cumulative daily wind speed at St. Ignatius (Sigm), Round Butte (Rdbm) and Creston (Crsm) Agrimet weather stations for 2006, 2007 and Jan – Aug 2008.

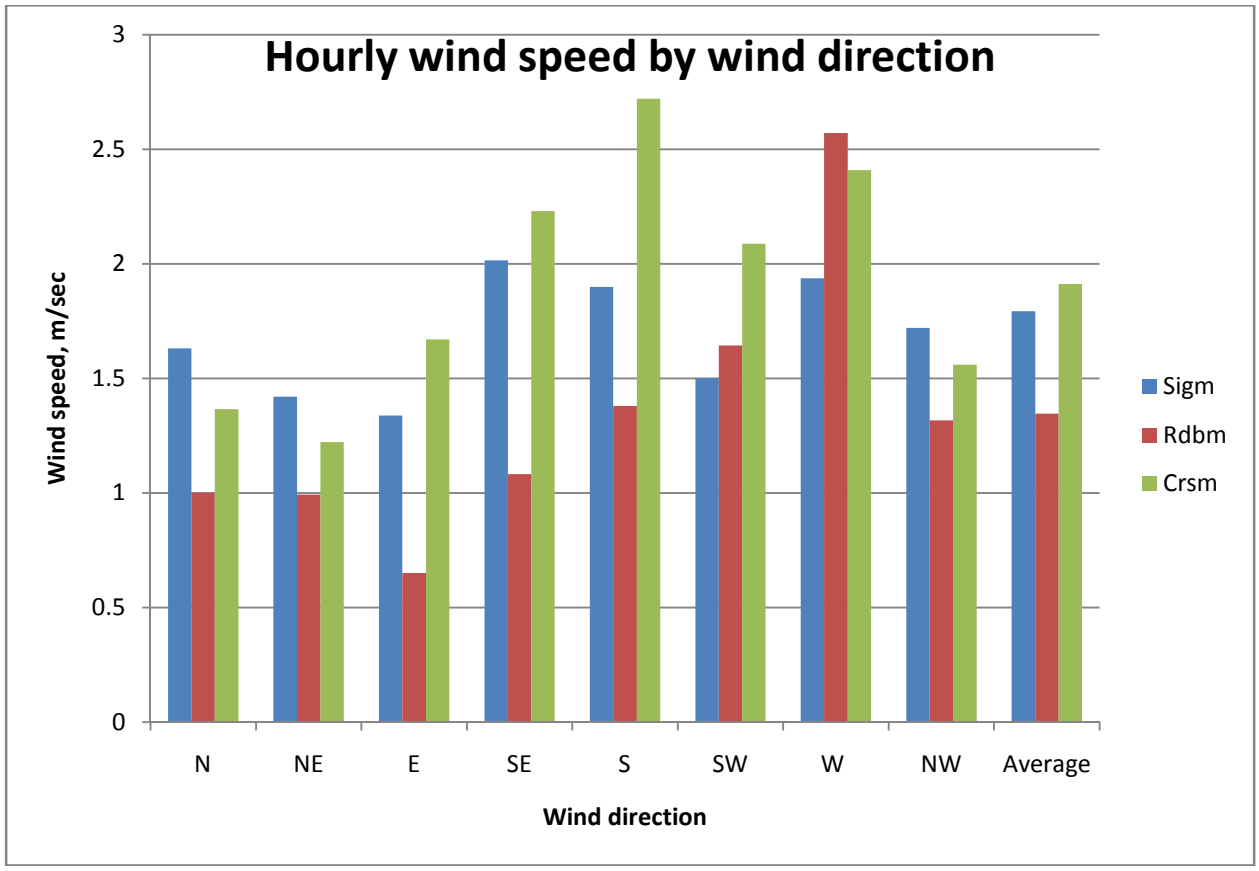

Figure 15. Average hourly wind speed by direction at St. Ignatius (Sigm), Round Butte (Rdbm) and Creston (Crsm) Agrimet weather stations for 2006, 2007 and Jan – Aug 2008.

Precipitation

Cumulative precipitation for each year is shown in Fig. 16. The differences in annual precipitation between stations may be caused by the precipitation gradient from west (low) to east (high) across the Mission Valley and possibly by turbulence in the airflows around the Round Butte station caused by nearby obstructions (tall bush-like vegetation, trees, buildings) compared to the more unobstructed locations of the St Ignatius and Creston stations.

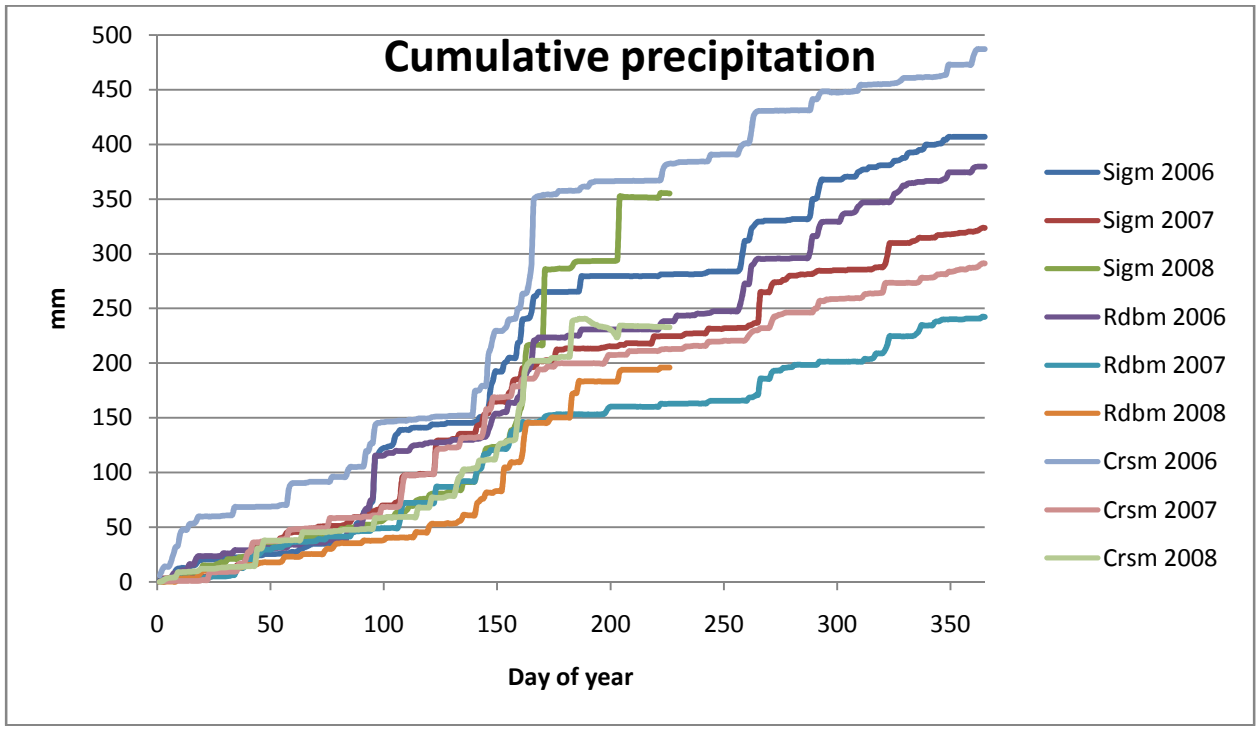

Figure 16. Cumulative precipitatin (mm) at St. Ignatius (Sigm), Round Butte (Rdbm) and Creston (Crsm) Agrimet weather stations for 2006, 2007 and Jan – Aug 2008.

Calculated reference evapotranspiration

Reference evapotranpiration, ET_r, is calculated using the ASCE-EWRI (2005) standardized Penman-Monteith equation and is applied for both the alfalfa reference and the grass reference. Alfalfa based ET_r is used in METRIC in the calculation of sensible heat flux, and are presented below. The ET_r values shown in this section were calculated following correction of R_s for St. Ignatius and Creston.

Figure 17 show the cumulative ET_r calculated for each weather station. ET_r runs slightly higher at St. Ignatius compared to the two other stations, especially in 2007. From Figure 18, which shows daily ET_r for the period May 1 to end of August for 2006, 2007 and 2008, it is seen that the largest deviation occurs by the end of July and beginning of August 2007, which coincides with a period with no or very little precipitation. Due to the location with less irrigated vegetation surrounding the St. Ignatius weather station the air is likely warmer and drier compared to air 'conditioned' by well-watered vegetation. For the remainder of the year, the St. Ignatius and Creston ET_r generally track each other, Figure 18 and 19.

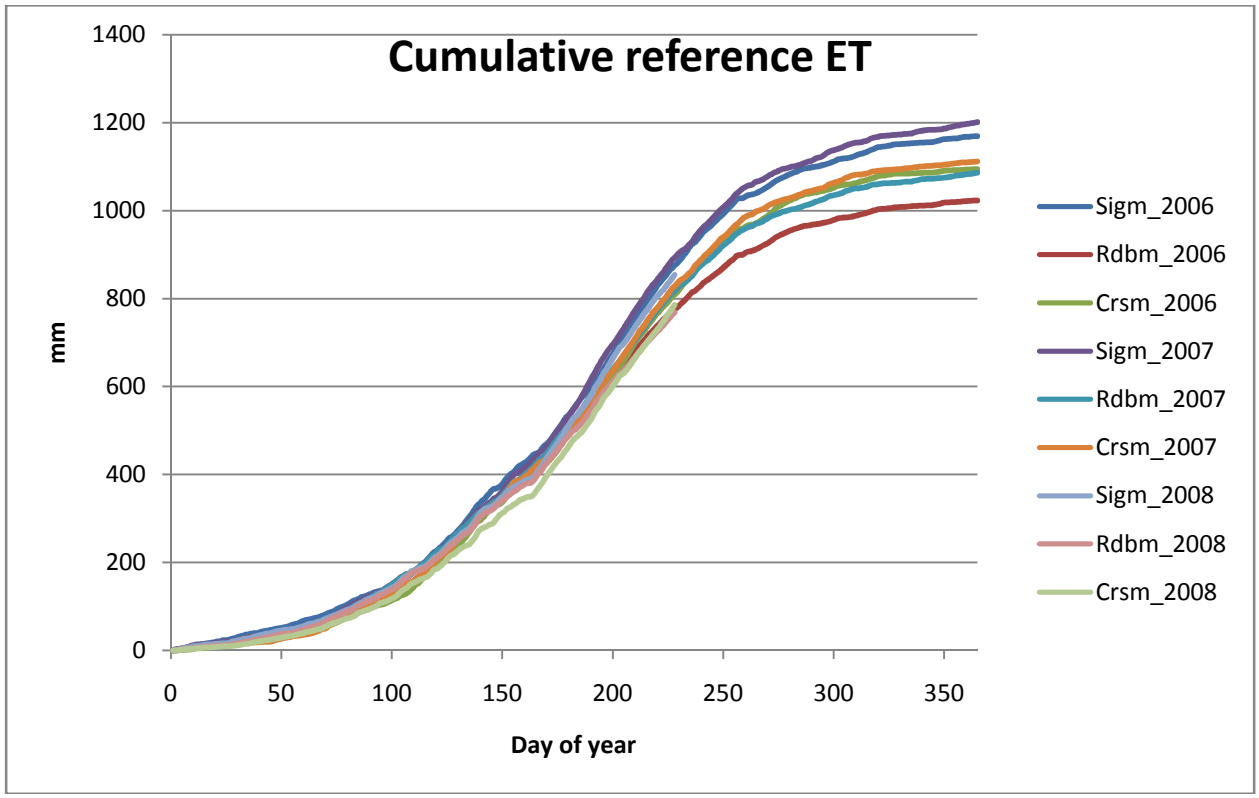

Figure 17. Cumulative reference ET (mm) at St. Ignatius (Sigm), Round Butte (Rdbm) and Creston (Crsm) Agrimet weather stations for 2006, 2007 and Jan – Aug 2008.

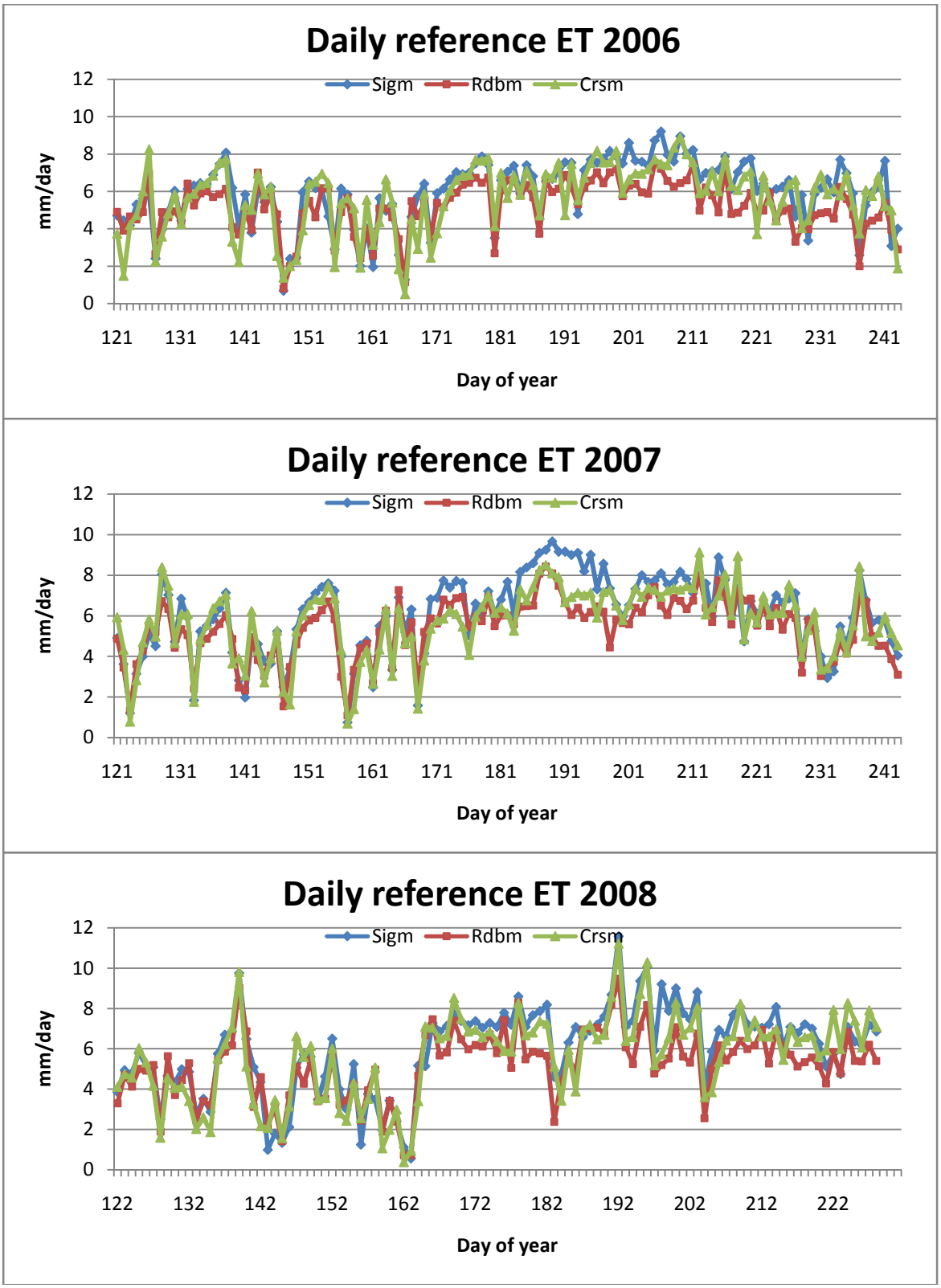

Figure 18. Daily reference ET (mm) between May 1 and August 31 for 2006 and 2007, and May 1 to August 15 for 2008 for St. Ignatius (Sigm), Round Butte (Rdbm) and Creston (Crsm) Agrimet weather stations.

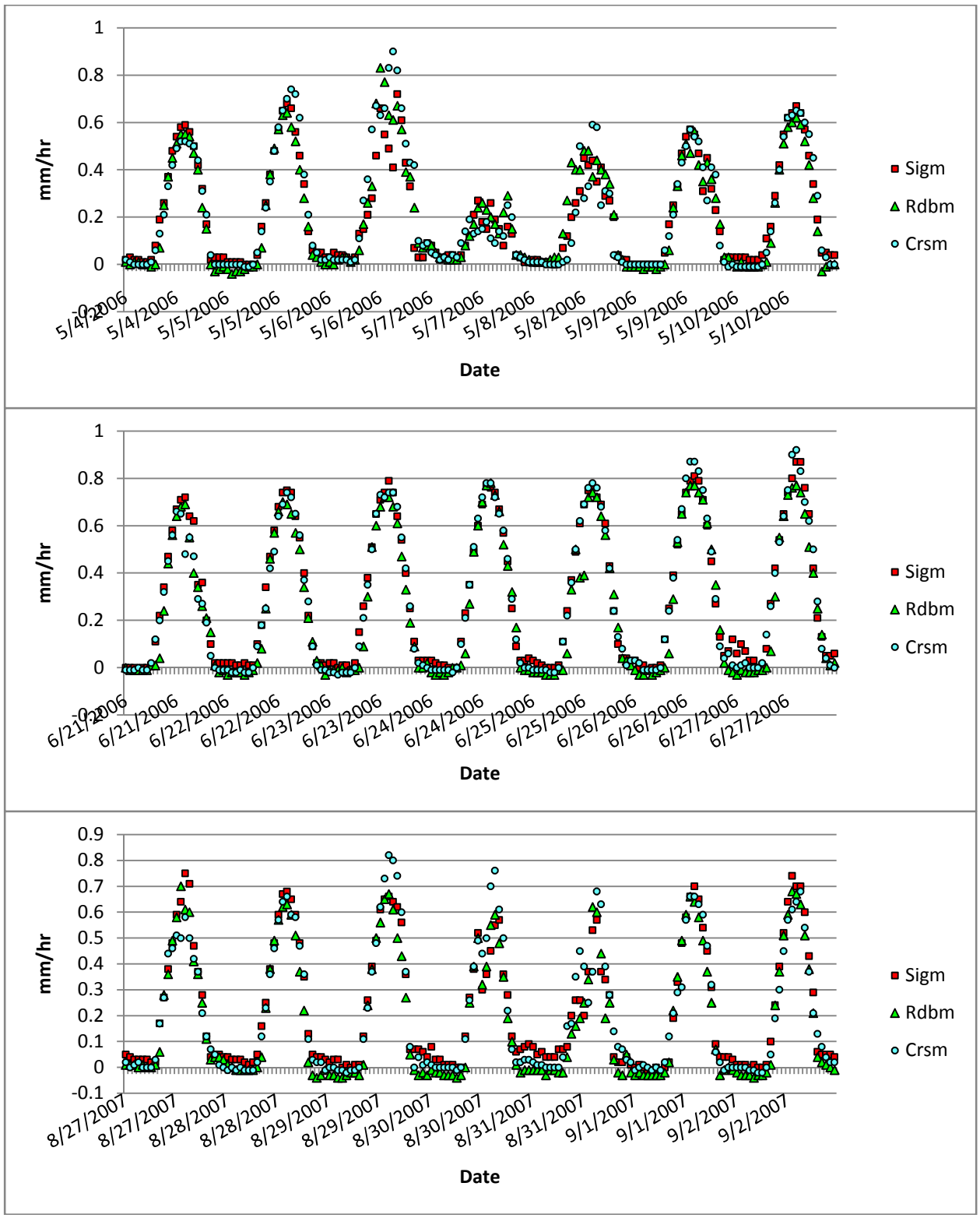

Figure 19. Hourly reference ET (mm) at St. Ignatius (Sigm), Round Butte (Rdbm) and Creston (Crsm) for a 7-day periods before satellite overpass dates.

Conclusion

The weather data from the St. Ignatius, Round Butte and Creston Agrimet weather stations have been downloaded and analyzed.

The measurements of air temperature and air humidity indicate that the St. Ignatius station is located in an area that is at times more arid than under reference conditions during prolonged periods with little or no precipitation in combination with high ET_r rates. However, only one such period has been identified in the dataset in end of July – mid August 2007.

Trees and buildings east of the Round Butte station shade the pyranometer and cause lower measurements during morning hours compared to the R_{s0} curve and the two other stations. In addition, the trees and buildings disturb the airflow from easterly directions rendering wind speeds to be lower than the two other stations.

The Creston station is closest to being located in reference conditions of the three stations. Wind speeds may be impacted locally by a relative sudden change in slope south of the station. However, the station is located north of the Flathead Indian Reservation.

Based on this analysis, both the St. Ignatius station and the Creston Agrimet weather stations may be used with METRIC (after correction of R_s). Since St. Ignatius is located within the study area and Creston is not, it is suggested that weather data from St. Ignatius be used as supporting meteorological information for the processing of satellite images using METRIC. It is also suggested, that for the dry two week period during July 3 to July 17 2007 that the weather data from St. Ignatius is substituted with weather data from Creston.

References

Allen, R.G., 1996. Assessing Integrity of Weather Data for Reference Evapotranspiration Estimation. J. Irrig. Drain. Engr., 122, 97-106.

Allen, R.G., et al., 2006. A Recommendation on the Standardized Surface Resistance for Hourly Calculation of Reference ET by the FAO56 Penman-Monteith Method. Agric. Water Manag., 81, 1-22.

Allen, R.G., Tasumi, M., Morse, A., Trezza, R., Wright, J.L., Bastiaanssen, W., Kramber, W., Lorite, I., Robison, C.W., 2007a. Satellite-Based Energy Balance for Mapping Evapotranspiration with Internalized Calibration (METRIC) – Applications. J. Irrig. Drain Engr., 133(4), 395-406.

Allen, R.G., Tasumi, M., Trezza, R., 2007b. Satellite-Based Energy Balance for Mapping Evapotranspiration with Internalized Calibration (METRIC) – Model. J. Irrig. Drain Engr., 133(4), 380-394.

ASCE-EWRI, 2005. The ASCE Standardized Reference Evapotranspiration Equation. ASCE, Reston, Virginia.

Appendix B
Selection of images for METRIC processing for the Flathead Indian Reservation, Montana
By J. Kjaersgaard and R. Allen, University of Idaho. July 2008.

Introduction and image selection criteria
This note describes the procedure for selecting Landsat satellite images to be processed using the METRIC ET procedure for the Flathead Indian Reservation, Montana. For this application, images from the Landsat 5 and Landsat 7 satellites are utilized due to their band combinations and high resolution. The image archive for Landsat 5 dates back to 1984 and the satellite is still in operation. Landsat 7 was launched in 1999, but the scan line corrector failed in May 2003 resulting in subsequent images having wedge shaped stripes of missing data across the scenes. There is no information contained in the stripes.

The Flathead Indian Reservation is conveniently contained in one Landsat scene path/row, i.e. path 41, row 27. A total of eight images were selected for processing, including the seven images as stated in the contract and one additional image from early or late season, respectively, that the UI will process for gratis. The images were selected so that they were distributed as evenly as possible throughout the growing season with preferably no more than 32 days between images so as to adequately follow evolution of vegetation development.

The most important criteria for the image selection is an assessment of the atmospheric conditions (i.e., cloudiness) at the time of the satellite overpass. The occurrence of conditions impeding the clearness of the atmosphere, such as clouds (including thin cirrus clouds and jet contrails), smoke, haze and similar over the study area may render an image unusable for processing in METRIC. Even very thin cirrus clouds have a much lower surface temperature than the ground surface and because METRIC needs surface temperature estimates to solve the energy balance, areas with cloud cover cannot be used in the surface energy balance estimations. In addition, in cases of partial cloud cover, land areas recently shaded by clouds may be cooler as they have not yet reached a thermal equilibrium corresponding to the clear sky energy loading, and will also have to be masked out.

Since one of the project goals is to study water distribution and use by irrigated agriculture it is probably desirable not to select a wet year, as this may partly blur the differences in crop water use between fields.

To aid the selection of images an image rating system has been employed where the usability of an image in terms of cloudiness and smoke was ranked as a fraction on a scale between “0” and “1”, where “0” is an unusable image (e.g. complete cloud cover) and “1” is a nice, usable image. If an image has partial cloud cover over the study area it is rated accordingly, e.g. if an estimated 70 % of the study area is cloud and cloud shadow free, it may be rated 0.7.

A graphical representation of the rating for path 41, row 27 for the period January 1997 to July 2008 is shown in Fig 1. Images are assessed using the USGS on-line image preview tool glovis at http://glovis.usgs.gov/.

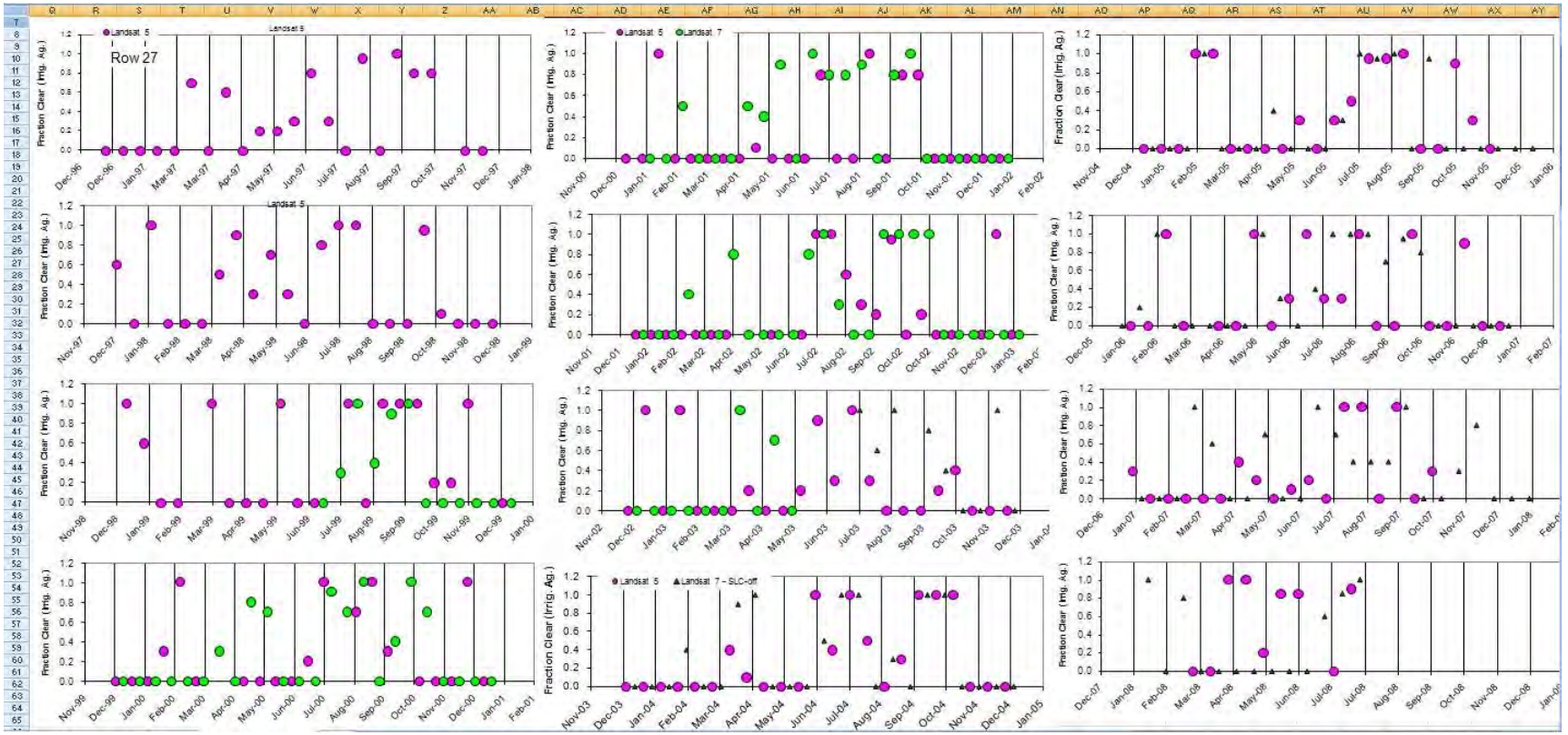

Fig 1. Graphical representation of the image ratings between January 1997 and July 2008. Pink circles are Landsat 5, green circles are Landsat 7 (SLC-on) and triangles are Landsat 7 (SLC-off).

Seasonal ET estimations aggregated using images from multiple years

None of the years 1998 – 2008 have a complete coverage of good cloud free images throughout the year. It is particularly important to have good, cloud free images during the spring and early summer, as the shape of the curve used to define the temporal development of ET is somewhat variable depending on crop type and crop management during this period. Unfortunately, the Mission valley has very few cloud free days during this period (April to early June) for nearly all years of record.

In addition, images from Landsat 7 (SLC-off) are generally less suited for the METRIC processing, as portions of the image contain no data. Even though the study area is located towards the center of the image, some parts will be covered by blank areas. Due to the temporal spacing between images, it is difficult to fill these gaps, resulting in "holes" when ET calculated from each image is aggregated to monthly and seasonal ET. Information must therefore be interpolated from adjacent image dates, which causes some loss in developmental information on ET.

To get a complete coverage over a full growing season, a "base" year has therefore been identified and images from other years have been used to fill in holes in the image sequence. This approach is feasible since the cropping patterns in western Montana tend to stay relatively constant between years, not least for the widespread and generally less-intensive cropping systems consisting of grass or grass/alfalfa intercropping for hay or forage.
For the high intensity cropping systems using a crop rotation between years, this approach will result in some error for individual fields. However, since the crop rotation pattern is assumed to stay relatively constant year to year in regard to total acreages of a particular crop, any biases in the ET estimations arising from different crop types for the same field at different years should cancel when ET is aggregated over a larger number of fields.

To evaluate and account for climatic variation among years, the cumulative number of Growing Degree Days (GDD) have been calculated for each year 1998 - 2008 based on temperature information from the St. Ignatius and Round Butte Agrimet weather stations. GDD is calculated as

$$GDD = (T_{min} + T_{max})/2 - T_{base} \qquad (1)$$

where T_{min} and T_{max} are daily minimum and maximum air temperature, respectively, and T_{base} is a "base" temperature below which none or very little plant development occurs. T_{max} is often capped at a threshold temperature, above which higher temperature does not promote additional plant development.

Commonly used thresholds for Eq. 1 are T_{base} = 10 °C and T_{max} capped at 30 °C. GDDs reported from the Agrimet network are based on these thresholds and are appropriate for corn and other crops requiring relatively high temperatures for their development. For alfalfa, small grain cereals and (cool season) grass, T_{base} values varies between 0 and 5 °C. Because of the relatively short growing season caused by low temperatures in the spring and fall, the Mission Valley area

is dominated by hay and forage C_3 grasses, alfalfa and small grains. Hence, a T_{base} = 0 °C and a T_{max} threshold of 30 °C appear to be reasonable and were used to calculate GDD. The accumulation of GDD was initiated on April 1 (March 30 for leap years). Cumulative GDD for each year in the period January 1998 - June 2008 from St. Ignatius and Round Butte are shown in Figures 2 and 3. The difference from the mean is shown in Figures 4 and 5.

The GDDs have been used to identify images compatible to the base year and, if needed, to adjust an image date to match the approximate crop growth stage relative to the base year.

Comparison of precipitation

Additionally, to avoid sampling too large of differences in the vigor and ET from non-irrigated vegetation between compatible years due to differences in precipitation, we have compared precipitation patterns among years. The annual average precipitation measured at the St. Ignatius and Round Butte weather stations are shown in Figure 6 and annual cumulative precipitation is shown in Figures 7 and 8. The differences in annual precipitation between stations may be caused by the precipitation gradient across the Flathead valley and possibly more turbulence in the airflows around the Round Butte station caused by nearby obstructions (tall bush-like vegetation, trees, buildings) compared to the airport location of the St Ignatius station.

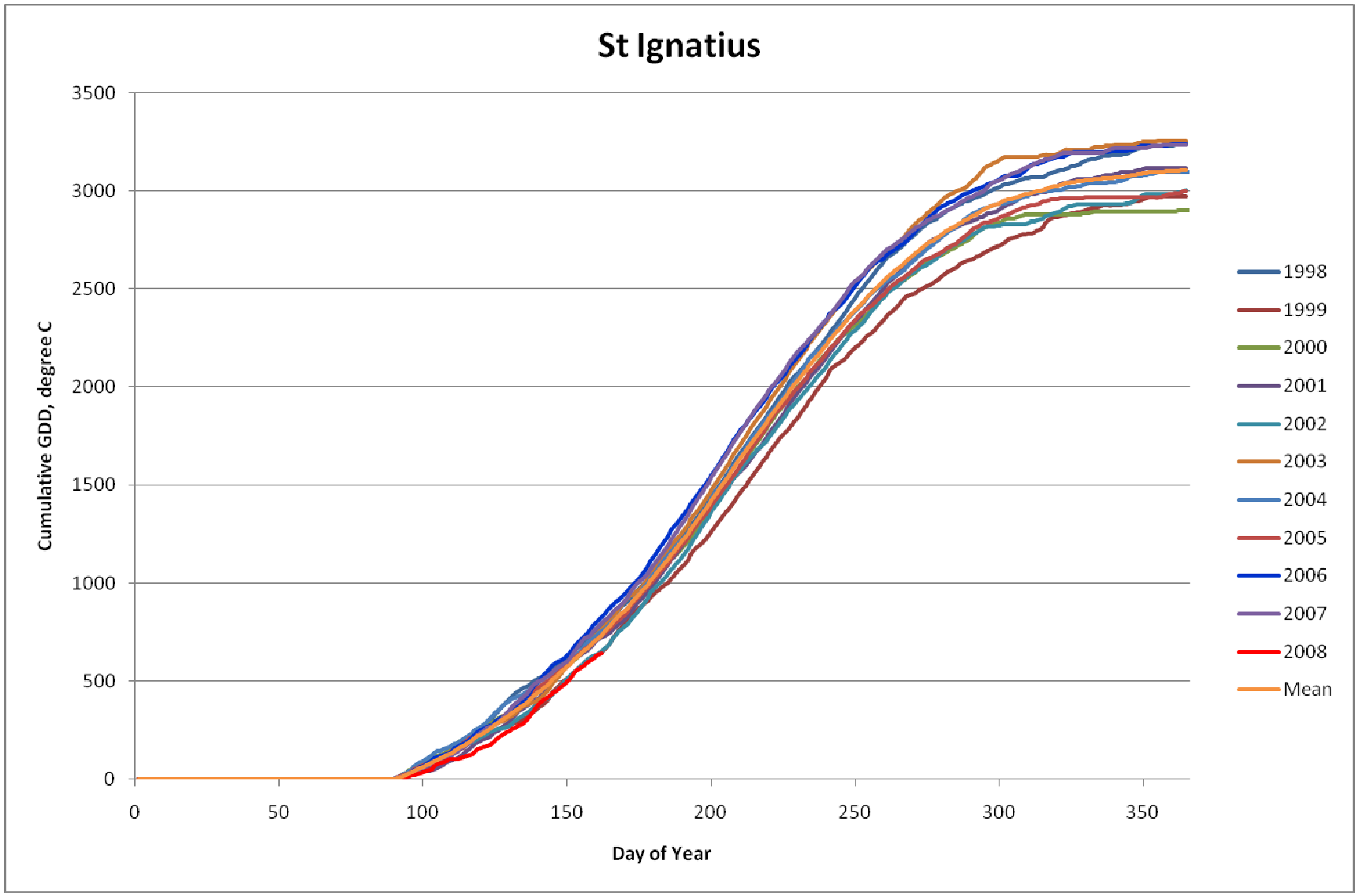

Fig 2. Cumulative Growing Degree Days (GDD) based on the St. Ignatius Agrimet weather station.

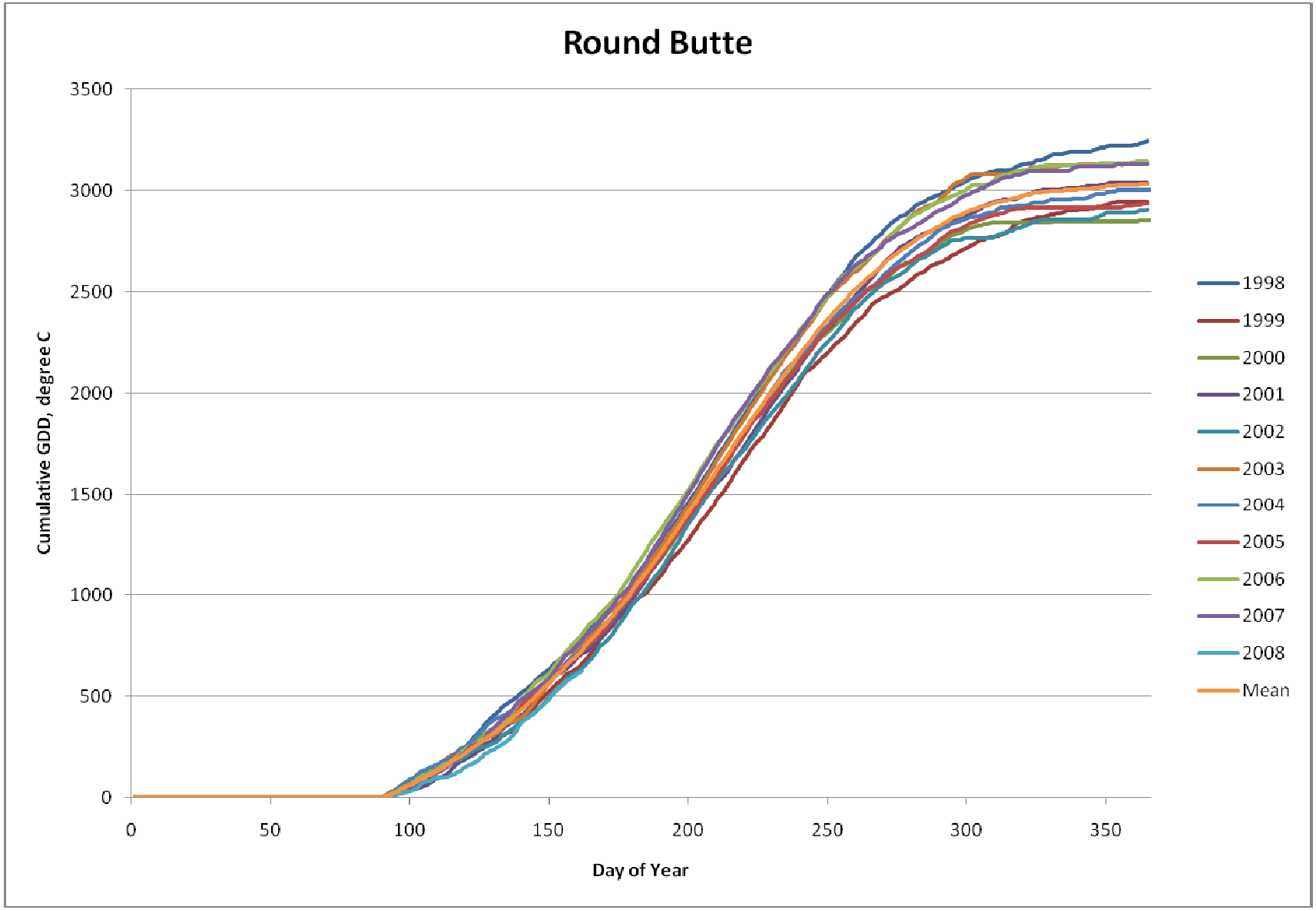

Fig 3. Cumulative Growing Degree Days (GDD) based on the Round Butte Agrimet weather station.

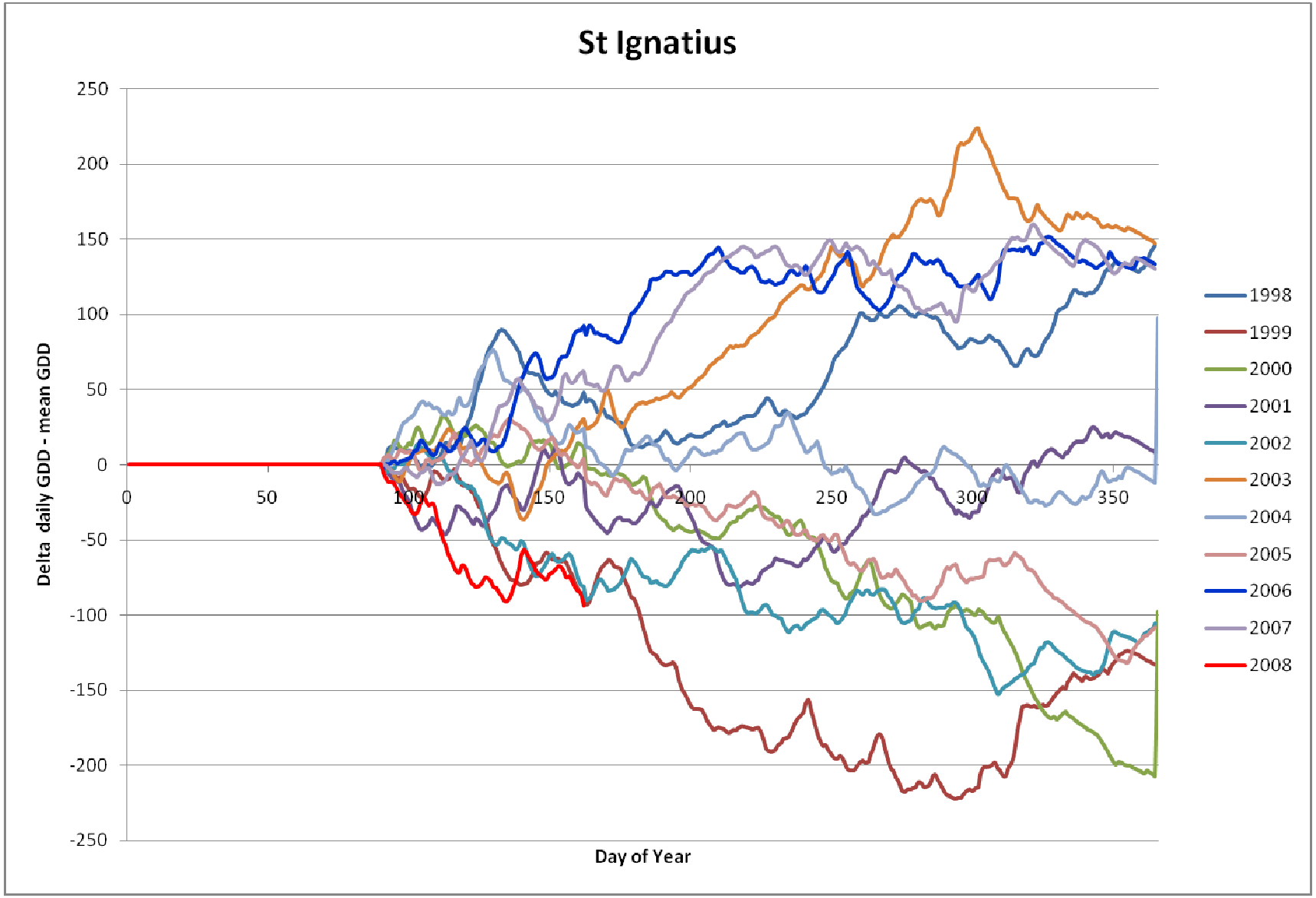

Fig 4. Difference between daily Growing Degree Day (GDD) per year and mean GDD over all 11 years calculated from the St. Ignatius Agrimet weather station. Degrees in °C.

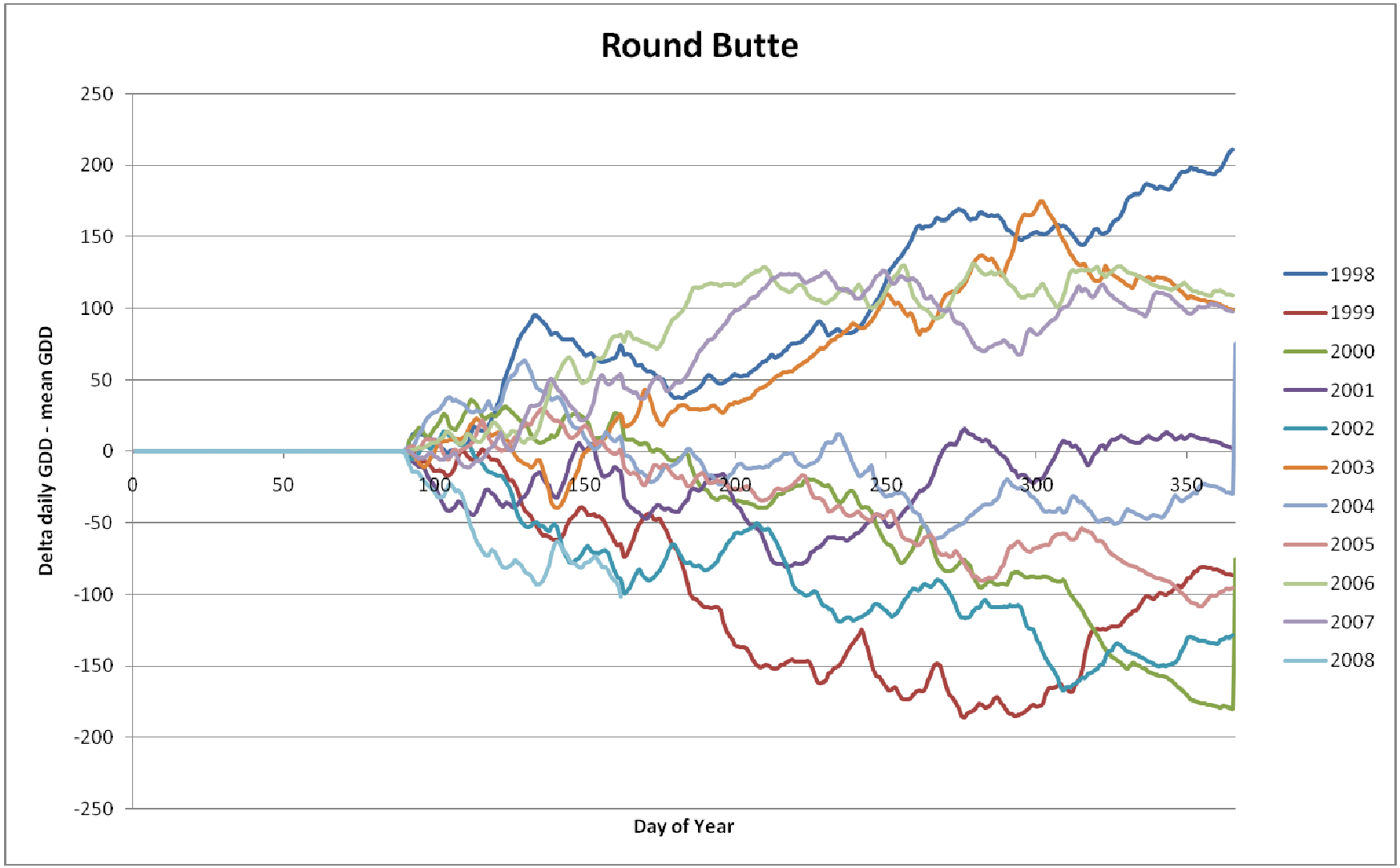

Fig 5. Difference between daily Growing Degree Day (GDD) per year and mean GDD over all 11 years calculated from the Round Butte Agrimet weather station. Degrees in °C.

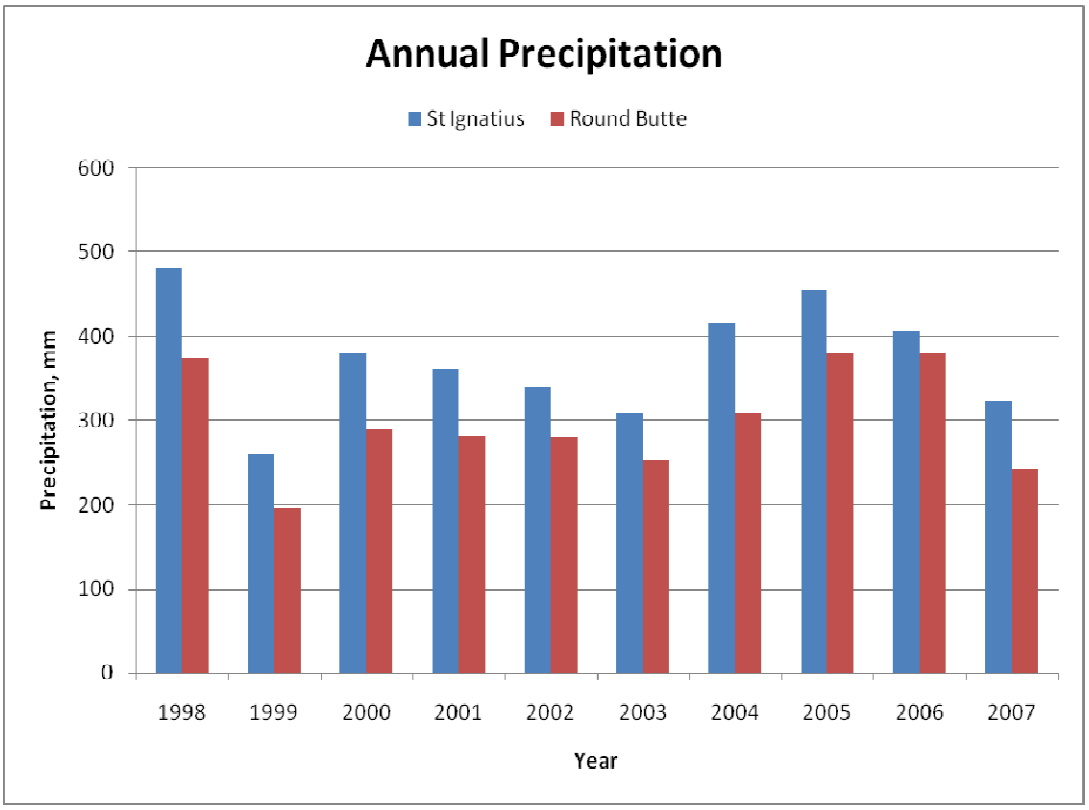

Fig 6. Annual precipitation (mm) recorded at the St Ignatius and Round Butte Agrimet weather stations for 1998 – 2007.

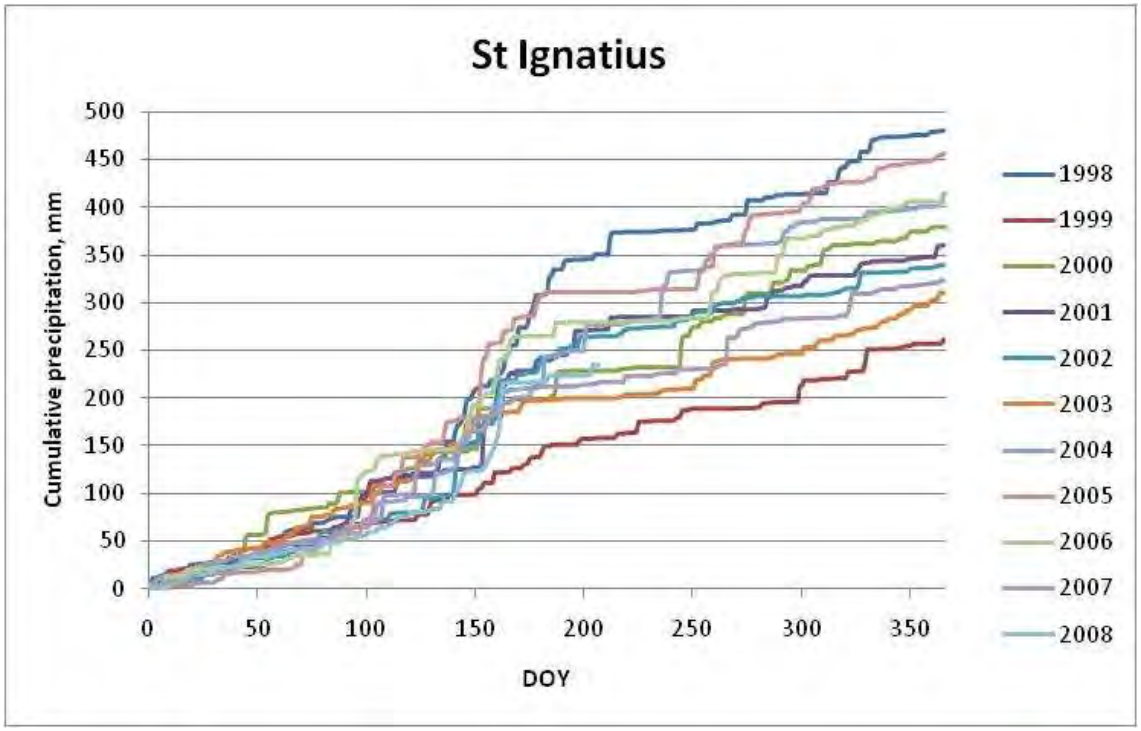

Fig 7. Cumulative daily precipitation measured at the St Ignatius Agrimet weather station for each year 1998 - 2008.

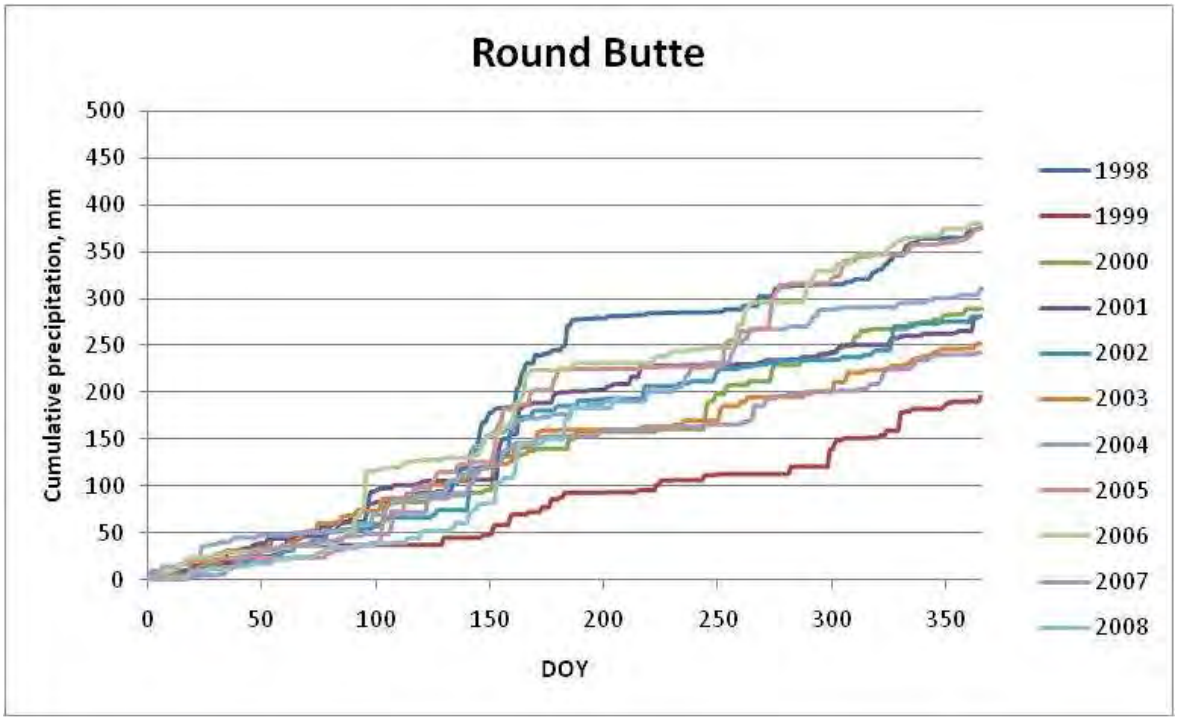

Fig 8. Cumulative daily precipitation measured at the Round Butte Agrimet weather station for each year 1998 - 2008.

Image selection

Based on the criteria and information discussed above, two sets of possible image dates have been identified, as summarized in tables 1 and 2. Year 2002 is used as a base year for option A in table 1, while year 2006 is used a base year for option B in table 2. As seen from Figures 4 and 5, 2002 was cooler than average for the 10-year period, while 2006 was warmer than the 10-year period.

For years other than the base year, the fourth column in tables 1 and 2 indicates which date in the base year the same GDD on the image date was reached. Differences between the first and fourth columns indicate how much the vegetation development in the non-base year image date may be advanced or retarded relative to the base year. The GDDs are based on the Round Butte weather station.

Option B was selected as the basis for the METRIC processing because of the more uniform image coverage, and because it is more recent compared to option A.

Table 1. Possible image dates for METRIC processing, option A. Suggested image dates are highlighted in yellow.

Image date	Year	Satellite	GDD date* Base=2002	Comments
Feb 19	00	L5	n/a	
Mar 20	99	L5	n/a	
Apr 8	03	L7	Apr 6	Not much green on fields
May 10	06	L5	May 16	Late year (06 vs. 99-03 for the rest of the images)
May 20	01	L7	May 23	Rating: 0.9 few cumulus over agric areas
May 23	99	L5	May 24	
Jun 21	01	L7	Jun 23	
July 2	02	L5		
July 10	02	L7		
July 12	00	L5	Jul 14	
July 18	02	L5		Maybe some smoke in N part
July 26	99	L5	July 21	
Aug 3	99	L7	July 29	
Aug 16	01	L5	Aug 18	
Aug 21	00	L7	Aug 26	
Aug 29	00	L5	Sep 2	
Sep 12	02	L7		
Sep 28	02	L7		
Oct 8	00	L7	Oct 10	Still some green on fields
Oct 14	02	L7		Smoke?
Oct 30	02	L7		Snow in SW part of valley – very little green on fields
Dec 3	00	L7	Nov 21	

*Corresponding date in 2002 based on GDD, i.e. which date in 2002 reached the GDD as this date in year X (example: the GDD on Apr 8 2003 = 50.3; in 2002, this GDD value was reached on Apr 6).

Table 2. Possible image dates for METRIC processing, option B. Suggested image dates are highlighted in yellow.

Image date	Year	Satellite	GDD date* Base=2006	Comments
Feb 19	06	L5	n/a	
Mar 4	05	L5	n/a	
Mar 28	08	L5	n/a	
Apr 8	03	L5	Apr 6	
Apr 13	08	L5	Apr 9	Very little green in agric area
May 10	06	L5		
May 18	06	L7		Note: Landsat 7 SLC-off
May 31	08	L5	May 22	Few cumulus, agric area cloud free
Jun 21	04	L5	Jun 15	
Jun 27	06	L5		
Jul 16	07	L5	Jul 14	
Jul 21	03	L5	Jul 17	
Aug 1	07	L5	Aug 1	
Aug 14	06	L5		
Aug 27	05	L5	Aug 18	
Sep 2	07	L5	Sep 2	
Oct 1	06	L5		
Oct 27	04	L5	Oct 6	

*Corresponding date in 2006 based on GDD, i.e. which date in 2006 reached the GDD as this date in year X (example: the GDD on Apr 8 2003 = 50.3; in 2006, this GDD value was reached on Apr 6).

Appendix C
Vertical shift in the thermal band in the Landsat 5 images over the Flathead Lake area
J. Kjaersgaard and R. G. Allen, September 2008

It has previously been found (Trezza and Allen, 2008) that the thermal band (band 6) of Landsat images is shifted, or misregistered, by up to 120 m in the north-south direction as compared to the remaining bands following terrain correction performed by the USGS Earth Resources Observation and Science, EROS. The thermal band is shifted in the southerly direction. The shift is generally considered to be consistent throughout the image.

The source of the shift is not clear, but it arises during the terrain correction preprocessing of the raw Landsat images performed by EROS using the NLAPS preprocessing system and where the 120 m pixels for the thermal band are resampled to 30 m pixel size. When the terrain correction is undertaken by other image preparation providers, this shift does not occur. The shift may or may not occur in increments divisible of 30 m.

It is important that the pixels of all seven bands in the Landsat image “line up” in order to perform a correct calibration when using the METRIC model to estimate the energy balance components.

The images used in the energy balance estimations in the Flathead Lake area were prepared (including terrain correction) by EROS. The images were screened and corrected for this thermal shift.

Screening
The screenings was done by displaying bands 2, 3, 4 (false color) and the thermal band side-by-side in ERDAS Imagine Viewers and identifying locations with sudden changes in land surface cover, such as a water-land interface, edges between irrigated fields and surrounding dry rangeland or desert. Normalized Difference Vegetation Index, NDVI and lapse corrected surface temperature, T_{s_dem} for approximately 20 pixels north and south of the land cover change wweresampled at a number of these break points throughout the Landsat image for each image date. Great care must be taken during the selection of break points to identify points that are representative for the area. The data was imported into a spreadsheet and the covariance was calculated while shifting the thermal pixel values incrementally 30 m north, i.e. 0, 30, 60, 90 and 120 m north. The covariances are used to indicate the magnitude of the shift. This magnitude is controlled by comparing break points throughout images visually.

An example of the shift is shown in Figure 1. On the left side of the figure is a portion of Flathead River shown in false color (shortwave bands 2,3 and 4), while the T_{s_dem} for the same portion of the river is shown on the right. In the false color image, green vegetation shows up as red, bare soil is tan to brown while water is dark blue. In the T_{s_dem} image temperatures are shown in grey scale with bright hues indicating warmer temperatures and darker hues indicating colder temperatures. The water in the river is colder than the predominantly bare soil along the river. The pixel sizes of the shortwave bands are 30 m and the original pixel size of

the thermal band is 120 m, causing the T_{s_dem} to have a coarser resolution and a more jagged appearance. The crosshair in the images is placed at the same location in accordance to the projection. While the crosshair is in the middle of the river on the false color image, it is north of the river on the T_{s_dem} image indicating the shortwave and long-wave bands do not overlap.

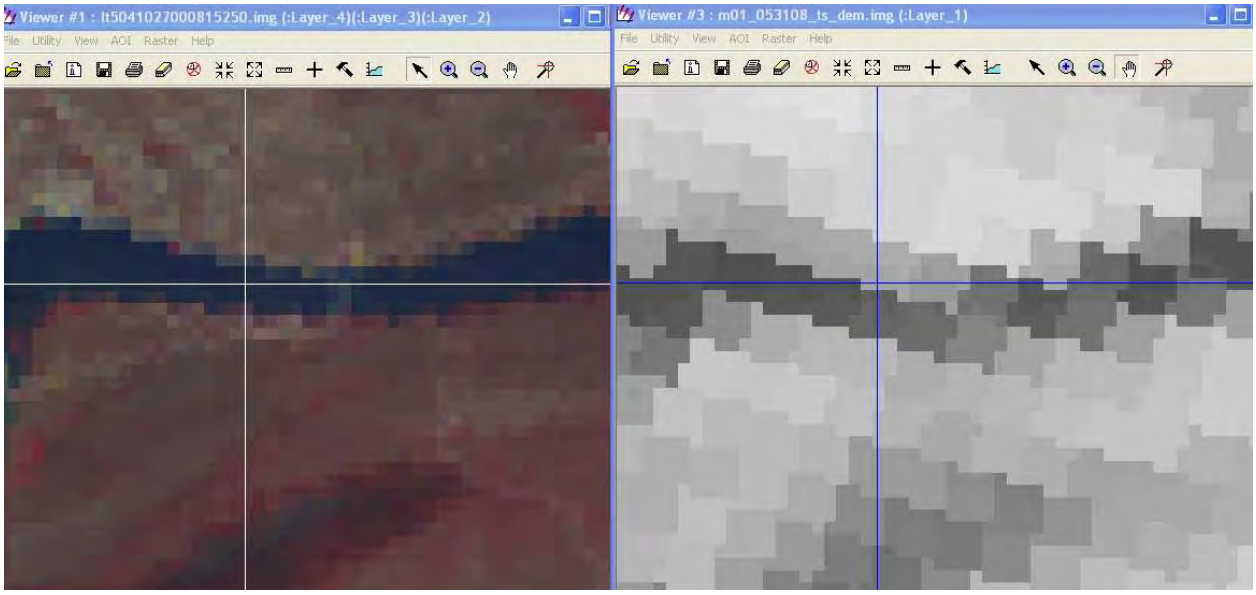

Figure 1. Incongruent depiction of the location of the Flathead River between a false color image (left) and elevation adjusted surface temperature map for May 31, 2008. The cross hair is at the same location.

Shift

As a result of the screening incongruencies were found between the shortwave and longwave band for all eight images. The vertical shift is shown in Table 1. No shift was found in the east-west direction.

Table 1. Vertical (north-south) shift between shortwave and longwave bands in the Landsat images.

Image date	Shift (m)
04/13-2008	60
05/10-2006	60
05/31-2008	60
06/27-2006	30
07/16-2007	60
08/01-2007	60
09/02-2007	60
10/01-2006	60

To correct the misalignment, the thermal bands were shifted upward relative to the shortwave bands by the distance shown in Table 1 prior processing. The shifting was done prior layer stacking by displaying band 6 in an ERDAS Imagine Viewer, open the Layer Info dialog, select Edit – Change Map Model, and add the shift (30 or 60 m) to the coordinate in the Upper Left Y box. The 7 bands (including the shifted band 6) are subsequently stacked the normal way.

It is noted, that the north and south edges of the shortwave bands and the thermal band no longer has the same geographical extent after the shift. This may cause problems with 'undefined numbers' along the north and south edges of the image (2 pixel layers thick) in some of the products from the METRIC processing. This can be avoided by e.g. defining an Area of Interest, AOI, limiting the METRIC calculations to be carried out for the largest common area i.e. only on pixels that have valid numbers for both the shortwave and the longwave bands.

A model to create a mask for the largest common area is shown in Figure 2. Inputs are the 7-band Landsat image, the DEM and the LU map. The background value must be specified in the two scalar boxes for the DEM and the LU (normally 0, if no background value is present in the image, the background value should be set to a value lower than the smallest pixel value occurring in the image). The output is a binary map, where pixels that are common across all

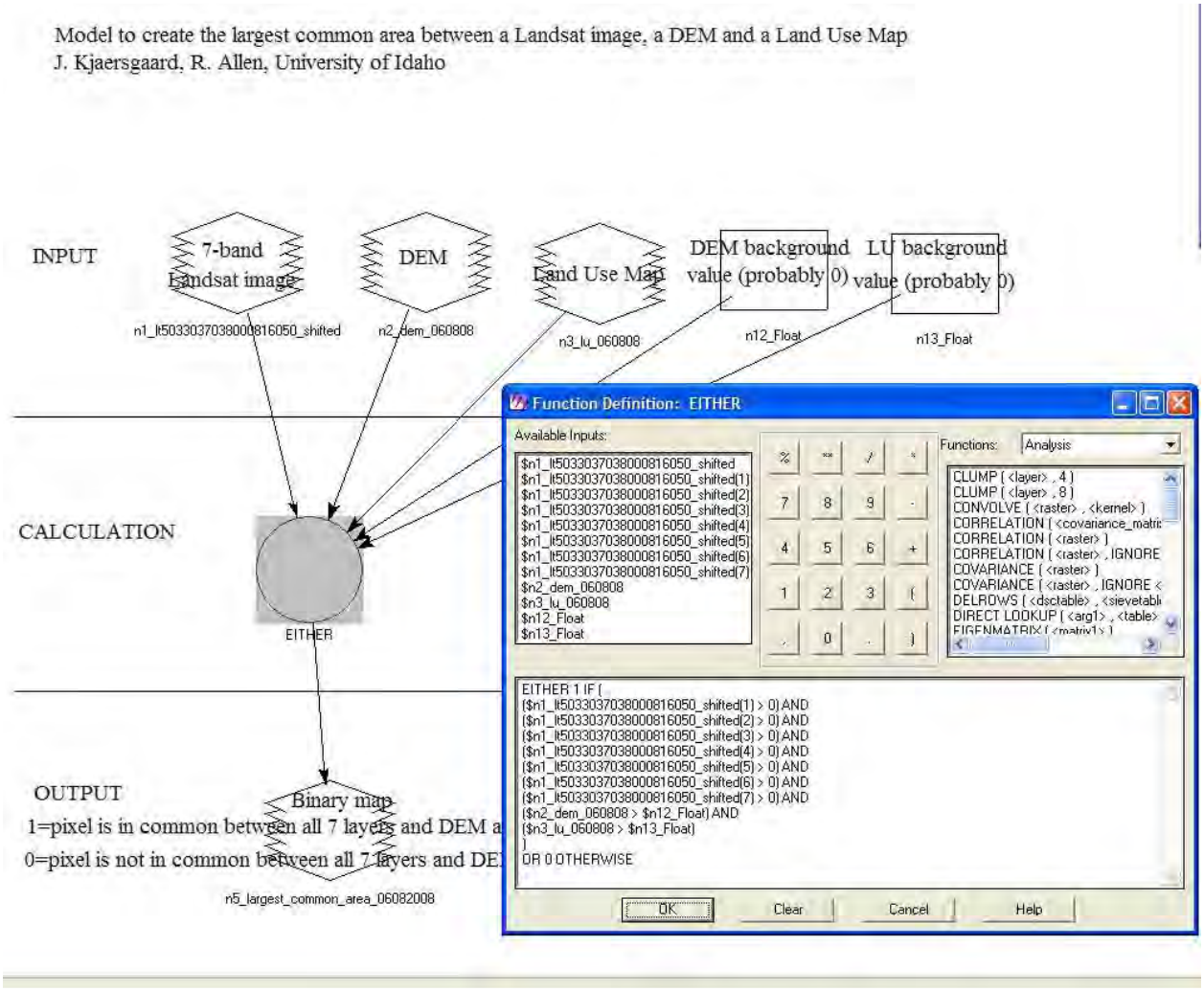

Figure 3. Model to calculate the largest common area between the 7-band Landsat image, the DEM and the Land Use map. In the model above the background value for the DEM and the LU must be specified (they are normally 0). The function is shown in the dialog on the right.

seven bands and the DEM and the LU have the value 1 and all pixels that are not present in all seven bands and the DEM and the LU have the value 0. This binary map can be used as the input file when creating the AOI as outlined by e.g. Kjaersgaard (2009).

References

Kjaersgaard, J., 2009. Defining an AOI in ERDAS Imagine to the exact outline of an existing image. Technical Report, University of Idaho, Kimberly, Idaho. 4 pp.

Trezza, R., Allen, R.G., 2008. Analysis of vertical shift in Band 6 of Landsat 5 images in the EROS L1T product. University of Idaho, Kimberly, Idaho. 25 pp. Accessed online on June 17 2009 at http://www.idwr.idaho.gov/GeographicInfo/PDFs/trezza-allen-thermal-band-shift.pdf

Appendix D.
Maps of Land-Use and Elevation for the Mission Valley, Mt application
J. Kjaersgaard and R. G. Allen, University of Idaho. September 2008

The purpose of this note is to summarize the land use maps (LU) and elevation maps available for the Mission Valley, MT application of METRIC.

Digital Elevation map
A digital elevation map, DEM, at 30 m resolution was downloaded in GeoTiff format from the national elevation dataset, NED at http://seamless.usgs.gov/. The map was converted into an Imagine file using the ERDAS import function and reprojected into the desired projection using cubic convolution. The DEM was downloaded as several overlapping sub-maps, which were "stitched" together in one operation using the "StackLayers" followed by the "Stack Max" procedures in ERDAS Imagine Modelmaker creating a seamless DEM for an area slightly larger than the p41 r27 Landsat scene. The boundaries of the DEM are tailored to fit the geographic extent of each Landsat 5 scene.

Land-Use map
Two LU maps immediately available at 30 m resolution were considered for use to support the METRIC processing, *viz.* the NLCD 2001 and the SILC. Both LU map systems cover offers full coverage at a 30 m resolution of the geographical area covered by the Landsat 5 image. The LU maps were reprojected into the desired projection using nearest neighbor.

National Land Cover Database (NLCD) 2001
The USGS has produced national land use maps since the 1960s. The most current maps are from the National Land Cover Dataset based on satellite imagery acquired in 2001 (NLCD 2001). A newer version, based on 2007 imagery, is currently being prepared by the USGS but is not yet available. The classification system as it applies to the Mission Valley and surrounding area is shown in Table 1. The NLCD land cover classification is identical for the entire United States and the classification lacks detail about e.g. crop type for agricultural land use or areas with natural vegetation. More information about the land use system can be found at http://landcover.usgs.gov/usgslandcover.php The NLCD 2001 was downloaded in GeoTiff format from the USGS seamless server, http://seamless.usgs.gov/. The map was drawn to cover the entire p41 r27 Landsat scene.

Table 1. National Land Cover Database 2001 classification. Also shown is assumed vegetation height for selected land use categories and the momentum roughness length, z_{om}.

Class	Classification category	Vegetation height (m)	z_{om} (m)
11	Open water		0.0005
12	Perennial ice/water		0.0005
21	Developed, open space		0.05
22	Developed, low intensity		0.05
23	Developed, medium intensity		0.05
24	Developed, high intensity		0.05
31	Barren land		0.005
41	Deciduous forest	15 – 20	0.5
42	Evergreen forest	10 - 15	0.5
43	Mixed forest		0.5
52	Shrub	2-5	0.2
71	Grassland/herbaceous	0.2	0.02
81	Pasture/hay		Agric *f*
82	Cultivated crops		Agric *f*
90	Woody wetlands	7 - 15	0.1
95	Emergent herbaceous wetlands	0.5	0.05

Satellite Imagery Land Cover (SILC) and MT-GAP

The satellite imagery land cover (SILC) program was started in the early 1990s at the University of Montana. The SILC map covering western Montana (including the p41 r27 Landsat image) was developed in 1996 using Landsat TM images acquired during 1991 – 1993 followed by ground truthing to minimize misclassifications. More information about this land cover classification program may be found at http://www.wru.umt.edu/project/silcpage/index.html. The 50 classes of the classification system are shown in Table 2.

The SILC map of Western Montana was used along with other SILC maps to generate the MT-GAP land use map. The MT GAP land use classification is part of a nationwide effort seeking to "identify the degree to which all native plant and animal species and natural communities are or are not represented in our present-day mix of conservation lands". GAP maps are produced by each state based on guidelines provided by USGS Biological Resources Division.

A MT-GAP land use map was downloaded for the entire state of Montana from http://www.wru.umt.edu/project/silcpage/index.html. Metadata for the MT-GAP may be found at http://www.wru.umt.edu/project/silcpage/mtcov30.htm. The downloaded file was compressed using gzip.

Table 2. Satellite Imagery Land Cover classification

Class	Classification category	Class	Classification category
1	Urban or developed lands	**26**	Western larch
2	Agricultural lands – dry	**27**	Utah juniper
3	Agricultural lands – irrigated	**28**	Douglas fir/lodgepole pine
4	Altered herbaceous	**29**	Mixed whitebark forest
5	Very low cover grassland	**30**	Mixed subalpine forest
6	Low/moderate cover grassland	**31**	Mixed mesic forest
7	Moderate/high cover grassland	**32**	Mixed xeric forest
8	Montane parkland and subalpine meadows	**33**	Mixed broad leaf and conifer forest
9	Mixed mesic shrubs	**34**	Standing burnt forest
10	Mixed xeric shrubs	**35**	Water
11	Silver sage	**36**	Conifer riparian
12	Salt desert shrub/flats	**37**	Broadleaf riparian
13	Sagebrush	**38**	Mixed conifer and broadleaf riparian
14	Mesic shrub-grassland association	**39**	Graminoid and forb riparian
15	Xeric shrub-grassland association	**40**	Shrub riparian
16	Low density xeric forest	**41**	Mixed riparian
17	Mixed broadleaf forest	**42**	Rock
18	Logdepole pine	**43**	Mines, quarries, gravel pits
19	Limber pine	**44**	Badlands
20	Pondarosa pine	**45**	Missouri breaks
21	Grand fir	**46**	Mixed barren sites
22	Western red cedar	**47**	Alpine meadows
23	Western hemlock	**48**	Snowfields or ice
24	Douglas fir	**49**	Clouds
25	Rocky mountain juniper	**50**	Cloud shadows

Recommendation of LU map

A major difference between the NLCD and the SILC LU maps is the acquisition dates of the satellite images they are based upon. The SILC map does not capture some more recent changes in land use. Some examples are e.g. found South of Polson (East of the Pablo reservoir), where several gravel pits are classified as agriculture, riparian or various forms of forest, and in the vicinity of the urban centers (especially around Polson) where recent housing developments have replaced other land use types. The NLCD maps captures more of these more recent changes in land use.

A comparison of the NLCD and SILC maps to Google Earth and high resolution NAIP aerial photos from 2005 show some inaccuracy in the classification of riparian areas in the SILC map. Examples include the Mission Valley Speedway arena (established in 1973 with the track asphalt sealed in 1977) classified as riparian, and several agricultural fields or sections of fields classified as riparian (perhaps due to (surface) irrigation at the satellite overpass moment) and as salt desert shrub/dry salt flats.

The SILC map lacks identification of most roads, large farmsteads and other permanent human made structures in the rural areas. These structures are generally assigned the same class as

the immediate surrounding area. Many of the larger road and farmsteads are correctly classified as “Developed” in the NLCD LU map.

Many agricultural fields (probably used for pasture) in the eastern portion of the Mission Valley along the Mission Range are classified as low/moderate grasslands in the SILC LU map. This land cover class is also used for the dry rangeland in the western portions of the Mission Valley. During a ground truth campaign on June 27 – 29 2008 it was found that vegetation in the agricultural fields in the eastern part of the valley generally has dense, green and uniform vegetation and is irrigated, while the vegetation in the rangeland in the western portion of the valley is more typical of drier conditions with sparse vegetation that does not cover the ground completely and is non-uniform regarding plant height, species and vigor.

The SILC LU map has more detail about the tree species in forested areas (primarily in mountainous areas) and land cover type in areas with natural vegetation (primarily in the dry, western porting of the reservation) compared to the NLCD map.

Based on the comparison, the NLCD LU map was found to be best suited to be used during the METRIC processing for all classification categories. The primary focus in the study is energy balance estimation for agricultural areas, where the NLCD map is more consistent and in better agreement with Google Earth and the NIAP photos than is the SILC map. Also, the higher degree of detail in the SILC map for areas with natural vegetation does not seem fully justified considering the many misclassifications between agricultural land and various natural vegetation types (typically classes 6 and 13 in table 2) types and visual comparison to Google Earth, NIAP photos and impressions and photos collected during a June 27 – 29 ground truth campaign in the Mission Valley.

Appendix E
Adjustments to METRIC during the Processing of the Landsat Images
By J. Kjaersgaard and R. G. Allen, University of Idaho, June 2009.

During the processing of the eleven 2008 Landsat images for the Mission Valley using METRIC, the model was adjusted to account for conditions that deviate from the description of a standard Level 1 METRIC model setup. These adjustments are referred to as Level 2 processing (Allen et al., (2008). Some of the Level 2 adjustments have been applied in previous applications of METRIC while other adjustments address factors specific to the Mission Valley. The adjustments are described in the following.

1. Elevation effects on surface temperature
The surface temperature (T_s) is used to estimate (among other things) the near surface air temperature gradient in METRIC. Changes in T_s caused by elevation must be accounted for using a lapse rate correction. The correction mimics the T_s of each pixel if all pixels were at the same datum elevation. For areas located at a higher elevation than a datum point, the correction will increase the T_s. The correction will decrease the T_s for areas located at an elevation below the datum. In METRIC, the elevation corrected T_s is only used during the estimation of sensible heat flux.
The environmental lapse rate (wet adiabatic) of 6.5 °C/km is used in most Level 1 METRIC processing applications. For Level 2 METRIC processing Allen et al. (2004) developed a procedure to customize the lapse rate estimations for each image which includes two modifications:

A) Use of different lapse rates for flat and sloped surfaces:
   The near surface atmospheric conditions are highly influenced by the ground surface. For flat areas an equilibrium lapse rate is developed depending on atmospheric conditions and surface characteristics. The environmental lapse rate may not sufficiently describe the lapse rate that develops over the flat areas present within the Landsat images, including the river valley and the flat desert areas. Sloped surfaces representing more mountainous terrain alters, mechanically, the vertical motion of the air masses, which may be described by a constant lapse rate. For the Mission Valley application two different lapse rates were determined and used for each image, with the transition between the “flat” and the “sloped” rates occurring at elevations above the highest laying desert floor areas, which was estimated to be at an elevation of 1000 m.
B) Customized “flat” lapse rates for each image
   The air lapse rate changes with water vapor content and weather conditions. It is reasonable to expect a unique lapse rate for each image, rather than a fixed rate for each image such as 6.5 °C/km. The technique to calibrate an image specific lapse rate developed by Allen et al. (2004) was adopted for the Mission Valley. The technique assumes that the surface/air temperature is well synchronized and is only applied to areas within the image that are relatively flat (slope less than 5 degrees) to reduce the impact of radiation loading on slopes.
   The lapse rate is derived by graphing T_s versus elevation, as shown in Figure 1.1. In the T_s versus elevation plots the line of highest temperature for each elevation level

represents conditions of low vegetation or bare soil. Similarly, the line with lowest temperatures for each elevation level represents areas with high vegetation and high evapotranspiration rates. The primary elevation range evaluated was 750-1400 m, since this elevation range covers most of the flat portions of the Mission Valley area.

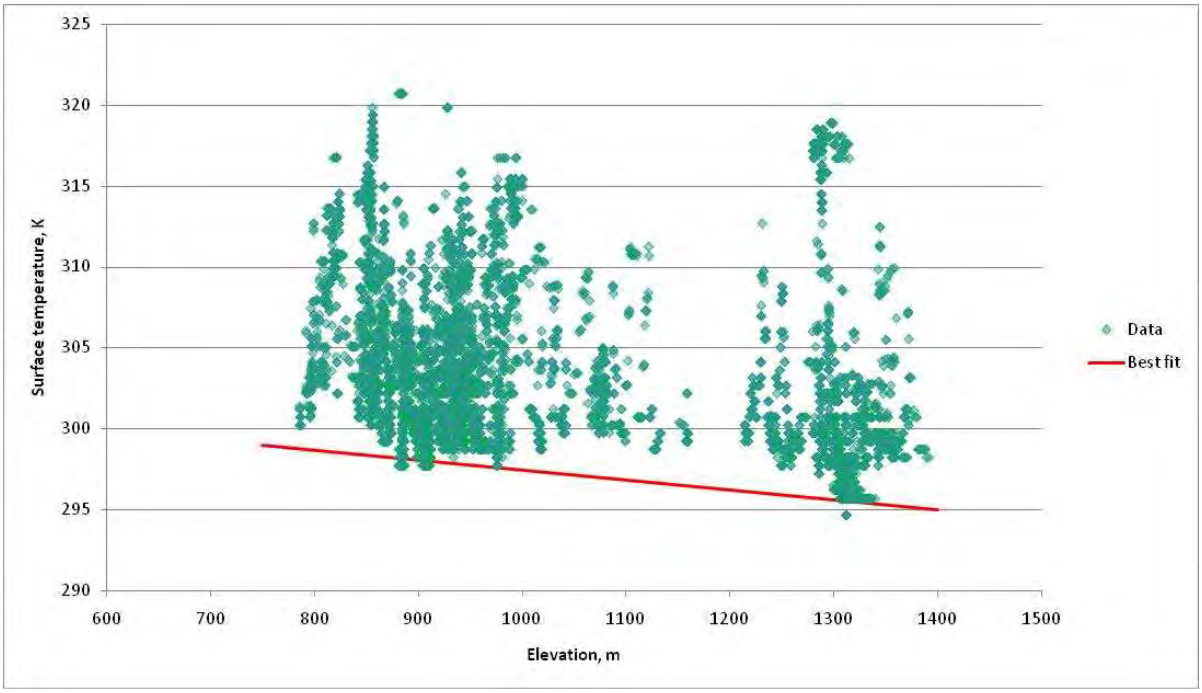

Figure 1.1. Determination of lapse rate for June 27 2006 based on a sample of 7700 sample points of elevation and surface temperature (T_s). The estimated lapse rate for horizontal areas is shown as a red line. All points are from surfaces having less than 5 degree slope.

Table 1.1. Lapse rates applied for each image.

Image date	Lapse rate (°C/km)	
	Flat	Sloped
04/13-2008	7	10
05/10-2006	7	10
05/31-2008	3	10
06/27-2006	6	10
07/16-2007	3	10
08/01-2007	7	10
09/02-2007	5	10
10/01-2006	7	10

The lapse rate calibration method could not be used for mountainous areas because the radiation loading on slopes alters the surface temperature of otherwise similar dry surfaces. In addition, there are very few dry surfaces near the mountain tops in the images. For mountainous areas in the Mission Valley region a dry adiabatic lapse rate of 10 °C/km applied. A lapse rate of 10 °C/km was assumed to be more appropriate than the wet adiabatic lapse rate of 6.5 °C/km because the relatively dry air in the mountains

normally will not have condensation of water vapor with increase in elevation. The "flat" and the "sloped" lapse rates applied for the Mission Valley are shown in Table 1.1. In addition, steep mountain slopes are more conducive to air masses following more vertical pathways through the atmosphere, and therefore more likely to follow the univerversal gas law, which suggests the 10 C/km.

2. Estimation of incoming longwave radiation on slopes

In METRIC, longwave incoming radiation R_{li} is estimated based on surface temperature (Allen, 2000; Allen et al., 2008). For sloped surfaces R_{li} is adjusted using an isotropic sky view factor to account for the reduction in hemispherical sky view angle "visible" to the slope compared to a horizontal surface, and adjusted for incident longwave radiation emitted from "visible" horizontal land surfaces.

In previous applications of METRIC it was found (Kjaersgaard and Allen, 2009) that for mountainous areas R_{li} is likely overestimated on south facing slopes (facing towards the sun) while R_{li} is underestimated on north facing slopes (facing away from the sun) due to the lower or higher emissions from opposing valley slopes that was not accounted for. The result is an overestimation of ET_rF on south facing slopes and an underestimation of ET_rF on north facing slopes. The mountains are characterized by having relatively steep slopes and most mountain slopes are facing other slopes across narrow valleys.

The errors in L_{in} in mountainous terrain occur because the R_{li} for each pixel is calculated based on the T_s of that pixel, only, without accounting for the terrain around or opposing the pixel. On north facing slopes, having a T_s that is relatively cooler because they face away from the sun, this results in a relatively lower R_{li} estimate not accounting for the R_{li} emitted from the opposing warmer south facing slope. Similarly, south facing slopes, having a T_s that is relatively warmer because they face the sun, which results in a too high R_{li} estimate since the opposing slope is a cool north facing slope.

The error may be accounted for by adjusting the surface temperature used for estimating R_{li} emitted from "visible" opposing surfaces for slopes greater than 5 degrees as

$$T_{s\_terrain} = \frac{T_s}{[1-(k-\frac{\pi}{2})\times\frac{10}{273}]} \qquad (2.1)$$

where $T_{s\_terrain}$ is the surface temperature used to estimate L_{in} emitted onto an incline from visible surfaces on slopes, T_s is the surface temperature estimated by METRIC and k is the terrain aspect angle minus the solar azimuth angle. k is zero when the terrain slope is facing the sun beam at a right angle and π when the slope is facing away from the sun. The resulting adjustment to T_s is up to circa ± 5.7 % depending on the orientation of the slope.

3. Stability correction in mountainous terrain

The convergence of flow lines as the wind passes over a sloped surface will impact the atmospheric stability correction. In addition, the general upward movement of air flow up a

slope tends to accelerate motions of buoyance, thereby increasing the impact of instability of the near surface air layers on aerodynamic conductance. In Level 2 METRIC processing this phenomenon is accounted for by adjusting the final iteration of the stability correction function for areas having a slope greater than 5 degrees. The correction takes on different forms depending on the stability of the atmosphere (see e.g. Allen et al., 2008 for reference on the stability correction).

For unstable conditions, i.e. if the Monin-Obukhov length (L) is less than zero the integrated stability corrections for momentum and heat transport, ψ_m and ψ_h, are adjusted as follows:

$$\psi_m = \psi_{m0} \times \left[1 + \frac{s-5}{45}\right] \text{ for L<0} \qquad (3.1)$$

and

$$\psi_h = \psi_{h0} \times \left[1 + \frac{s-5}{45}\right] \text{ for L<0} \qquad (3.2)$$

where s is slope greater than 5 degrees and ψ_{m0} and ψ_{h0} are the stability corrections for momentum and heat transport (Paulson, 1970; Webb, 1970, c.f. Allen et al., 2008).

For neutral atmospheric conditions, defined as when L is equal to zero, no correction is applied.

For stable conditions, i.e. if the Monin-Obukhov length (L) is greater than zero the integrated stability corrections for momentum and heat transport, ψ_m and ψ_h, are adjusted as follows:

$$\psi_m = MIN(\psi_{m0} \times 0.1, \psi_{m0} \times \left[1 - \frac{s-5}{45}\right]) \qquad \text{for L>0} \qquad (3.3)$$

and

$$\psi_h = MIN(\psi_{h0} \times 0.1, \psi_{h0} \times \left[1 - \frac{s-5}{45}\right]) \qquad \text{for L>0} \qquad (3.4)$$

where s is slope when greater than 5 degrees and ψ_{m0} and ψ_{h0} are the stability corrections for momentum and heat transport (Paulson, 1970; Webb, 1970, c.f. Allen et al., 2008).

4. Estimation of momentum roughness length for tall vegetation

The current 'agricultural function' used to estimate momentum roughness length, z_{om} for agricultural crops in METRIC is based on a linear relationship between z_{om} and crop height

$$z_{om} = 0.12h \qquad (4.1)$$

where h is crop height for dense agricultural crops. The relationship in Eq. 4.1 is used in e.g. FAO56 (Allen et al., 1998). Crop height h (m) is estimated based on LAI as

$$h = 0.15LAI \qquad (4.2)$$

where LAI is Leaf Area Index. The relationship in Eq. 4.2 can be compared to height vs. LAI for common agricultural crops in the Fig. A2-2 in appendix 2 of the METRIC manual (Allen et al. 2008).

The functions in Eq 4.1 and 4.2 assume a linear relationship between LAI and z_{om}, i.e. higher vegetation density (expressed as LAI) translates linearly into higher z_{om}. This assumption does not reflect the roughness conditions of e.g. orchards, forests or othewr areas with tall vegetation. For orchards and surface cover types of tall vegetation the z_{om} increases as the vegetation gets denser until some threshold density is reached. This is because that as long as the stand density of trees is somewhat sparse, the zero plane displacement height is close to the ground. As the trees grow taller, or more trees are added to the sparse stand, the roughness increases until the point where the vegetation density is high enough to bring the zero plane displacement height from the ground and up into the canopy. As the stand density increases beyond the threshold density, the surface becomes more aerodynamically smooth and the roughness decreases.

To estimate the z_{om} of tall vegetation a function developed by Perrier (1992) was employed (also described in the ASCE Hydrology Handbook (1996), p 197 – 199):

$$z_{om} = \left(\left(1 - \exp\left(\frac{-aLAI}{2}\right)\right)\exp\left(\frac{-aLAI}{2}\right)\right)h_p \qquad (4.3)$$

The parameter "a" is an adjustment factor for LAI distribution within the canopy with a = (2*f*) for $f \geq 0.5$ and a = $(2(1\text{-}f))^{-1}$ for $f < 0.5$. The factor *f* is the proportion of LAI lying above h/2, i.e. *f* = 0.3, 0.5 and 0.7 indicates sparsely topped canopy, uniform canopy and top heavy canopy, respectively. Based on photographic documentation and visual field observations a value for *f* of 0.6 was found to be appropriate for most tall vegetation types.
The height h_p (m) of the tall vegetation is estimated as

$$h_p = 2.5LAI \quad (4.4)$$

which corresponds to a maximum stand height of circa 15 m. The relation between LAI and z_{om} is shown in Figure 4.1 and the z_{om}/h ratio as function of LAI is shown in Figure 4.2.

Equation 4.3 and 4.4 was used to estimate the Z_{om} for areas of fruit orchards, forests and riparian vegetation during the METRIC processing. These vegetation typed were identified using the land use map.

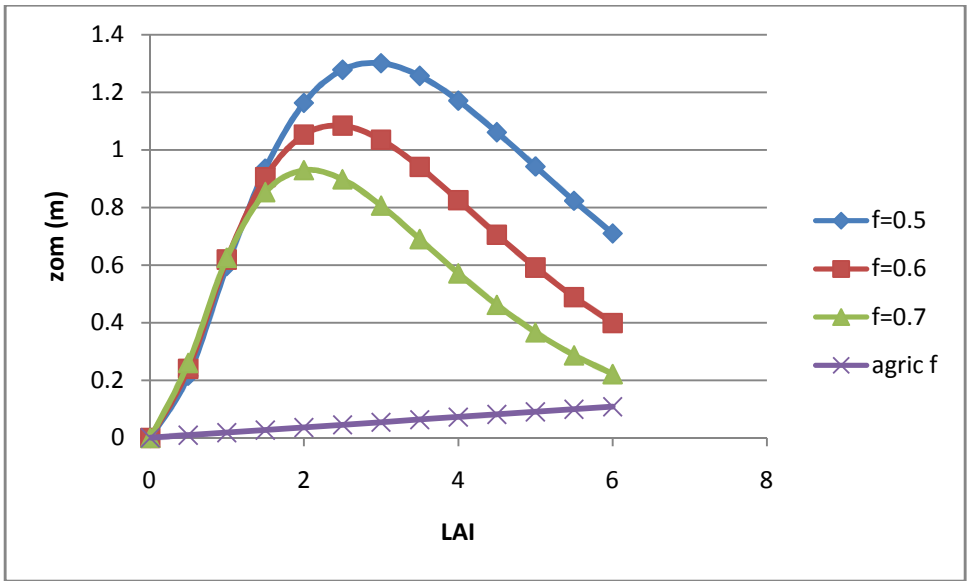

Figure 4.1. Momentum roughness length (z_{om}) estimated using eq. 4.3 as function of LAI for different values of f. Also shown is the agricultural function, eqs. 4.1 and 4.2

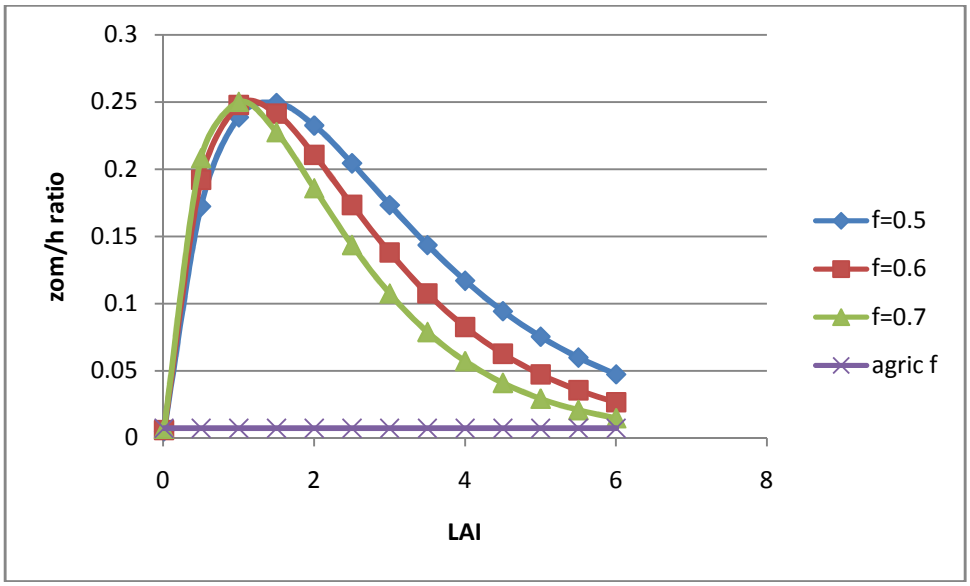

Figure 4.2. Ratio of momentum roughness length (z_{om}) to the height of tall vegetation h_p as function of LAI for different values of f. Also shown is the agricultural function, eqs. 4.1 and 4.2

5. Total hemispherical albedo estimation

The albedo from a vegetated surface depends not only on the reflective properties of the canopy but also on the proportion of sunlit and shadowed areas within the canopy and on visible ground. For tall vegetation including the forests in the Mission Valley the trees have some spacing between individual trees and shadows cast by one tree onto a neighboring tree. These shaded areas are may reduce the apparent reflection sensed by nadir looking satellites, such as Landsat, leading to estimates of albedo which are too low. Trezza and Allen (2009) compared the bidirectional albedo (it depends on solar elevation angle and sensor angle)

estimated using Landsat imagery to the directional hemispherical albedo estimated from the MODIS satellite imagery. They suggested calculating total hemispherical albedo from the bidirectional albedo estimates from Landsat as

$$albedo_{tot\_hem} = MAX(0.12, (0.16 - 0.16\cos(\theta)) + albedo_{bidir}) \qquad (5.1)$$

where $albedo_{tot\_hem}$ is the total hemispherical albedo, θ is the solar zenith angle and $albedo_{bidir}$ is the bidirectional albedo estimated from Landsat imagery.

Equation 5.1 was used to estimate the total hemispherical albedo for forests, orchards and tall riparian vegetation during the METRIC processing.

6. Tall vegetation canopy temperature

The development and algorithms of a procedure to estimate the canopy temperature of tall vegetation is described in Appendix F.

References

Allen, R.G., 2000. RAPID long-wave radiation calculations and model comparisons. Internal Report, University of Idaho, Kimberly, Idaho.

Allen, R.G., Tasumi, M., Trezza, R., Kjaersgaard, J.H., 2008. METRIC Applications Manual. Version 2.0.4. University of Idaho, Kimberly, Idaho. 164 pp.

Kjaersgaard, J. H., Allen, R.G., 2009. Adjustment of longwave incoming radiation on slopes. Technical Note, University of Idaho, Kimberly, Idaho. 2 pp.

Trezza, R., Allen, R.G., 2009. Albedo analysis for pecan trees in the LRG area. Technical Report, University of Idaho, Kimberly, Idaho. 19 pp.

Appendix F
Development of an Algorithm to Estimate Vegetation Temperature in Canopies of Tall Vegetation

J. Kjaersgaard and R. G. Allen, University of Idaho, March 2009.

Complex canopies of tall vegetation such forests and orchards as have a mixture of sunlit canopy, shaded canopy, sunlit soil, and shaded soil surfaces. Each of these surfaces tends to reflect a different fraction of solar radiation and tends to have different surface temperature. The mixture of surface temperature observed from a satellite depends on the view angle of the satellite, on the sun angle, and on the height and density of the vegetation. In the case of Landsat satellites, the view angle of the satellite is from nadir, meaning the satellite points vertically downward and therefore sees only radiation that is emitted or reflected in a completely vertical direction upward.

In the application of METRIC to the Mission Valley area, an adjustment was made to the surface temperature observed by Landsat to reduce biases in the temperature caused by the nadir view angle, which is subject to viewing a disproportionate amount of shadows and sunlit soil, as compared to a hemispherically integrated view of surface temperature. The adjustment of the surface temperature measurement to better approximate canopy temperature of forests is considered to provide an improved estimate of sensible heat transfer within the METRIC model and thus, better estimates of evapotranspiration. The sunlit canopies of mature tree stands are the primary source of energy exchange since these are the areas of most solar energy interception and the areas having the most aerodynamic exposure.

For a two-source condition of thermal emission (vegetation and soil), Norman et al. (1995) suggested calculating radiometric temperature as

$$T_s=[f_c\, T_c + (1- f_c)\, T_s] \qquad (1)$$

where f_c is fraction canopy cover, and T_c and T_s are vegetation canopy temperature and soil surface temperature.

For a three-source condition, as experienced with tall vegetation, this can be extrapolated to

$$T_s = f_c\, T_c + f_{shadow}\, T_{shadow} + f_{sunlit}\, T_{sunlit} \quad (2)$$

where f_c, f_{shadow} and f_{sunlit} are the relative fraction of vegetation, shadow and sunlit ground surface, respectively when viewed from nadir so that $f_c + f_{shadow} + f_{sunlit} = 1$. T_c, T_{shadow} and T_{sunlit} are the temperature of the canopy, the shaded ground surfaces and the sunlit ground surfaces, respectively.

The effective temperature of the energy exchange location can be estimated by solving Eq 2 for T_c when assuming T_s is the surface temperature estimated from Landsat using METRIC.

T_{shadow} and T_{sunlit} are estimated as a function of the temperatures of the hot and the cold anchor pixels and the wet bulb temperature estimated based on air temperature and humidity information from a suitable nearby weather station.

Some of the areas identified as forest in the 2001 NLCD land use map are relatively young forests following recent cuttings where the radiometric footprint is dominated by the bare ground between the young trees and sparse low vegetation resulting in low vegetation indices. The energy exchange between the surface and the atmosphere in these young stands is primarily occurring at the ground surface as opposed to more mature stands, where most of the energy exchange occurs at some height above the ground surface in the canopy of the trees. Following this, the estimation of effective T_c (T_{c_eff}) from the tree canopies is limited to

$$\begin{aligned} T_{c\_eff} &= T_s && \text{for LAI} \le 1 \\ T_{c\_eff} &= 2(LAI-1)T_c + (1-2(LAI-1))T_s && \text{for } 1 < \text{LAI} < 1.5 \\ T_{c\_eff} &= T_c && \text{for LAI} \ge 1.5 \end{aligned} \qquad (3)$$

where LAI is leaf area index.

In some of the young stands herbaceous vegetation partially or fully covers the ground between trees. The “greenness” of the cover vegetation will increase the vegetation index of those orchards leading to an increase in vegetation indices above the thresholds for correction of T_c.

The estimation of fraction ground cover of vegetation and fraction of the ground surface that is shaded by vegetation or sunlit when viewed from nadir is described in the following.

1. Estimation of fraction vegetation cover and clumping factor

Norman et al. (1995) and Kustas and Norman (1999) suggest calculating fractional canopy cover (f_c) for a uniformly distributed canopy that is viewed from nadir as

$$f_c = 1 - \exp(-0.5LAI) \qquad (4)$$

For row crops with a more ‘clumped’ canopy (such as row crops and trees) a clumping factor (Ω) is used to adjust the LAI, *viz*. ΩLAI, for the uneven canopy distribution across the land area. Ω ranges from 0 to 1, where 1 indicates no clumping (spatial uniform canopy distribution) and 0 indicates extreme clumping. Kustas and Norman (1998) quote values for Ω when viewed from nadir (Ω(0)) of 0.7-0.8 for row crops. Table 1 lists some values of Ω(0) for mature stands of different tree species (Campbell and Norman, 1998). Based on photographic documentation and Table 1, a general Ω(0) value of 0.7 for mixed forest seems reasonable.

The f_c of the forests as “seen” by a nadir looking satellite can thus be estimated as

$$f_c = 1 - \exp\left(-0.5\Omega(0)LAI\right) \qquad (5)$$

with Ω(0) = 0.7.

The value of 0.7 for Ω is only to be used when the tree crowns is viewed from nadir. The Ω changes with the view angle. This impacts the amount of solar radiation intercepted by the canopy depending on the zenith angle of the sun at a given time. Ω can be estimated as a function of the solar zenith angle (θ) as (Campbell and Norman, 1998)

$$\Omega(\theta) = \frac{\Omega(0)}{\Omega(0) + [1-\Omega(0)]\exp\left[-2.2(\theta)^p\right]} \qquad (6)$$

where θ is the solar zenith angle, Ω(0) is the clumping factor when the crowns is viewed from nadir and p = 3.8 – 0.46D, D is the ratio of vegetation height vs. width (Campbell and Norman, 1998). A value for D of e.g. 2 indicates that the crown is twice as high as it is wide. For mixed forest, a value for D of 3 appears to be reasonable. Table 1 lists values of D for stands of different tree species.

Table 1. Canopy clumping factors Ω when viewed from nadir and vegetation height vs. width (D) for mature, healthy stands of different tree species (after Campbell and Norman, 1998).

Species	Ω(0)	D
Sugar Maple (Wisconsin)	0.95	~ 1
Oak (North Carolina)	0.90	~ 1
Aspen (Saskatchewan)	0.70	1.5-2
Jack Pine (Saskatchewan)	0.50	3-4
Black Spruce (Saskatchewan)	0.40	5-6

2. Estimation of fraction shaded ground

When the solar zenith angle is greater than zero the tree crowns will cast a shadow on the ground that is visible to the nadir looking satellite. The fractional area covered by a shadow cast by the crowns (including the shaded areas under the trees) f_{s_tot} is estimated as (Campbell and Norman, 1998)

$$f_{s\_tot} = \frac{1-\exp\left(-0.5\Omega(\theta)LAI\right)}{\cos\left(\theta\right)} \qquad (7)$$

where Ω(θ) is estimated based on solar zenith angle using Eq 6. The division by cos(θ) is to project the shadow onto a horizontal plane. Equation 7 is limited to $0 \le f_{s\_tot} \le 1$.

The shadow cast by the crowns are either wholly or partly under the crown itself, or may be cast on the ground next to the tree or under or onto neighboring trees. The nadir looking satellite does not “see” the entire shadow cast by the crowns because the view is partly

obstructed by the tree crowns. The fraction of shadow visible when viewed from nadir is estimated as described below.
When estimating the momentum roughness length for the calculation of sensible heat flux in METRIC it is assumed that mixed forest tree height (h) in meters can be estimated as

$$h = 2.5LAI \qquad (8)$$

The effective height $z_{leafless}$ above the ground where there are no leaves intercepting the solar radiation can be estimated as

$$z_{leafless} = h \times f \qquad (9)$$

where f is a factor (f<1) describing the proportion of bottom needleless or leafless portion of the tree and not casting a shadow to the total height of the tree. A value of f of e.g. 0.3 indicates that the lower 3/10 of the tree has no foliage and thus casts no shadow. An f value of 0.25 appears reasonable for mixed forests (the foliage is distributed over the top three quarters above the ground of the trees, while the bottom quarter is leaf-free). The fraction of the canopy that has a shadow under it (which is not visible to the satellite because it is covered by the canopy) can be estimated as

$$f_{nonvisible} = 1 - \frac{f_{shape}\left(\frac{z_{leafless}}{\tan(\pi/2-\theta)}\right)}{w} \qquad (10)$$

where:

$f_{nonvisible}$ = The fraction of the ground under the vegetation that has a shadow cast on it, limited to $0 \le f_{nonvisible} \le 1$,

f_{shape} = Factor to adjust for differences in shape between the trees and their shadow when viewed from nadir (tentatively set to 1),

$z_{leafless}$ = Distance in m from the ground to the lower edge of the foliage, calculated in Eq 9

θ = Sun zenith angle, radians

w = Vegetation width in m, calculated as h/D (h is from Eq 8, D was assumed to be 3 in Eq 6),

The principles behind Eq 10 are sketched in figure 1.

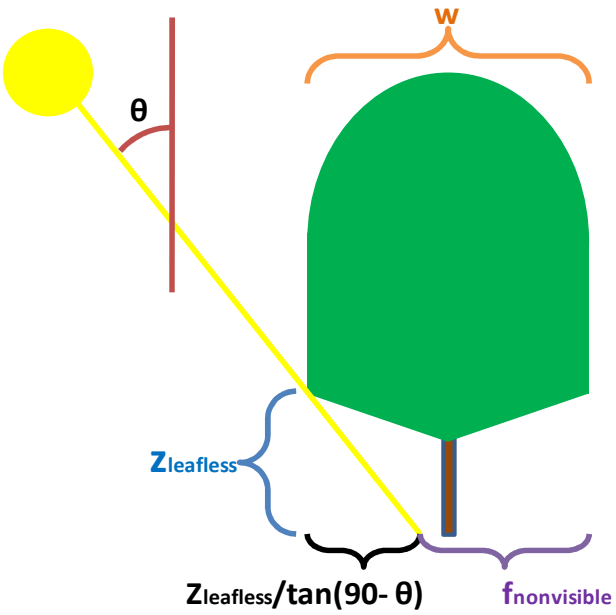

Figure 1. Calculation of the fraction ground area under a tree that has a shadow cast on it (Eq 10) (schematic).

The fraction area of the ground that has a shadow visible from nadir can then be estimated as

$$f_{shaded} = MIN(1 - f_c, f_{s_{tot}} - f_c \times f_{nonvisible}) \qquad (11)$$

3 Estimation of fraction sunlit ground

The fraction of the ground that receives direct solar radiation visible from nadir (f_s) can be estimated as

$$f_{sunlit} = MAX(0, 1 - f_c - f_{shaded}) \quad (12)$$

4 Examples of fractional ground cover

Estimated fractional ground cover (Eq 5) for is sketched for solar zenith angles of 15°, 35° and 55° in figures 2-4.

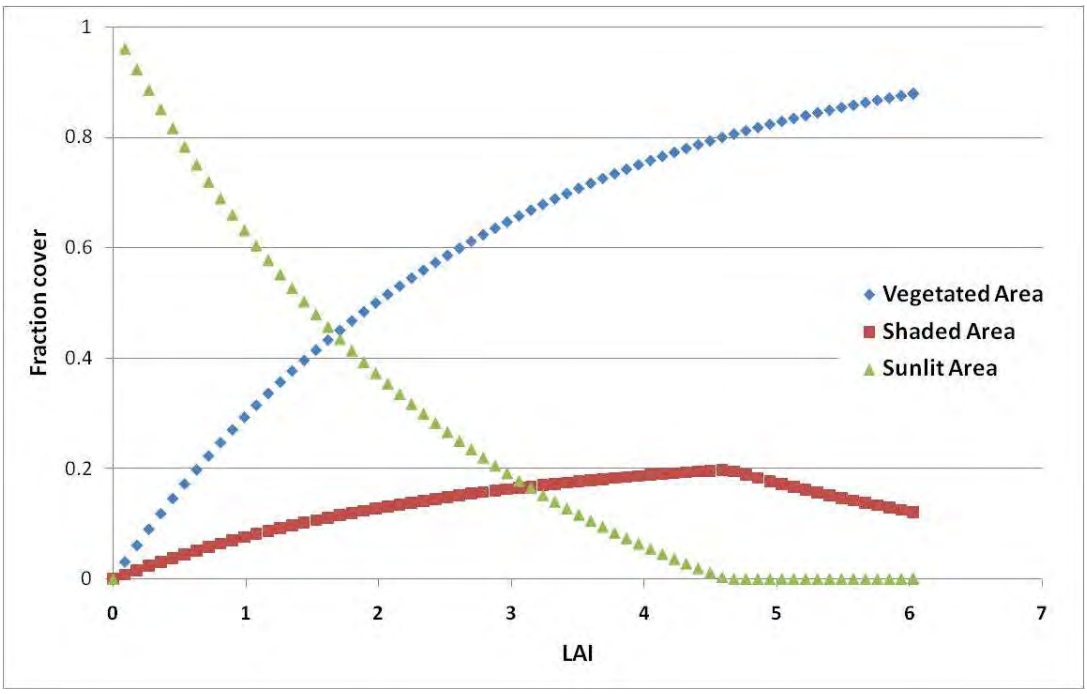

Figure 2. Fractional ground cover estimated for forest with a solar zenith angle of 15°.

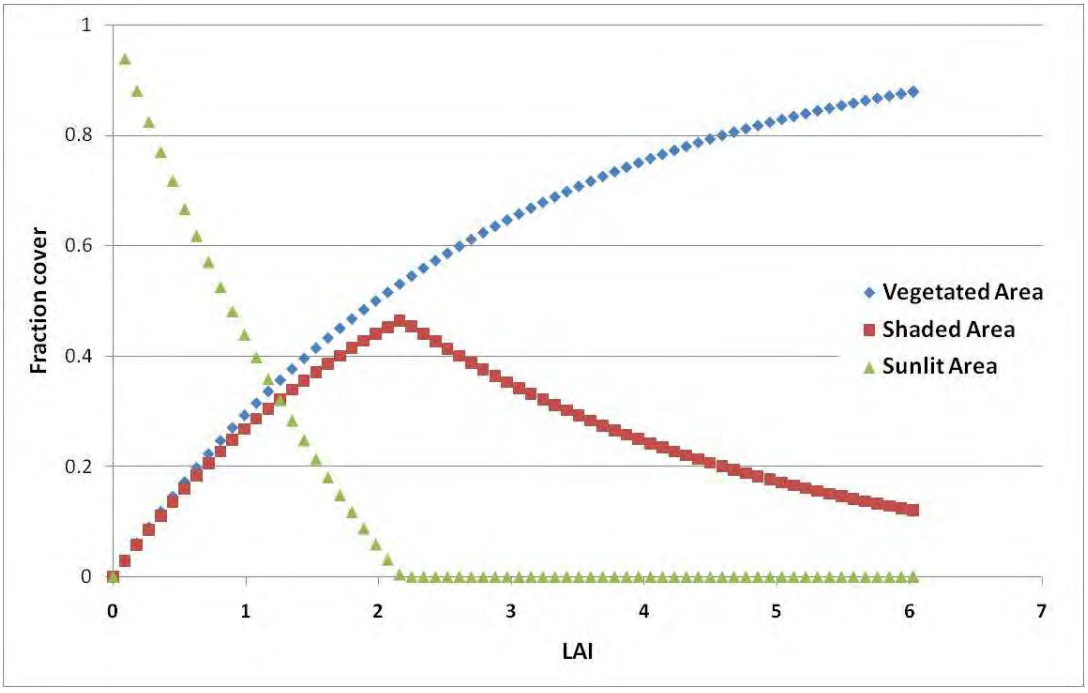

Figure 3. Fractional ground cover estimated for forest with a solar zenith angle of 35°.

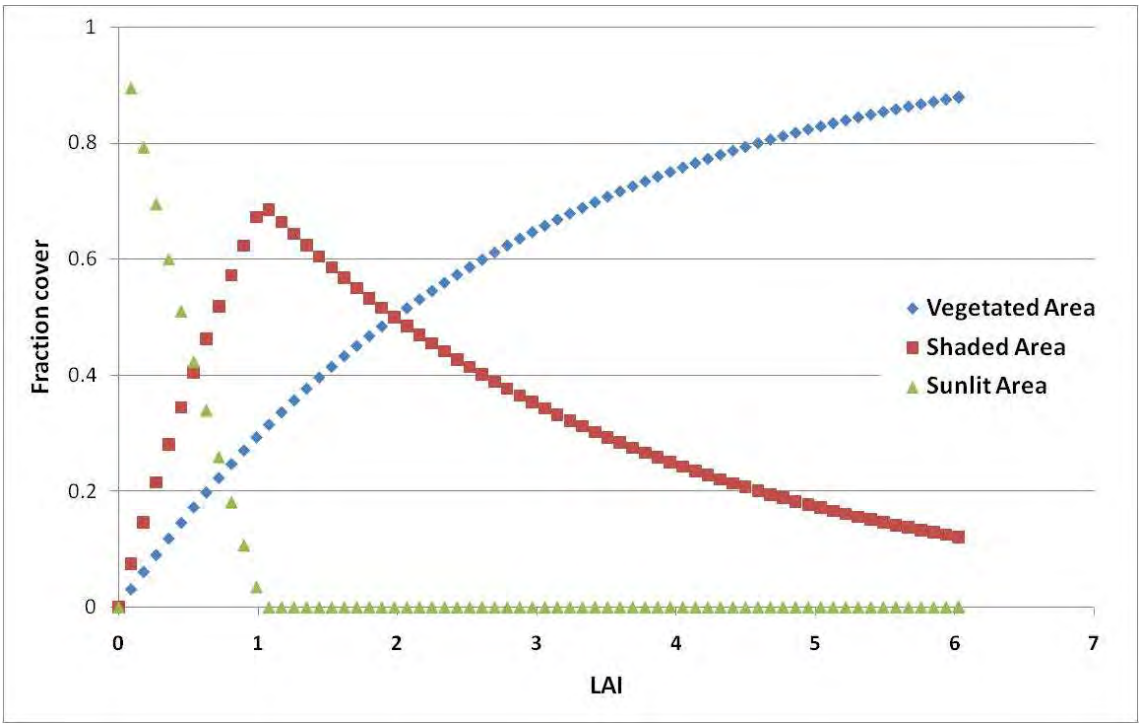

Figure 4. Fractional ground cover estimated for forest with a solar zenith angle of 55°.

5. Estimation of T_{shadow} and T_{sunlit}

The main properties controlling the surface temperature of the shaded areas are evaporative cooling and the radiation exchange between the ground and the vegetation. In forests residual evaporation of soil moisture from antecedent rainfall or snow melt will generally occur from the soil surface at low rates over extended periods of time. In shaded areas, without direct solar radiation to supply energy for evaporating the soil moisture, the shadowed, moist surfaces may approach the wet bulb temperature. The radiation exchange between the ground and the vegetation will tend to heat the ground to a temperature above the wet bulb temperature. The shaded ground surface temperature may therefore, on average, be approximated as $T_{shadow} = T_{coldpixel} – (T_{coldpixel} - T_{wetbulb})/3$, Table 2. Field measurements may confirm this approximation. $T_{coldpixel}$ is the surface temperature of the cold calibration pixel of METRIC, which is generally for full cover uniform vegetation. $T_{wetbulp}$ is estimated as outlined by Jensen et al. (1990) based on $T_{drybulb}$, dew point temperature and atmospheric pressure reported for the St. Ignatius weather station.

The sunlit portion of the ground visible to the satellite when viewed from nadir is likely to be warmer than the temperature of the cold pixel primarily due to the energy loading from the sun. The temperature is likely to be not as high as the temperature of the hot calibration pixel of METRIC (representing dry bare soil in an open area) because of some energy is consumed in evaporating water from areas of moist soil within the tree canopies, because the sunlit area may have been exposed to sunlight for only a limited amount of time prior to satellite overpass time, and because the heating of the surface may create some buoyancy over the sunlit

portions where warmer air rises and is periodically replaced by cooler air from areas with shadows. The sunlit ground surface area is therefore approximated, on average, as $T_{sunlit} = T_{coldpixel} + (T_{hotpixel} - T_{coldpixel})/3$, Table 2. Field measurements may confirm this approximation. Figure 5 shows the temperature data of Table 2 in graphical form.

Table 2. Temperatures for the cold anchor pixel and hot anchor pixel of METRIC, the wet bulb temperature, the dry bulb temperature and estimations of T_{shadow} and T_{sunlit}.

Date	Tcoldpixel	Thotpixel	Twetbulb	Tdrybulb	Tshadow	Tsunlit
04/13-2008	295.2	306.7	279.2	286.3	289.9	299.0
05/10-2006	289.4	310.4	274.8	286.5	284.5	296.4
05/31-2008	291.5	306.7	285.3	291.0	289.4	296.6
06/27-2006	298.2	318.5	290.9	299.0	295.8	305.0
07/16-2007	298.2	322	287.5	302.0	294.6	306.1
08/01-2007	297.7	319	281.4	297.8	292.3	304.8
09/02-2007	294.7	312.3	286.7	297.4	292.0	300.6
10/01-2006	290.3	300	278.5	293.7	286.4	293.5

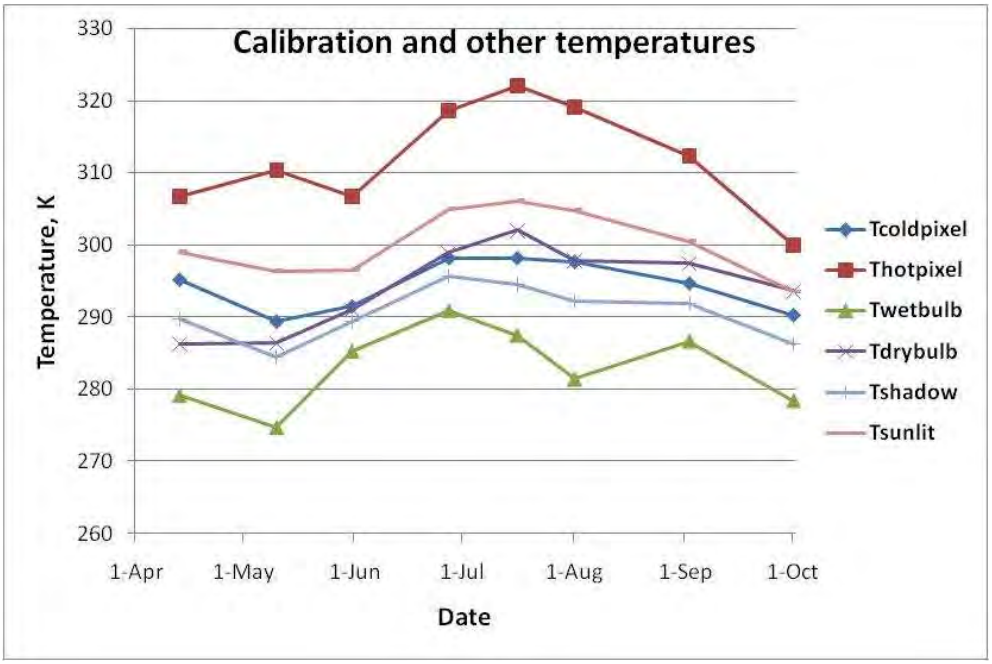

Figure 5. Temperatures for the cold anchor pixel and hot anchor pixel of METRIC, the wet bulb temperature, the dry bulb temperature and estimations of T_{shadow} and T_{sunlit}.

References

Campbell, G.S., Norman, J.M., 1998. An introduction to environmental biophysics. Springer, New York. 286 pp.

Jensen, M.E., Burman, R.D., Allen, R.G., 1990. Evapotranspiration and Irrigation Water Requirements. ASCE Manual No. 70. ASCE, New York. 332 pp.

Norman, J.M., Kustas, W.P., Humes, K.S., 1995. Source approach for estimating soil and vegetation energy fluxes in observations of directional radiometric surface temperature. Agric. For. Meteorol. 77, 263-293.
Kustas, W.P., Norman, J.M., 1999. Evaluation of soil and vegetation heat flux predictions using a simple two-source model with radiometric temperatures for partial canopy cover. Agric. For. Meteorol. 94, 13-29.

Appendix G
Generation of Monthly and Seasonal ET and ET_rF on Satellite Overpass Days
By J. Kjaersgaard and R. Allen, University of Idaho, April 2009.

Estimates of the fraction of alfalfa based reference evapotranspiration (ET_rF) were generated using the METRIC image processing model for eight image dates in the Mission Valley area. The image dates and satellite source are shown in Table 1. These products were interpolated over dates between Landsat images to produce monthly average crop coefficients and total monthly evapotranspiration, as described below. ET_rF is similar to the well-known crop coefficient (K_c) and represents the ratio of actual ET to the reference ET. In METRIC, the alfalfa reference ET_r is used for calibration and determination of ET_rF.

Table 1. Image dates and satellite used in the estimation of ET_rF for the Mission Valley area

Image date	Satellite
04/13-2008	Landsat 5
05/10-2006	Landsat 5
05/31-2008	Landsat 5
06/27-2006	Landsat 5
07/16-2007	Landsat 5
08/01-2007	Landsat 5
09/02-2007	Landsat 5
10/01-2006	Landsat 5

Cloud masking
Most of the satellite images had some degree of clouds within the image. Due to the lower temperature of the surface of the clouds and the opaque nature of clouds and other major atmospheric disturbances in the shortwave bands used for the METRIC application, the ET_rF estimates for areas covered by clouds (including thin cirrus clouds), jet contrails and smoke are non-representative of the ET_rF at the ground surface. The shadows cast by clouds on the ground surface are generally cooler than sunlit portions which may lead to an overestimation of ET_rF by METRIC. Areas with cloud cover and other major atmospheric disturbances and their shadows must therefore be identified and masked out.

The cloud recognition was based on visual identification of clouds within each image and the cloud masking was done manually. When masking for clouds, areas of up to a kilometer around both the clouds and the cloud shadows were masked. This ensured that thin, almost transparent edges of the clouds as well as portions of the ground, just upwind of the current shadow, that do not yet have the same surface temperature as they would have had if there had been no shadow cast on them were masked out. The cloud masked images are shown in Figure 1.

The gaps in the ET_rF maps occurring as a result of the cloud masking were filled in using time weighted ET_rF values interpolated from the previous (already gap filled) image and the nearest following satellite image date having a valid ET_rF estimate (Trezza et al. 2007). During the gap

filling, the interpolated values for the desert areas were adjusted for differences in residual soil moisture between the image dates.

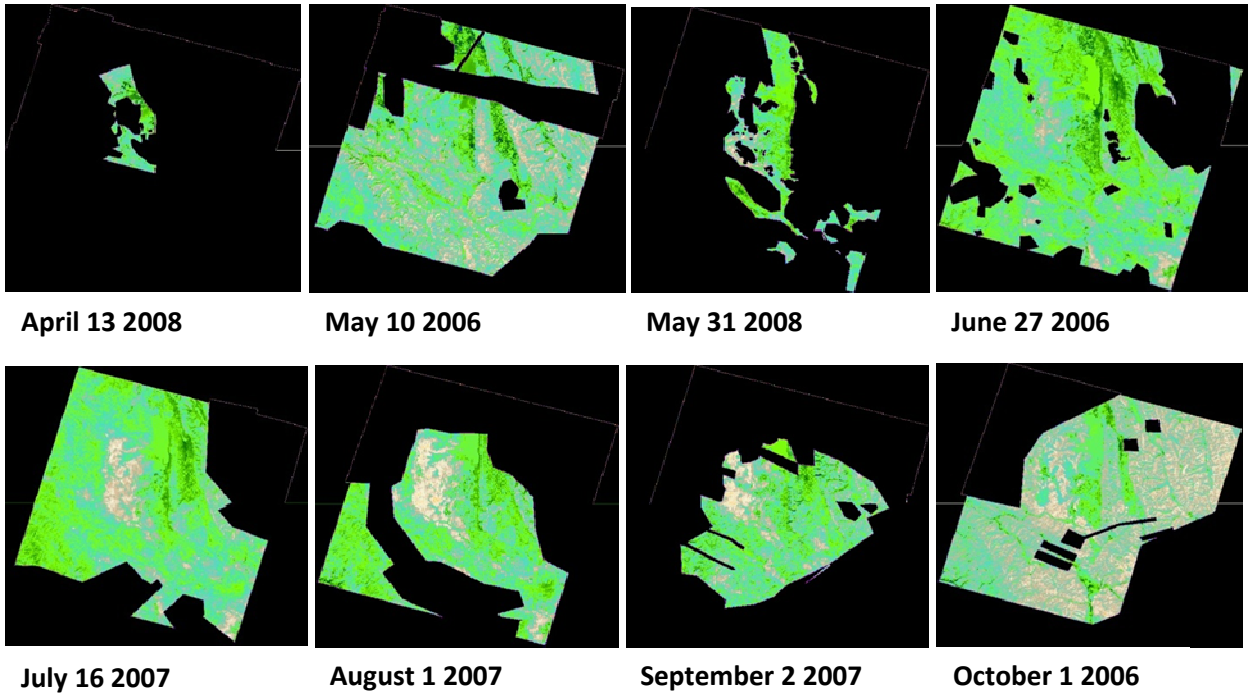

Figure 1. Cloud masked images of ET_rF for each satellite overpass day. Four of the images had no cloud cover present in the image.

Some areas within the images, such as the mountainous area east of the Mission Range, had some degree of cloud cover in all images. The monthly ET_rF for some of these areas are thus based on interpolated values. Because of the ET_rF values in these areas with high degree of cloud cover are interpolated, the monthly and ET estimates have a greater uncertainty and possible a bias compared to areas free from cloud cover.

Fortunately, the agricultural areas in the Mission Valley were cloud free for all image dates, except on April 13 where thin cirrus clouds were present over roughly half the valley and on May 31 where a small portion of the valley had cloud cover.

Because the April 13 is the first image in the image sequence and because it is acquired one month prior to the following image, this image was gap filled using a relationship between the normalized difference vegetation index (NDVI) and ET_rF rather than interpolation from the following image. The relationship between NDVI and ET_rF for the April 13 image was established by fitting regression functions to over 2100 pixels sampled in the cloud free portions of the Mission Valley. Because of the difference in vegetation characteristics separate relationships were developed for agriculture and for natural vegetation. The coefficients for the relationship are shown in Table 2. The relationship for agriculture is shown in Figure 2. The gaps from the cloud masking within the Flathead Reservation were filled using these relationships.

Table 2. Linear regression coefficients and sample size, n, for the relationship between NDVI and ET_rF.

Vegetation type	Slope	Offset	n
Agriculture	0.75	0.26	1396
Natural vegetation	1.50	0.10	745

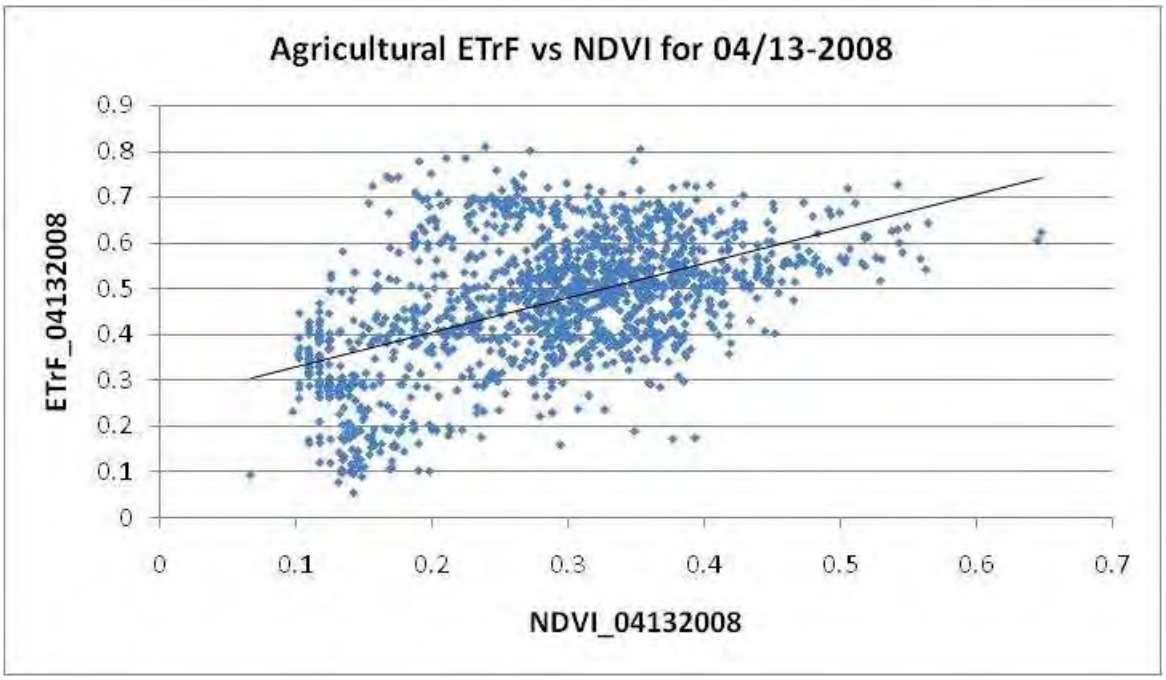

Figure 2. ET_rF versus NDVI for approximately 1400 pixels located in agricultural fields in the Mission Valley on 04/13-2008. The black line indicates the best fit.

Estimation of daily ET_rF using a cubic spline model

The daily estimates of ET_rF for the satellite overpass dates were extrapolated between image dates using a cubic spline model. The cubic spline model used for the extrapolation has been described by Allen et al. (2008) and Trezza et al. (2009). The spline creates a smooth curve for ET_rF between images to simulate the day to day development of vegetation.

The spline estimates the ET_rF value for each day of a month (such as e.g. the month of June) based on the ET_rF values estimated for the image date(s) for that month (June 27, see Table 1), plus two image dates earlier than the month (May 10 and May 31), and two image dates later than the month (July 16 and August 1).

There were not two independent ET_rF images available prior the months of April and May to be used for the splining of the ET_rF. At this early period of the growing season crop development is stagnant or very slow, and changes in vegetation cover is very small. In 2008 the residual ET_rF from bare soil as predicted by the soil water balance model remained relatively constant (around $ET_rF = 0.25$) during the second half of March and first half of April. This was because small precipitation events occurred roughly every other day at amounts sufficient to replenish the soil water lost to the atmosphere by evaporation. A similar balance between precipitation and evaporation occurred in mid-March – mid-April in 2006 and 2007 as well. It was therefore

assumed that the ET_rF map from April 13 was representative for the ET_rF occurring on March 26 and March 31 also. The April 13 image was therefore used as an input to the spline interpolation on March 26 and March 31. This resulted in a somewhat "flat" development in ET_rF during the first week of April. Similarly, the image from October 1 was scaled for differences in soil moisture and vegetation development and used to indicate the ET_rF for November 1 and November 15 in order to spline the ET_rF for the month of October.

The splined daily ET_rF values sampled from randomly selected fields of agricultural crops, rangeland and forest for the period April through October are shown in Figure 3. Some of the oscillations in ET_rF within the middle part growing season of the agricultural crops reflect the impacts of cutting or intensive grazing on the ET_rF.

Some of the highest values for ET_rF in Figure 3 are caused by the nature of the cubic spline interpolation process where the midpoint of the splined curve between two high ET_rF points from adjacent images in time will tend to extend above the values of either of these points, especially if those two images are surrounded by images having lower ET_rF values (at any particular pixel). These extensions above computed ET_rF are generally balanced by similarly low values of ET_rF that occur between two adjacent images having low ET_rF computed for a particular pixel so that growing season estimates for ET should not be substantially impacted.

Estimation of monthly ET and ET_rF

Daily values of ET for each pixel within the images was estimated using

$$ET_{daily} = ET_{r\_daily} \times ET_rF_{daily} \qquad (1)$$

where ET_{daily} is the daily evapotranspiration (mm/day), ET_{r_daily} are daily values of alfalfa based reference evapotranspiration (mm/day) and ET_rF_{daily} are the daily ET_rF values. ET_r was estimated using hourly input data from the St. Ignatius Agrimet weather station using the University of Idaho RefET software. The hourly values of ET_r were subsequently summed to daily values.

Daily values of ET were summed to monthly totals (mm/month) as

$$ET_{month} = \sum_{i=m}^{n} ET_{daily} \qquad (2)$$

where ET_{month} is the cumulative monthly ET (mm/month), and m and n are the first and last day of the month.

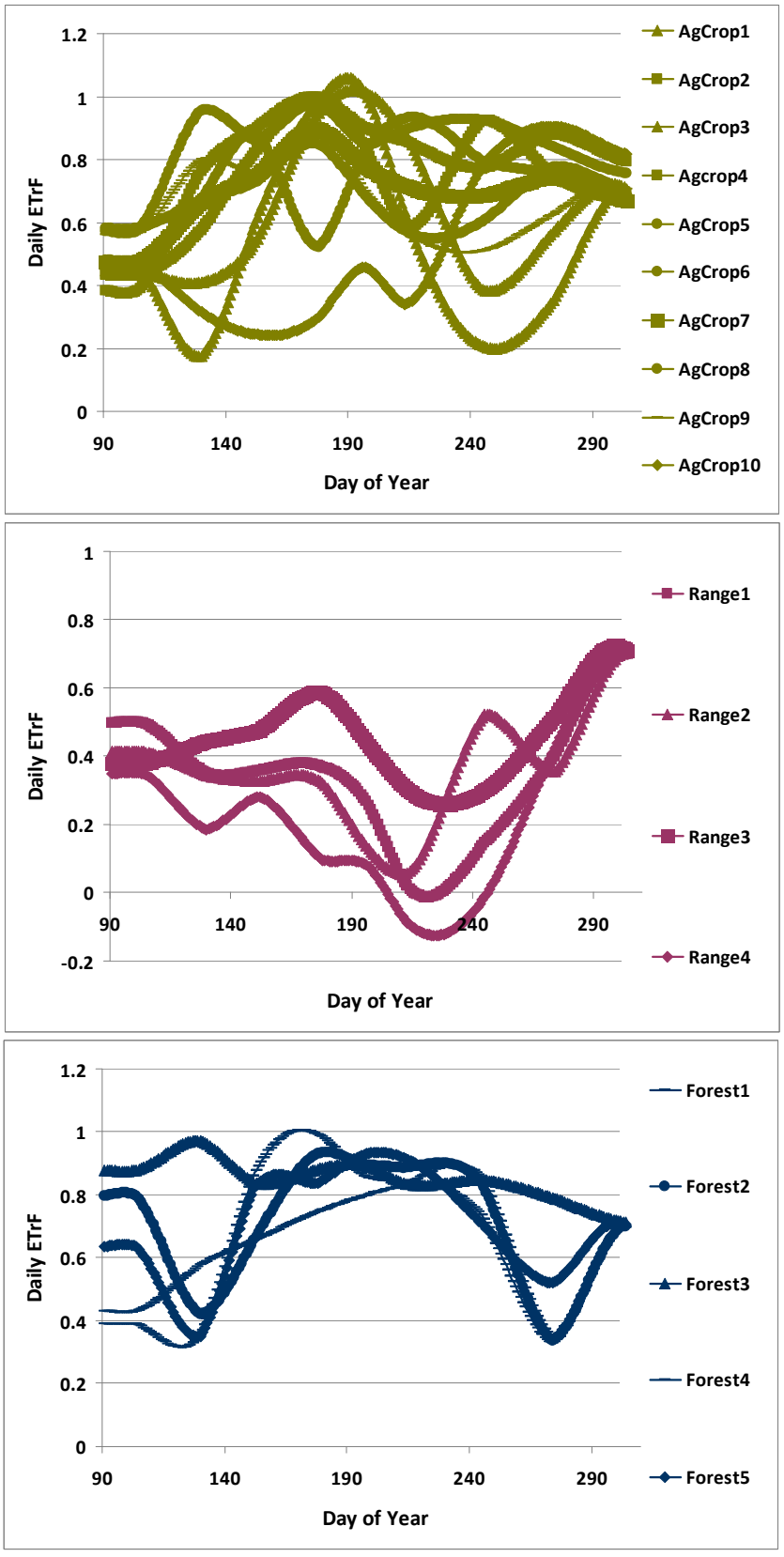

Figure 3. Daily ET_rF splined between image dates for randomly selected fields of agricultural crops, rangeland and forest..

The satellite images processed using METRIC were from three different years and consequently the estimates of monthly and seasonal ET and ET_rF will show some dependence on which year's weather data were used to calculate ET_r. For this reason, monthly and seasonal ET were calculated using four different sets of ET_r from the St. Ignatius weather station as summarized in Table 3. This resulted in four sets of monthly and seasonal ET_rF and ET values. All four sets were transferred to the MT-DNRC.

Table 3. Source years of meteorological information used to calculate ET_r.

Method reference	Calculation of ET_r (based on data from the St. Ignatius Agrimet weather station)
2006	2006 weather data
2007	2007 weather data
2008	2008 weather data
Mean	Average ET_r from 2006, 2007 and 2008

The monthly fraction of ET_rF_{month} were estimated using

$$ET_rF_{month} = \frac{ET_{month}}{ET_{r\_month}} \qquad (3)$$

where ET_{month} is the monthly ET (mm/month) and ET_{r_month} is the monthly ET_o obtained by summing ET_r estimates from each day of that month. The monthly and seasonal ET_r is shown in Table 4 for 2006, 2007, 2008 and as the mean of the three years.

Table 4. Monthly, seasonal (April through October) and annual ET_r (mm) estimated from the St. Ignatius weather data set

Month	2006	2007	2008	Mean
January	32	22	24	26
February	34	25	31	29
March	63	76	65	68
April	98	99	97	97
May	160	146	142	149
June	156	170	167	164
July	229	248	229	236
August	189	184	173	184
September	105	115	97	106
October	53	58	53	55
November	35	31	22	29
December	17	26	16	19
April-Oct Total	990	1020	959	990
Year Total	1169	1201	1117	1162

In some cases, due to statistical uncertainty and insufficient model calibration, some land use types may take on slightly negative values in the final ET_rF map generated at each satellite

image date. During the calibration process, very dry desert areas are normally considered to have an ET_rF close to zero. Due to the heterogeneity of the desert areas (slight differences in soil characteristics, vegetation and similar) the ET_rF values will hover around zero, with some ET_rF values slightly above zero while others are slightly below zero. When spatially averaged over a medium to large area, variations will tend to cancel out.

In the ET_{month} products generated from METRIC, a floor was applied so that negative values were set to zero. When generating the seasonal ET estimates from the monthly ET estimates, a possible negative estimate of ET in one month may somewhat counteract a positive ET estimate the following month which may lead to an overall underestimation in seasonal ET. Because for some land use types, such as desert where the negative ET values are countered by positive ET values when viewed over a larger area (e.g. several km^2), this may lead to a slight positive bias in the estimates.

No floor was used when generating the ET_rF_{month} product hence the negative values are included in the ET_rF_{month} maps. This will allow the user to avoid creating a bias from dry desert or similar areas when summarizing the values over a larger area.

Estimation of seasonal (April through October) ET and ET_rF
Seasonal estimates (April through October) of total ET, ET_s (mm/season) and seasonal ET_rF, ET_rF_{season} were calculated as

$$ET_{season} = \sum_{i=m}^{n} ET_{month} \qquad (4)$$

where ET_{season} is the cumulative seasonal ET (mm/season), and m and n are the first (m=4) and last (m=10) month of the season, and

$$ET_rF_{season} = \frac{ET_{season}}{ET_{r\_season}} \qquad (5)$$

where ET_{r_season} is the seasonal ET_r obtained by summing ET_r estimates from each day of the season.

The primary focus in the application of METRIC in the Mission Valley was to estimate the ET from irrigated and non-irrigated agricultural land (including orchards and range land). The ET_{month} and ET_{season} estimates from other land cover types such as for asphalt roads (including rural roads), which have a different ground heat flux and surface roughness as compared to other urban structures. The ET from a road is normally very low as the surface is almost impermeable so there is very little residual ET once the surface is dry. Excess water during precipitation events will either run off the road (often through storm drains) or removed by traffic, reducing the annual evaporation from the road surface to as little as 10 % of the precipitation.

References

Allen, R.G., Tasumi, M., Trezza, R., Kjaersgaard, J.H., 2008. METRIC Applications Manual. Version 2.0.4. University of Idaho, Kimberly, Idaho. 164 pp.

Trezza, R., Allen, R.G., Garcia, M., 2007. Methodology for Cloud Gap Filling in METRIC. University of Idaho, Kimberly, Idaho. 7 pp.

Trezza, R., Allen, R.G., Garcia, M., Kjaersgaard, J.H., 2008. Using a Cubic Spline to Interpolate between Images. University of Idaho, Kimberly, Idaho. 9 pp.